A FREEZE-DRYING PROCESS FOR FABRICATION OF POLYMERIC BRIDGES FOR PERIPHERAL NERVE REGENERATION

by

Howard Martin Loree II

Bachelor of Science in Mechanical Engineering,
Massachusetts Institute of Technology 1986

SUBMITTED TO THE DEPARTMENT OF MECHANICAL ENGINEERING IN PARTIAL FULFILLMENT OF THE REQUIREMENTS FOR THE DEGREE OF

MASTER OF SCIENCE

at the

MASSACHUSETTS INSTITUTE OF TECHNOLOGY

May 1988

Signature of Author _____
Department of Mechanical Engineering
May 27, 1988

Certified by _____
Professor Ioannis V. Yannas
Thesis Supervisor

Accepted by _____
Professor Ain A. Sonin
Chairman, Department Committee on Graduate Students

A FREEZE-DRYING PROCESS FOR FABRICATION OF POLYMERIC BRIDGES FOR PERIPHERAL NERVE REGENERATION

by

Howard Martin Loree II

Submitted to the Department of Mechanical Engineering on May 27, 1988 in partial fulfillment of the requirements for the degree of Master of Science.

Abstract

The goal of this research is a manufacturing technique for biodegradable collagen-glycosaminoglycan (CG) polymers with controlled pore structure. When used to bridge a 15-mm gap in the rat sciatic nerve, these polymers have induced regeneration of myelinated and unmyelinated axons along the entire gap length. In the current stage of development, the cylindrical bridges are ensheathed in 20 mm long sections of 1.5 mm diameter silicone tube. Three characteristics of the bridge pore structure are thought to affect nerve regeneration. These are average pore diameter, pore channel orientation with respect to the long axis of the bridge, and bridge degradation rate. Preparation of bridges involves four primary steps: (1) making a suspension of CG particles in 0.05 M acetic acid, (2) filling a length of silicone tube with the suspension, (3) lowering the tube axially into a cooling bath to form oriented ice dendrites in the CG suspension, and (4) freeze drying the tube to sublime the ice, leaving a porous foam within the tube. An apparatus has been constructed to test the proposed manufacturing process. Three manufacturing parameters affect the bridge pore structure: entry velocity of bridges into the cooling bath, undercooling, and concentration of CG in the suspension. In our apparatus, these parameters can be varied across the following ranges: entry velocity, 2.0×10^{-5} m/s to rapid quench; undercooling, 10 to 70 °C; and CG concentration, 0.12 to 0.48 %w/w. For analysis, bridges are cut into longitudinal and cross sections and then photographed using scanning electron microscopy or using embedding and sectioning and light microscopy. Calculations of average pore diameter and orientation are done by a computerized image analysis system. The research also includes theoretical modeling of the heat and mass transfer processes that occur during dendritic solidification of water in the CG suspension. The objective of this modeling is an understanding of the mechanism of solidification in CG suspensions and the effect of CG concentration and cooling rate on dendrite geometry. Experimental results show that bridges with uniform pore diameter and uniform orientation can be prepared reproducibly. Pore diameter can be adjusted between 30 and 300 microns. Pore orientation can be adjusted from strongly axial to strongly radial. Pore diameter decreases as undercooling increases. As CG concentration increases, pore structure changes from fibrillar to lamellar, with pore diameter remaining constant. Pore orientation becomes more radial as velocity increases.

Thesis Supervisor: Professor Ioannis V. Yannas
Title: Professor of Polymer Science and Engineering

Dedication

This thesis is dedicated to the individuals whose contributions made it possible:

Jesus Christ, to whom my entire life is dedicated. May the lessons learned during the course of this thesis make me a better servant in His Kingdom.

My parents, for their constant love and encouragement.

Prof. Ioannis Yannas, for choosing me to work in his laboratory and for wisely counseling me through all phases of the project.

Ariel Ferdman, Roy Hughes, Jim Kirk, Hollie Mahaney, and Gene Skrabut for their invaluable technical advice.

Prof. Borivoje Mikic for helping me develop the heat transfer model.

Allison Hubel and Mehmet Toner for their assistance with the cryomicroscopy experiments and their technical advice on solidification processes.

Mark Moormans, for being my best friend and for extending me the computer privileges used in writing this document.

Al Chang for finding a practical use for the PNS bridges and for spurring me on by his example of excellence.

Lou Bonhomme, Jude Colt, Donna Duffy, Vic Gobbell, Yuri Kinoshita, Simon Lewis, Ted Moore, Randy Saunders, and Mark Shelley for their encouragement and support during this project.

Table of Contents

List of Figures

List of Tables

Chapter 1

Introduction

1.1 Background

The goal of this research is a manufacturing technique for biodegradable collagen-glycosaminoglycan (CG) polymers with controlled pore structure. The most immediate application of these polymers is in the development of peripheral nervous system (PNS) bridges with controlled pore diameter and orientation. PNS bridges have induced regeneration of severed rat sciatic nerve across a gap of 15 mm. Bridges are produced through a process of controlled dendritic solidification and freezedrying of CG suspension. Pore structure can be adjusted by varying the cooling rate during solidification and changing the concentration of CG in the suspension. Several methods of specimen preparation and microscopy have been used to image the structure of CG foams, including epoxy embedding and sectioning followed by light microscopy and metal plating followed by scanning electron microscopy. Stereological analysis of micrographs has been done both manually and with a computerized image analyzer.

1.2 Nerve Regeneration

As described in the thesis of Chang[1], a severed nerve will degenerate rapidly. The distal portion loses axons, since axons are separated from nerve cell bodies in the spinal cord. Myelin and Schwann cells also degenerate, leaving only the endoneurial tubes in the gross extracellular matrix of the nerve trunk. Muscles innervated by the severed nerve soon atrophy because they are no longer in communication with the central nervous system. The proximal stump of the severed nerve sprouts new growths that attempt to make connection

with their target organs. Unless the distal nerve trunk is available for guidance, the axonal growths wander aimlessly and die.

Currently, severed peripheral nerves are surgically repaired by suturing the stumps directly together. Nerve growths from the proximal end can follow the distal endoneurial tubes to the target organs. There is no known mechanism guaranteeing that each axon will return to its original target organ. However, neurotrophic factors secreted by the distal portion of the the nerve and the neuromuscular junctions may help guide the axons to their proper targets.

Previous work has addressed the problem of nerve regeneration across extended gaps. Frequently used techniques involve putting the stumps into the ends of an empty tube (entubating) to contain the growth of axonal sproutings and to localize the effect of neuronotrophic factors. An empty silicone tube has been used with limited success across a 10 mm gap[2]. Biodegradable tubes have also been used[3].

1.3 Peripheral Nerve Bridges

A new avenue of peripheral nerve regeneration has been developed by Dr. Ioannis V. Yannas and colleagues at the M.I.T. Fibers and Polymers Laboratory. This research has applied a collagen-glycosaminoglycan (CG) polymer matrix to the regeneration of an entubated severed nerve. The CG matrix with oriented pore structure is thought to serve as a template into which various nerve cells can grow and reestablish the nerve trunk across the gap. Oriented collagen gels are known to elicit a strong contact guidance response when used as a substratum for nerve axons[4]. The CG matrix is broken down by collagenase secreted by infiltrating cells. The matrix resistance to collagenase degradation can be adjusted through glutaraldehyde crosslinking[5].

Figure 1-1 contrasts a CG peripheral nervous system (PNS) bridge with an empty

silicone tube. In the current stage of development, the cylindrcial nerve bridges are ensheathed in 20 mm long sections of 1.5 mm diameter silicone tube. PNS bridges have induced successful induced regeneration of myelinated and unmyelinated axons along a 15 mm gap in the rat sciatic nerve[6, 7]. Figure 1-2 depicts a PNS bridge placed in a gap in the rat sciatic nerve.

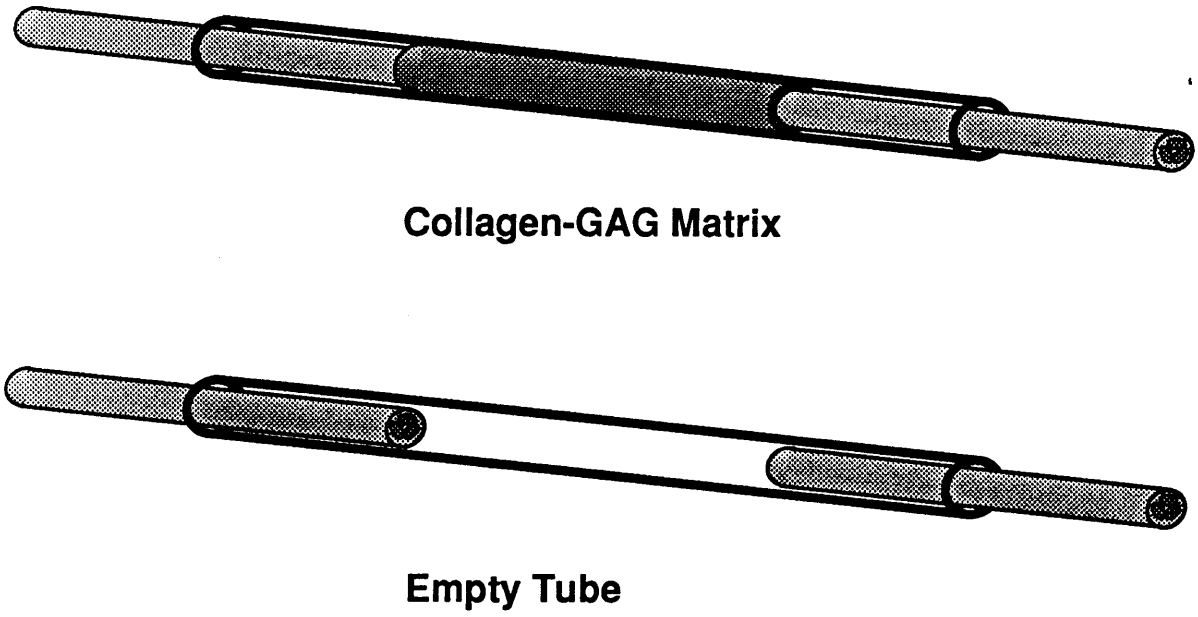

Figure 1-1: PNS bridge vs. Empty Silicone Tube, Chang (1988)

The use of CG polymers to promote tissue regeneration is not a new idea. Over the past 17 years, the Fibers and polyumers Laboratory has developed and tested CG polymer foams as an artificial skin to graft full-thickness skin wounds[8, 9]. Without CG artificial skin, a full-thickness skin wound rapidly contracts and forms scar tissue. In the presence of artificial skin, the wound contracts slowly and regenerates a neodermis very similar to normal dermis. A schematic of artificial skin is shown in Fig. 1-3.

The performance of a PNS bridge is subject to two measures. The first is a histological assay of the regenerated severed nerve. Using embedding, sectioning, and light

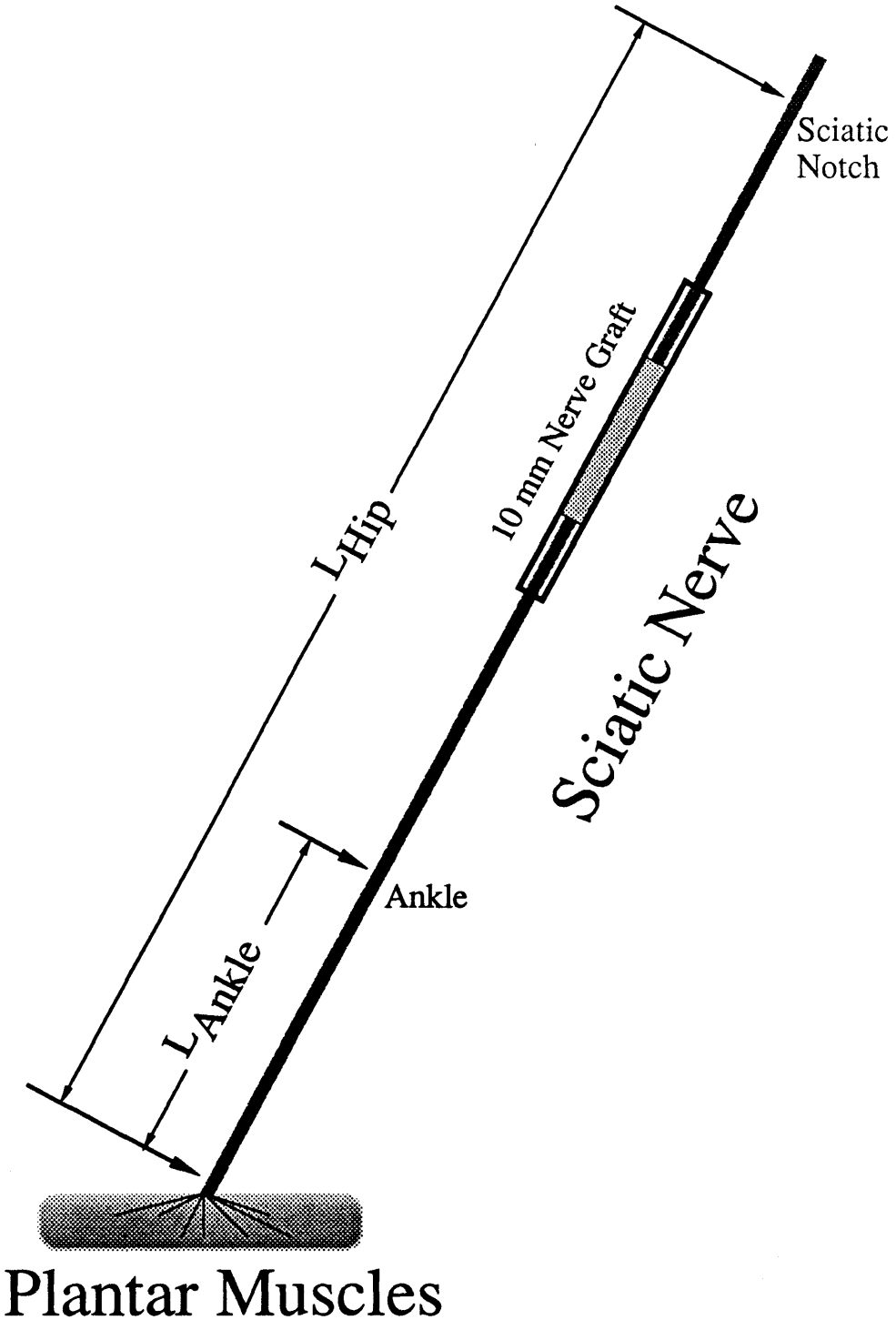

Figure 1-2: Schematic of Grafted Sciatic Nerve, Chang (1988)

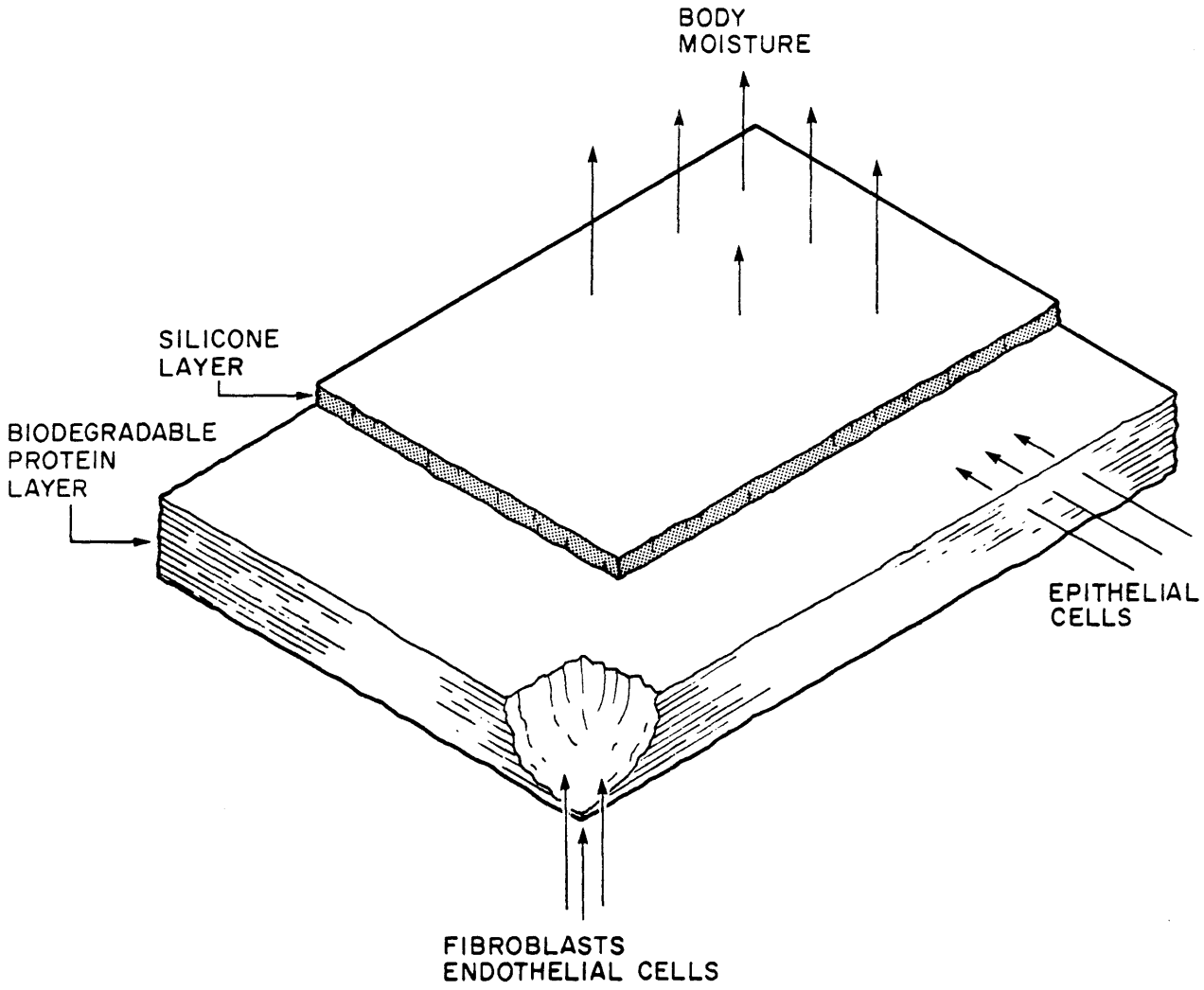

Figure 1-3: Schematic of Artificial Skin, Orgill (1983)

microscopy techniques, the number of axons and blood vessels crossing the gap can be counted at distinct times subsequent to implantation of the bridge. The second index is the electrophysiological response of the regenerated nerve. Electrical stimuli are applied to the nerve, both distal and proximal to the transection site, and the compound muscle action potentials (CMAP's) effected in the foot plantar muscles are monitored. Two quantities are measured: the CMAP amplitude resulting both from hip and ankle stimulation of the nerve and the time between nerve stimulation and the onset of CMAP's, known as the distal

motor latency. Figure 1-4 shows that electrical stimulation of the nerve at the ankle elicits no CMAP's until the 12th week. When first measured, the latency is about 2-3 times higher than normal. Up till 20 weeks, the latency rapidly decreases. Then the latency decreases at a more gradual rate until it stabilizes to a value 50% higher than normal by the 25th week. The latency history for stimulation of the nerve at the hip follows a similar course.

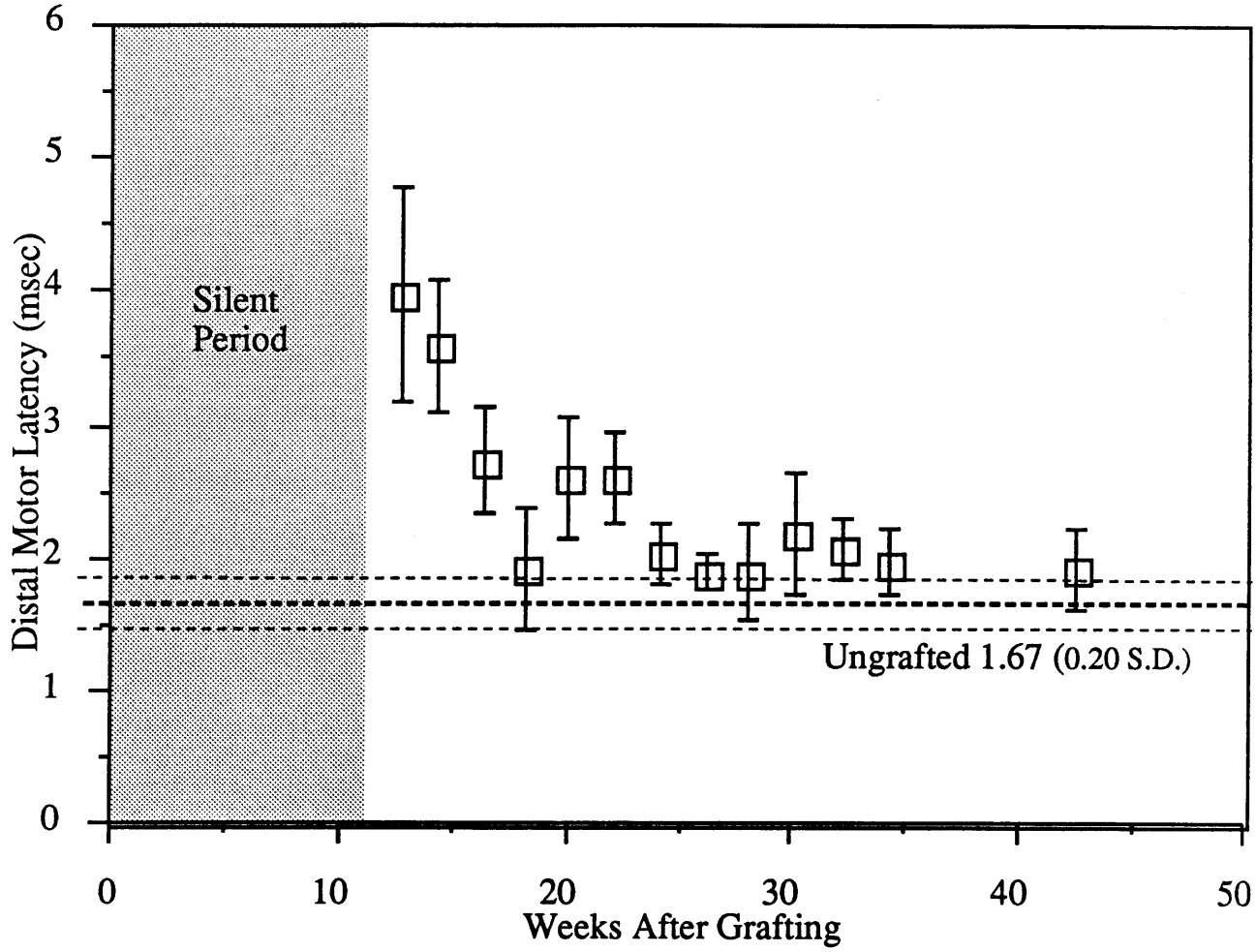

Figure 1-4: Distal Motor Latency vs. Time after Grafting, Chang (1988)

The motivation for the research in this thesis is determination of the optimal pore structure of PNS bridges for nerve regeneration. The work of Ferdman[5] shows that there is an optimal pore structure for the performance of artificial skin. With skin, the performance index is D_{50}, the time after grafting required for a skin wound to contract to 50% of its original area. The longest D_{50} gives the best skin regeneration and, as illustrated in Fig.

1-5, can be obtained for a mean pore diameter of 50 microns. For mean pore diameter lower than 40 or greater than 100 microns, the wound contraction is very rapid. Distal motor latency for regenerated peripheral nerves may be a similar strong function of PNS bridge pore diameter and pore orientation.

1.4 PNS Bridge Manufacturing Process

A production method for peripheral nerve bridges was first developed in the Fibers and Polymers Laboratory by James F. Kirk. Preparation of bridges involves four primary steps: (1) making a suspension of CG particles in .05 M acetic acid, (2) filling a length of silicone tube with the suspension, (3) lowering the tube axially into a cooling bath to form oriented ice dendrites in the CG suspension, and (4) freeze drying the tube to sublime the ice, leaving a porous foam within the tube. An apparatus has been constructed to test the proposed manufacturing process. Three manufacturing parameters affect the bridge pore structure: entry velocity of bridges into the cooling bath, undercooling, and concentration of CG in the suspension. In our apparatus, these parameters can be varied across the following ranges: entry velocity, 2.0×10^{-5} m/s to rapid quench; undercooling, 10 to 70 °C; and CG concentration, 0.12 to 0.48 %w/w.

1.5 Dendritic Solidification of CG Suspension

1.5.1 Ice Physics

Solidification of water can occur by two different mechanisms. In the first process, the water is supercooled, its temperature brought below the 0 °C melting temperature. A nucleation site presents a thermodynamically favorable condition for solidification and freezing starts. The latent heat of freezing passes from the ice-water interface to the supercooled water and ice grows in dendrites. A snowflake is formed by such a process.

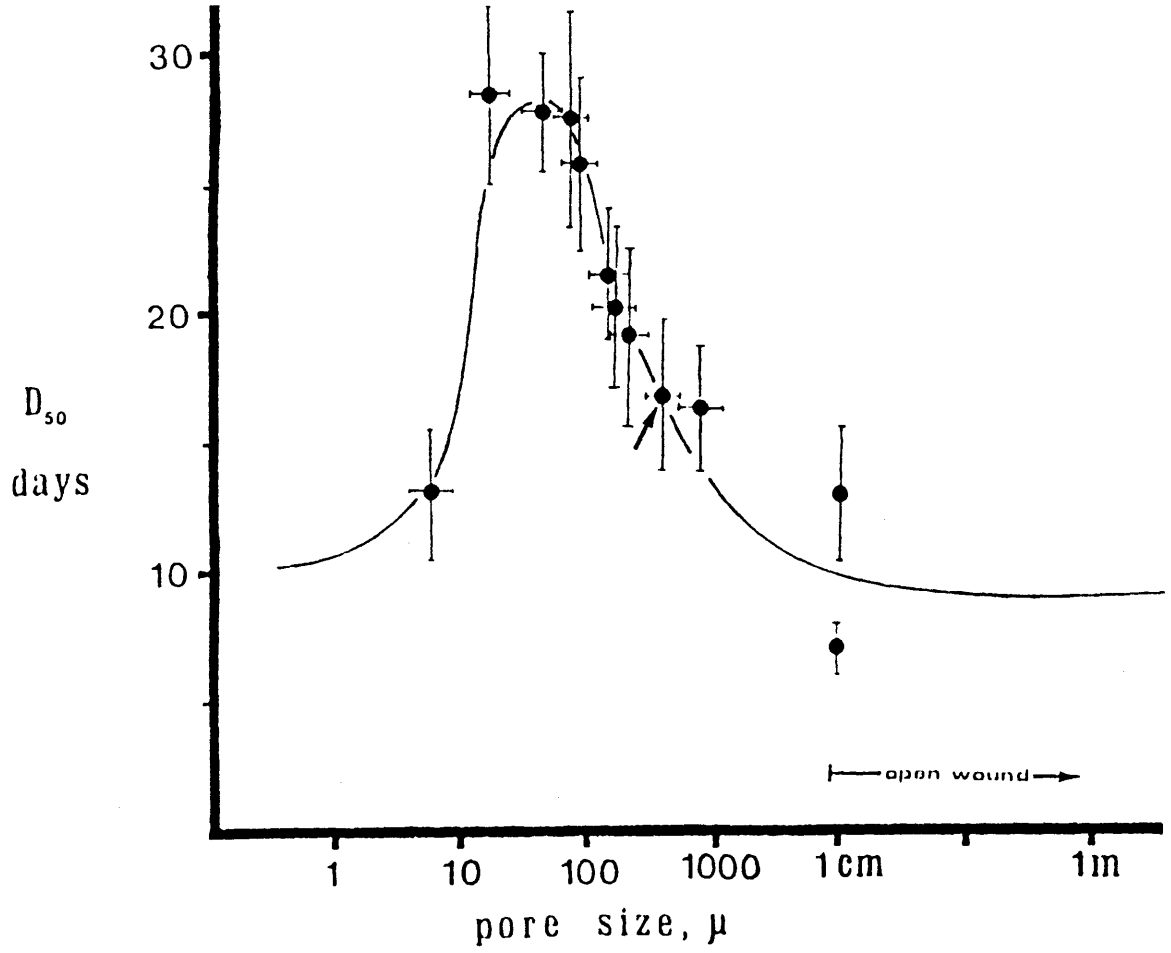

Figure 1-5: Effects of Pore Size on D_{50} in Guinea Pigs, Ferdman (1985)

In the second process, the bulk of the water remains above the melting temperature. If the wall of the container is maintained at a supercooling temperature, ice can form at the wall. Growth of the ice front occurs as the latent heat of freezing of the liquid near the ice front is carried away by conduction through the ice that has already formed. The surface of the ice remains planar for low cooling rates but becomes unstable and assumes a dendritic geometry for fast cooling rates. Such a process is responsible for the freezing of water in home plumbing during cold weather.

The second process is employed in the production of PNS bridges. The freezing rate is directly related to the magnitude of the temperature gradient across the ice front. The orientation of dendritic ice growth is up the temperature gradient or normal to the isotherms in the CG suspension. This orientation is the same as that of the dominant heat flux vector at the freezing front.

1.5.2 Collagen-Ice Interactions

The interaction of particles and a moving solidification front is a topic of considerable interest to metallurgists and cryobiologists. Most theoretical work has focused on the physics of spherical inclusions. Although collagen-GAG molecules are cylindrical filaments rather than spheres, the theory gives at least a qualitative understanding of processes that push a body ahead of a solidification front and processes that capture the body in the solid phase.

The most complete monograph on the subject of inclusions is found in the thesis of Aubourg[10]. Aubourg identifies a critical velocity V_c of the solidification front for capture of a body that it pushes. In all work reviewed by Aubourg, some form of the power law relation $V_c = CR^n$ is applicable. R represents the particle radius and n is a value that increases with R. Competing forces act on a particle as it is pushed ahead of an advancing solid-liquid interface. Viscous drag acts to force the particle into the interface. Van der

Waal's forces repel the particle from the interface due to differences in interfacial free energy. Critical velocity is generally a decreasing function of melt viscosity. Particles may be pushed for some distance before V_c is attained and inclusion occurs.

Myers and Flemings[11] studied the behavior of SiO_2 inclusions in Iron/Copper alloys and found that the majority of inclusions were captured in interdendritic spaces.

Korber, Ran, Cosman, and Cravalho[12] studied the inclusion of latex spheres by an advancing ice-water interface. The sphere diameters ranged from 5.7 to 11.9 microns, about an order of magnitude thicker than the average pore wall thickness observed in CG foams. For the 5.7 micron spheres, V_c= 13 microns/second while for the 11.9 micron spheres V_c= 7 microns/second. Three regimes of interface velocity were distinguished. For $V<V_c$, the spheres were pushed along by the front. For $V=V_c$, the spheres were gradually included in the solid phase as they were pushed along. For $V>V_c$, the spheres were encapsulated so quickly that they remained in their original positions. If such a model was applied to solidification of a CG suspension, then the first two regimes would correspond to CG particles packed into lamellar walls separating dendrites. The last regime would model the situation where CG particles remained uniformly distributed in a fine fibrillar structure. A dendritic breakdown of the otherwise planar interface occurred for conditions in which V greatly exceeded V_c.

Uhlmann, Chalmers, and Jackson[13] studied the interaction between small particles and an ice-water interface. The critical velocity for solid particles in the ice-water system exceeded the velocity (typically about 20 microns/second) at which the planar interface broke down into cells and dendrites. For comparison, the standard lowering velocities used in PNS bridge production are 16.7 and 83.5 microns/second. These nominal interface velocities are of the right order of magnitude for both dendritic breakdown and particle inclusion. Particles were observed trapped between cell boundaries, often with lines of particles between cells. The average cell dimension was 50 microns. V_c was relatively

independent of particle diameter for diameters lower than 15 microns. V_c was not correlated to the average charge on a particle. Therefore, we expect that the highly charged particles should obey this general behavior.

Cisse and Bolling[14] studied the the trapping and rejection of insoluable particles during the freezing of water. They observed that groups of particles were often carried at velocities in excess of V_c for individual particles. They observed the preferential trapping of particles between well developed dendrites, a simple geometric entrapment.

According to Doillon, etal[15], collagen fibers in the pan cast foams are composed of aggregated collagen fibrils. The fibrils range in diameter from 100 to 300 nm, forming fibers with diameters ranging from 700 to 1200 nm. These dimensions may be much smaller than the particle diameters encountered by a moving solidification front in the suspension, since the glycosaminoglycan added to make a CG suspension causes clumping of fibers.

1.6 Freeze-Drying of Frozen CG Suspension

After dendritic solidification of CG suspension, the suspension can be converted to a dry foam through the process of lyophilization (freeze-drying) from an aqueous state. During freeze-drying, ice is removed by sublimation, leaving an empty pore in the place of every ice crystal. Since freeze-dryingis a diffusion based process, the solute phase is not disrupted by the drying process[16], though a certain pore shrinkage factor may be introduced as the CG foams collapse under their own weight.

1.7 Control of Pore Diameter in CG Foams

The physical processes controlling dendrite diameter are governed by complex thermodynamic relations. Because of the nature of the freeze drying process used in CG foam production, pore diameter relates exactly to the diameter of ice dendrites formed in a solidifying CG suspension. Previous thesis research concludes that the pore diameter in CG foams can be controlled by varying three manufacturing conditions: undercooling, concentration of CG in suspension, and pH of the suspension.

The thesis work of Irving[17] focused on the effect of undercooling on the average pore width in pan cast CG foams. The results of the research are summarized in Fig. 1-6. The mean pore width in the CG foams was observed to decrease with decreasing freezing temperature. The numerical relationship between the mean pore width and the freezing temperature was roughly linear, with the values ranging from 150 microns at -50 °C to 500 microns at -10 °C. The observed pore width deviated from the calculated mean pore width by approximately +/- 20%. Pore morphology varied over the 40 degree experimental range of freezing temperature. At low temperatures, the pores were roughly circular. At high temperatures the pores were elongated.

Chen's thesis research[18] demonstrated the effect of CG concentration of the on the average pore width in pan cast CG foams. As shown in Fig. 1-7, mean pore width decreases as CG concentration increases. When plotted in semi-log coordinates, the log of mean pore width decreases linearly with increasing CG concentration. At all concentration in the range 0.5 to 1.3 % w/w, the observed pore width deviated from the calculated mean pore width by approximately +/- 10%. Although Chen did not check the effect of CG concentration in the range used for PNS bridge production, theory would extrapolate a similar logarithmic decrease in mean pore width with concentration.

The effect of suspension pH on the pore structure of pan cast CG foams was

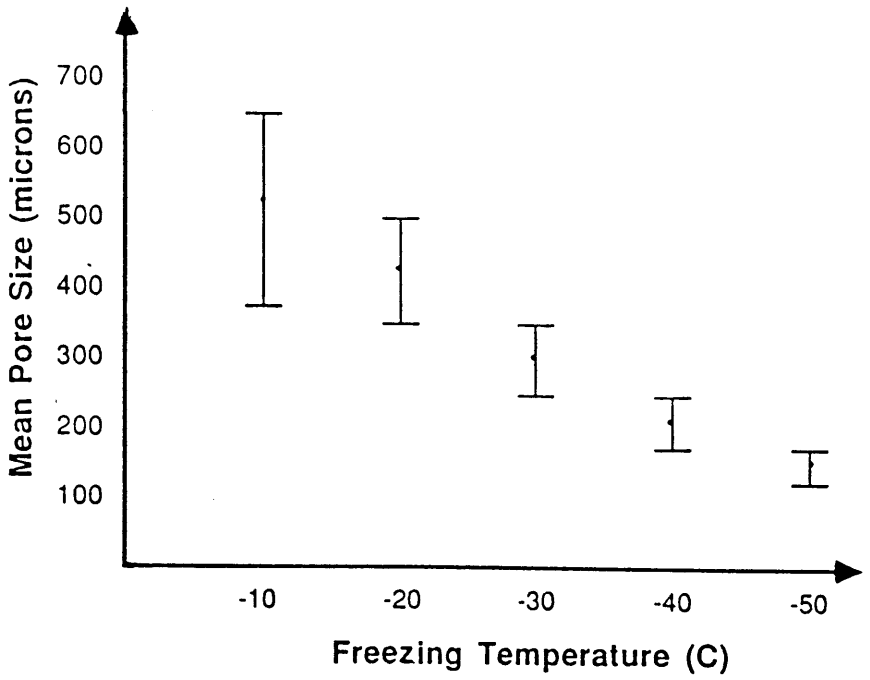

Figure 1-6: Mean Pore Width vs. Freezing Temperature (-ΔT) for CG Foams Cast in Pans: C = 0.48 %w/w, Heather Irving (1986)

examined by Doillon etal[15]. At an undercooling of 30 °C, mean pore width was varied from 44 to 110 microns by changing the pH from 2.1 to 3.5. The observed pore width showed +/- 10% deviation about the calculated mean throughout this range of pH. The effect of PH on pore width was much weaker than the effect of undercooling on pore width. By maintaining a suspension pH of 3.5 and varying the undercooling from 80 to 30 °C, the mean pore width was changed from 14 to 110 microns with a +/- 10% deviation.

An explanation for the effect of pH on pore width was offered by Doillon. As the pH decreases, collagen fibers swell and bind water. Ice crystals are small due to a shortage of free water so small pores result from freeze-drying. With an increase in pH, there is no swelling of collagen fibers, allowing an abundance of free water. Ice crystals can grow large, leading to large channel-like pores after freeze-drying.

Repeated freeze drying of preformed CG foams has been used as a means of controlling mean pore diameter[19].

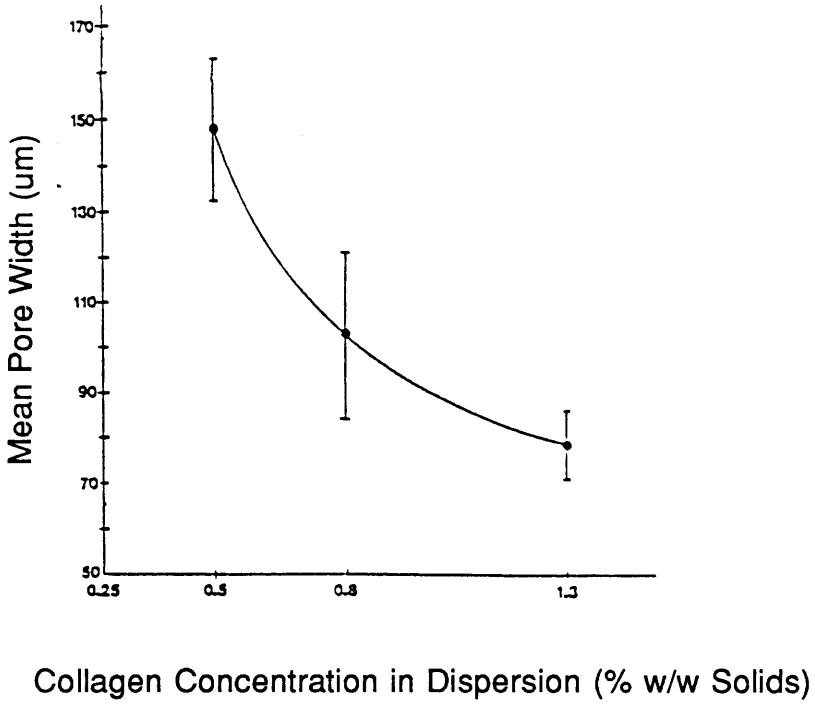

Figure 1-7: Mean Pore width vs. CG Concentration for Foams Cast in Pans: $\Delta T = 40$ to 45 °C, Elizabeth Chen (1982)

1.8 Previous Approaches to Pore Geometry Measurement

Several approaches have been used to chacterize and measure the pore geometry of CG foams. These approaches have involved both light microscopy and scanning electron microscopy (SEM) in conjunction with both manual and computerized image analysis.

Chen[18] was the first to apply the principle of quantitative stereology to the measurement of pore structure in artificial skin. She embedded CG membranes in a low viscosity epoxy medium, allowed the epoxy to harden, cut the block, and polished its surface. Chen photographed cross-sections of the membranes using a reflected light microscope. She then traced the pore structure in the photographs and scanned the tracings with an image analyzer to obtain a distribution of pore width and an index of pore orientation. Tracing was necessary because the image analyzer models pores only as ideal

closed figures, while pores in the light micrograph often do not appear closed. Chen's method was effective but very time consuming.

Wong[20] adapted Chen's technique for use with transmission light microscopy. She embedded CG foams in Epon or methacrylate, sectioned the blocks to 1-5 micron thickness, mounted the sections on slides, stained them, and photographed them with a transmission light microscope. Like Chen, Wong traced the pore structure in the photographs and scanned the tracings with an image analyzer to obtain a distribution of pore width. Mahaney[21] first applied Wong's technique to the study of pore geometry in peripheral nerve bridges.

Dagalakis[19] developed a simple but effective technique of manually measuring pore width from SEM micrographs. Irving[17] used the technique with some modifications. She prepared samples of CG foams, photographed them using SEM, and traced the pore structure. By tracing, Irving overcame the primary disadvantage of the SEM micrograph in stereological analysis: a large depth of field. She then drew a series of lines at random orientations across the tracings and measured the average distances between interceptions of lines and pore outlines. The line intercept method gives a good rough measure of pore width and does not require a closed pore structure.

Chapter 2

Theory

Although the research performed in this thesis was primarily experimental, some theoretical research was required in the design of the nerve bridge production method. In addition, theory was needed to predict pore structures produced under various untried manufacturing conditions. Because pore structure of PNS bridges is determined exclusively by the process of solidification of the aqueous CG suspension, a theoretical understanding of dendritic solidification, collagen-ice interactions, and macroscopic heat transfer processes was needed. Because of the complexity of these processes, a highly simplified model for PNS bridge freezing was considered.

Nerve bridges are produced by freezing an aqueous suspension of CG under controlled conditions. The suspension is packaged in a silicone tube surrounded by a cylindrical jacket. The device is lowered axially at constant velocity into a cooling bath maintained at uniform temperature. The manufacturing parameters subject to adjustment are the entry velocity (V), the undercooling (ΔT), and the concentration of CG in the suspension (C). Figure 2-1 illustrates a proposed transfer function relating these manufacturing parameter inputs to the bridge geometry outputs: average pore diameter (d), distribution of pore diameter (SD_d), and orientation index (OI). A primary goal of theoretical modeling is to qualitatively describe this transfer function.

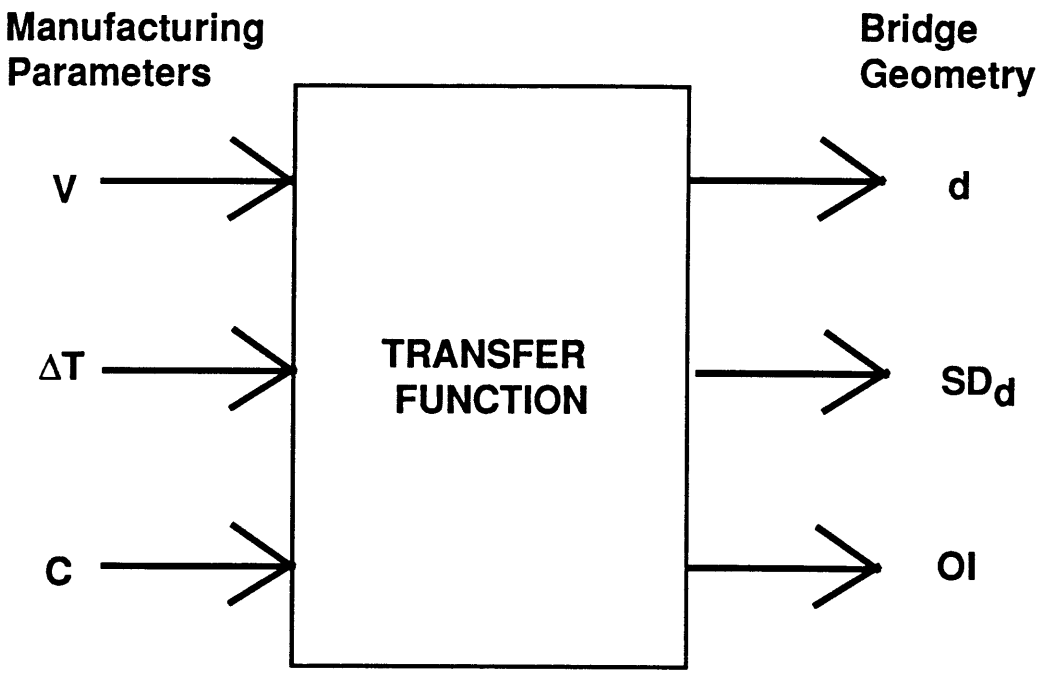

Figure 2-1: Proposed Transfer Function for PNS Bridge Production

2.1 Control of Pore Orientation

During the freezing of a PNS bridge, the bridge is lowered at a constant velocity into a well stirred cooling bath at temperature T_b. Figure 2-2 illustrates the geometry and heat transfer processes occurring at the freezing front in a PNS bridge. The constant velocity condition insures that the temperature gradients near the freezing front remain constant. Otherwise, the gradient would decrease as the ice front moved up a stationary tube and heat had to be conducted through an increasing length of frozen suspension. The bath is maintained at a constant supercooled temperature by a LN_2 cooling coil and a feedback temperature controller.

At the freezing front, heat can be transfered from the solidifying suspension in two primary directions. If the freezing front is below the bath surface, most heat leaves in the radial direction via the flux vector q_r. Heat conducts through the ice layer advancing radially inward from the tube wall, through the tube wall, and into the cooling bath. If the

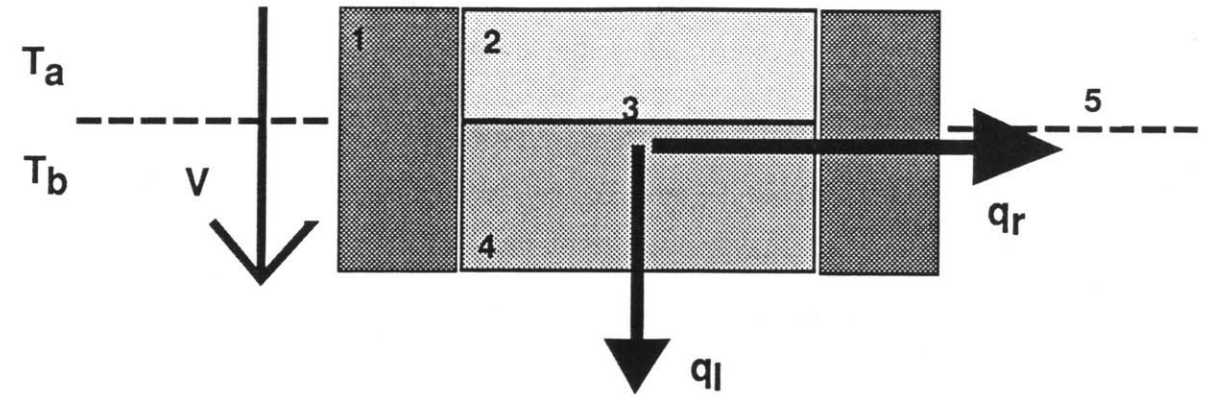

1. **PVC Tube Wall**
2. **Liquid Suspension**
3. **Freezing Front**
4. **Frozen Suspension**
5. **Bath Surface**

$$\Delta T = T_{freeze} - T_b$$

Axial Dendrite Orientation

$$q_l >> q_r$$

Slow cooling:

low ΔT

low **V**

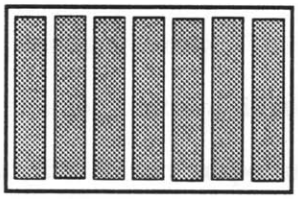

Radial Dendrite Orientation

$$q_l << q_r$$

Rapid cooling:

high ΔT

high **V**

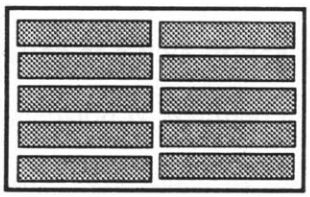

Figure 2-2: Dendritic Solidification and Heat Transfer at Freezing Front

freezing front is at (or slightly above) the bath surface, then heat leaves the front in the axial direction via the flux vector q_l. Heat conducts down through a column of frozen CG suspension and rapidly leaves the tube via radial conduction.

As illustrated in Fig. 2-2, ice dendrites grow in the direction of the dominant heat flux vector. For conditions of slow cooling (low ΔT, low V), the freezing front is near the bath surface so axial heat flux prevails and ice dendrites assume an axial orientation. If the cooling is rapid (high ΔT, high V), the freezing front is well below the bath surface. Radial heat flux prevails, leading to a strong radial orientation of ice dendrites.

2.2 Heat Transfer Modeling

A heat transfer model for solidification of the CG suspension in a PNS bridge has been developed[22]. Figure 2-3 describes the geometric and material properties used in the model. Note that there are three components of a PNS bridge during freezing. These are the CG suspension, the silicone tubing, and a PVC jacket maintaining uniform dilation of the bridge. The liquid suspension is modeled as water and the frozen suspension is modeled as ice. This is an appropriate model because the concentration of CG in the aqueous suspension is low. Because of its thickness and low thermal conductivity, the PVC jacket acts as a significant thermal resistance and thermal capacitance.

Figure 2-4 shows the geometry of inward radial solidification of a PNS bridge as it is lowered into a cooling bath. For simplicity, the liquid CG suspension is assumed to be at freezing temperature before the bridge enters the cooling bath. The quantity δ is the distance that the freezing front has moved from the wall. The bridge centerline is at δ=r. The primary heat flux vector is radial, with the PVC jacket as the limiting conductance. Two temperature differences are defined. ΔT is the difference between freezing temperature and bath temperature. ΔT^* is the difference between freezing temperature and the temperature at the inside wall of the PVC jacket. For slow cooling rates, ΔT^* is the

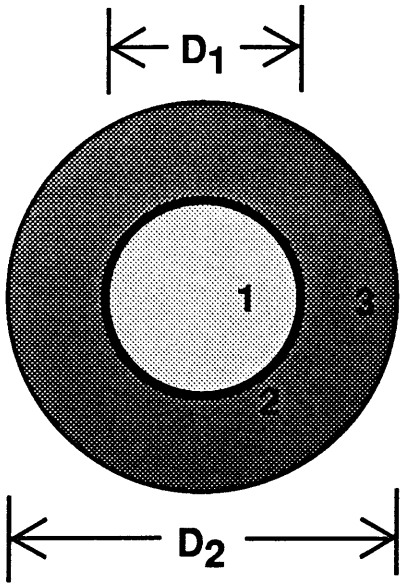

Components:

1. CG Suspension
2. Silicone tubing
3. PVC jacket

Geometry:

D_1 = 2.7 mm

D_2 = 6.4 mm

$A_1 = 5.73 \times 10^{-6}$ m^2

L = 0.127 m

Material Properties:

Liquid CG Suspension (model as water):

c_{pw} = 4205 J/kgK

ρ_w = 1000 kg/m^3

k_w = 0.58 W/mK

Frozen CG suspension (model as ice):

c_{pi} = 2100 J/kgK

ρ_i = 917 kg/m^3

k_i = 2.215 W/mK

$h_{fg} = 3.33 \times 10^5$ J/kg

PVC jacket (with silicone tubing):

k_j = 0.168 W/mK

$\alpha_j = 0.372 \times 10^{-6}$ m^2/s

Figure 2-3: Geometric and Material Properties for Heat Transfer Modeling

same as ΔT, since time of lowering is much longer than the lag time for heat conduction through the jacket. For fast cooling rates, ΔT^* is somewhat less than ΔT.

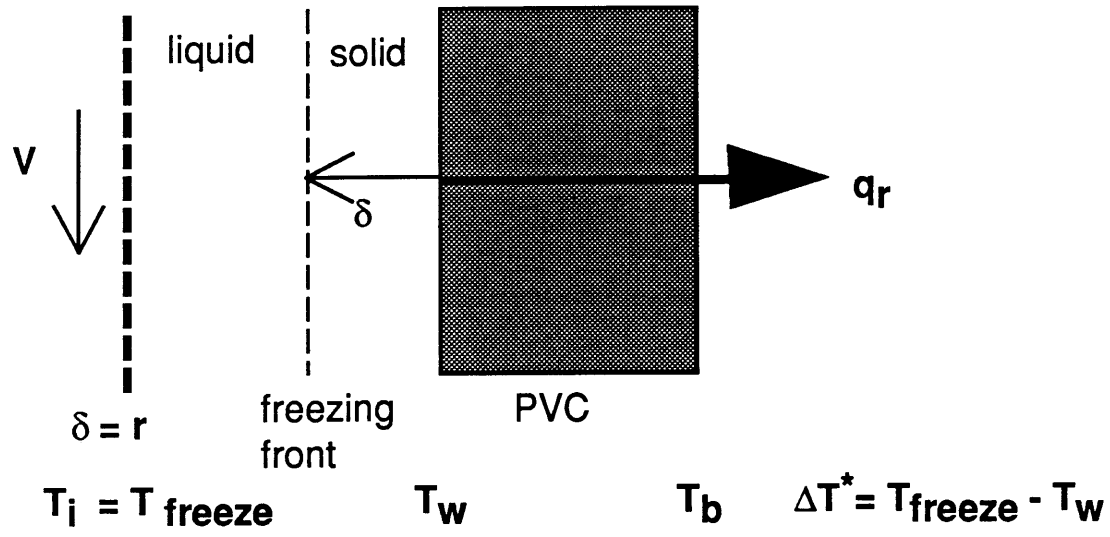

Figure 2-4: Schematic of Inward Radial Solidification of a PNS Bridge

2.3 Transient Conduction in the PVC Jacket

In order to estimate the difference between ΔT^* and ΔT for various cooling rates, it is necessary to model the transient conduction in the PVC jacket. The details of the model are shown in Fig. 2-5. Two assumptions are necessary to the model: an estimated heat transfer coefficient and uniform material properties (those of PVC) across the jacketed bridge. A Biot number of 1.04 is calculated (A). Therefore, the thin fin approximations do not apply to the nerve bridge tube during freezing. The Fourier number is developed as a linear function of entry velocity (B,C,D). Using a standard transient conduction graph[23], the difference between ΔT^* and ΔT for slow and rapid cooling was derived. For slow cooling rates, ΔT^* is indeed the same as ΔT (E). For fast cooling rates, ΔT^* is only 80% of ΔT (F).

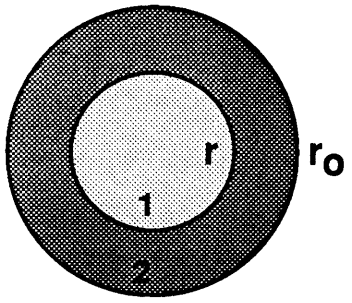

Components:
1. CG Suspension
2. PVC jacket

$h_{est} = 25\ W/m^2K$

$$\frac{r}{r_o} = \frac{D_1}{D_2} = 0.42$$

$$Bi = \frac{k_j}{h_{est} r_o} = 1.04 \qquad A$$

$$Fo = \frac{\alpha_j t}{r^2_o} = \frac{\alpha_j}{r_o V} \quad ; t \sim L/V \sim r_o/V \qquad B$$

Slow Cooling ($V = 2.0 \times 10^{-5}$ m/s): $Fo = 5.82$ C

Rapid Cooling ($V = 10^{-4}$m/s): $Fo = 1.16$ D

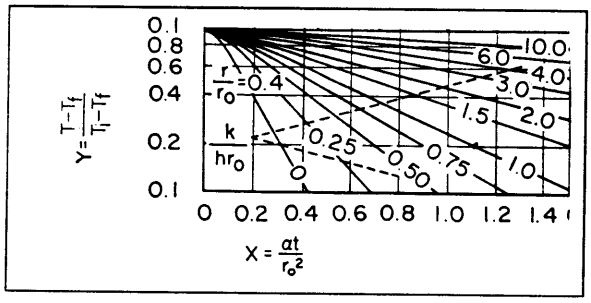

Temperature history in a circular cylinder subject to a sudden change in environmental temperature

Slow Cooling ($Y << 1$): $T_w - T_b = 0$; $\Delta T^* = \Delta T$ E

Rapid Cooling ($Y = 0.2$): $T_w - T_b = 0.2(T_i - T_b)$; $\Delta T^* = 0.8\Delta T$ F

Figure 2-5: Transient Conduction through PVC Jacket

2.4 Defining Radial Freezing Time and Freezing Front Depth

Figure 2-6 shows the derivation of a heat flux balance by applying the change of phase relation at the freezing front and the Fourier law between the ice front and the outer surface of the jacket (A). Integrating this expression (B) yields t_r, a characteristic time for radial freezing (δ=r) (C). A correction factor of 0.1 is applied to t_r to account for the increase in freezing front velocity near the bridge centerline.

We can also define a characteristic distance L below the bath surface at which the bridge freezes to the centerline. L is simply the product of T_r and V (D). As the bridge is lowered into the cooling bath, the annular freezing front grows and traces out a parabolic trajectory. The value of L is a strong function of both entry velocity and undercooling. For slow cooling it is less than 1 mm (E) and for fast cooling slightly more than 1 mm (F). Under quench conditions, L goes to infinity since the parabolic profile is reduced to a cylindrical annulus advancing toward the bridge centerline. The lower the value of L, the flatter is the shape of the freezing front and the more axial is the orientation of dendritic growth. For high values of L, the freezing front assumes a steep parabolic profile and dendrite orientation is radial. In the quench case, the orientation of dendrites is completely radial.

2.5 Mikic Number and the Effect of V and ΔT on Orientation

While the concept of characteristic freezing front depth is useful, it is much more useful to have a dimensionless number describing the effect of undercooling and entry velocity on dendrite orientation. Figure 2-7 illustrates the development of this number, the Mikic number. We must initially define a characteristic convective time for graft lowering. For simplicity this value t_c is just a function of velocity and an arbitrary length scale chosen to be the inside radius of the PVC jacket (A). The Mikic number is now defined as a ratio between the radial freezing time and the convective time (B).

Fourier Law with phase change: $q_r = \frac{k_j \Delta T^*}{\delta} = \frac{d\delta}{dt} h_{fg} \rho_w$ A

Integrate: $\frac{k_j \Delta T^* t}{\rho_w h_{fg}} = \frac{\delta^2}{2}$ B

Define a characteristic time for $\delta = r$: $t_r = \frac{\rho_w h_{fg} r^2}{10 k_j \Delta T^*}$ C

Define a distance **L** below the bath surface at which the bridge freezes to $\delta = r$: $L = t_r V$ D

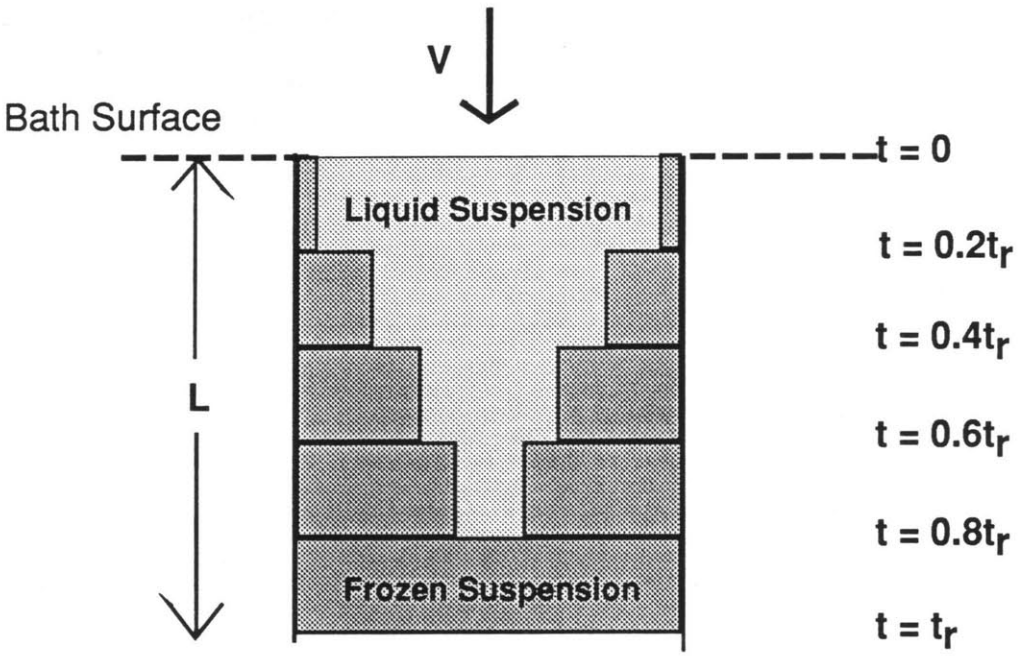

Slow Cooling (ΔT = 10 °C, **V** = 2.0 x 10^{-5} m/s): **L** = 0.89 mm E

Rapid Cooling (ΔT = 40 °C, **V** = 10^{-4} m/s): **L**=1.39 mm F

Figure 2-6: Definition of Radial Freezing Time and Freezing Front Depth

Figure 2-7 qualitatively illustrates the shape of isotherms in the freezing PNS bridge for different values of Mi. For a low Mi (slow cooling conditions), the isotherms are shallow, flat paraboli. For a high Mi (rapid cooling conditions), the isotherms are steep paraboli. The freezing front can be considered the characteristic isotherm for a given Mi. As shown in Fig. 2-7, the shape of the freezing front and therefore the orientation of dendrites may be predicted from the magnitude of Mi. Theory predicts that Mi<<1 produces strong axial orientation, while Mi>>1 produces strong radial orientation. For conditions M approximately 1, the theory cannot give a clear prediction, but intuition says M<1 should produce axial pores and Mi>=1 should lead to radial pores. Figure 2-8 summarizes the Mikic number predictions of pore orientation for typical bridge manufacturing conditions.

Define a convective time:

$$t_c = \frac{L}{V} = \frac{r}{V} \quad ; L \sim r \qquad A$$

Define a dimensionless ratio **Mi** describing the effect of **V** and ΔT on dendrite orientation:

$$Mi = \frac{t_r}{t_c} = \frac{\rho_w h_{fg} r V}{10 k_j \Delta T^*} \qquad B$$

Isotherms:

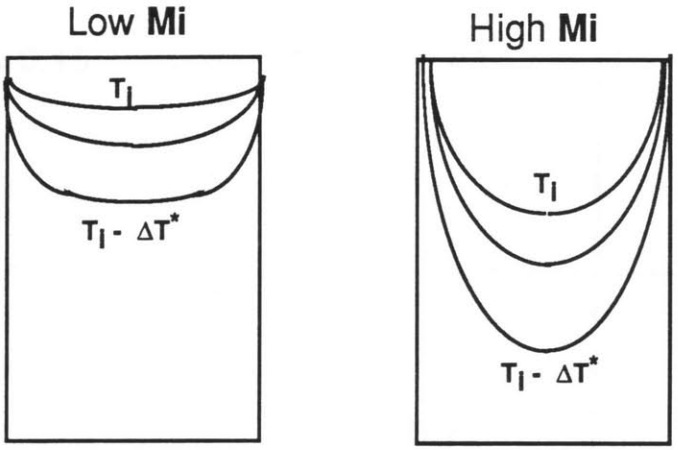

Freezing front profiles:

$Mi_1 < Mi_2 < Mi_3 < Mi_4$

$L_1 < L_2 < L_3 < L_4$

Strong Axial Orientation	Strong Radial Orientation
Mi <<1	**Mi >> 1**

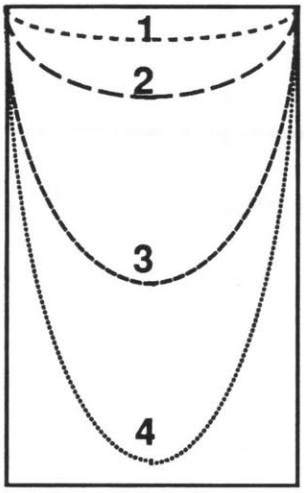

Figure 2-7: Definition of Mikic Number and its Effect on Dendrite Orientation

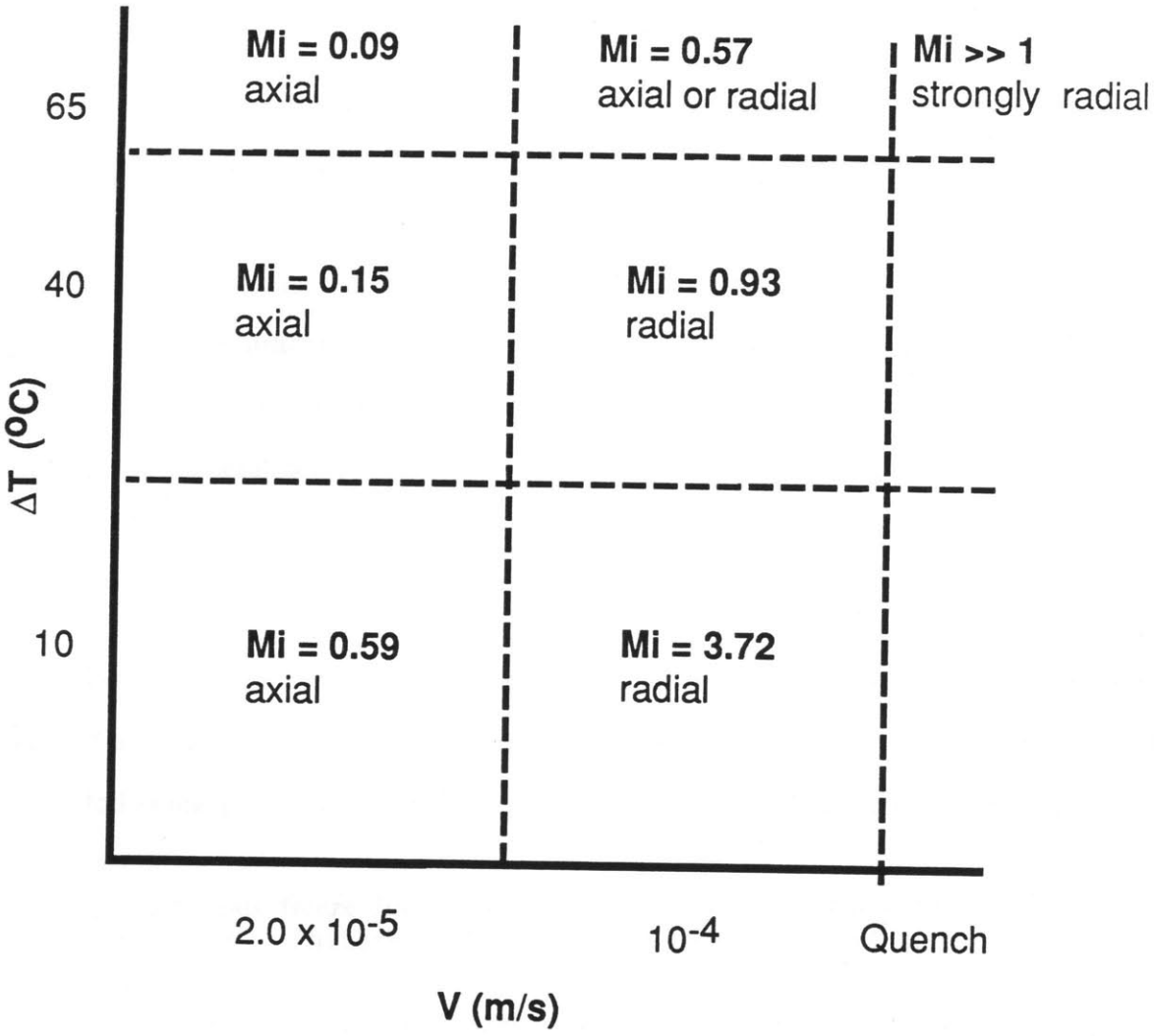

Figure 2-8: Prediction of Orientation for Typical Values of Undercooling and Entry Velocity

Chapter 3

Materials and Methods

Several techniques were developed as part of the production method for peripheral nerve bridges. A sequence of manufacturing steps was devised, including preparation of CG suspension and assembly of nerve bridge tubes . An apparatus was developed for freezing nerve bridge tubes under controlled conditions. Experiments were performed to evaluate the performance of the freezing apparatus and the effect of manufacturing conditions on pore structure. Finally, methods of SEM and light microscopy imaging and manual and computerized image analysis were developed in order to characterize the pore structure of peripheral nerve bridges.

3.1 Production of CG Suspension

The collagen-glycosaminoglycan (CG) suspension (.48 %w/w in .05 M acetic acid) is prepared according to the protocol developed by Yannas etal.[8] and outlined by Skrabut [24] the following processing steps are performed at room temperature unless otherwise noted.

1. Grind fibrous freeze-dried bovine hide collagen in a Wiley Mill (Arthur J. Thomas Co., Philadelphia, PA) with a 20 mesh screen and liquid nitrogen cooling.
2. Blend 1.65 g of collagen with 600 ml of 0.5 M acetic acid (glacial acetic acid, Mallinckrodt Chemical Co., Paris, KY) at 15000 rpm (Granco overhead blender, Granco Co., Kansas City, MO) for 1 hr at 4° C (Brinkman cooler model RC-2T, Brinkman Co., Westbury, NY).
3. Dropwise add 120 ml of 0.11 % w/v Chondroitin-6-sulfate solution (From shark cartilage: no. C-4384, Sigma Chemical Co., St. Louis, MO) to the blending collagen dispersion over 15 min at 4° C.
4. Blend 15 additional minutes at 4° C.
5. Centrifuge at 2300 rpm (1300 g) for 2 hr at 4° C (Damon centrifuge model CRU-5000, Damon International Equipment Co., Needham Heights, MA).

6. Decant 420 ml supernatant.
7. Reblend at 11,000 rpm for 15 min at 4° C.
8. Store in a capped centrifuge bottle at 4° C.

3.2 PNS Bridge Manufacturing Steps

The following steps are used in the production of peripheral nerve bridges. All steps are performed at room temperature unless noted. Please note that a nerve bridge (a PNS bridge) is a 25 mm section of silicone tubing filled with a CG foam matrix. A nerve bridge tube (PNS bridge tube) is a 125 mm length of silicone tube with CG suspension inside, fitted with a PVC jacket, ready for freezing. Figure 3-1 illustrates the components of a PNS bridge tube before freezing.

1. Dilute the .48 %w/w CG suspension to the desired concentration by adding 0.5 M acetic acid.
2. Dearate CG suspension in a 1500ml Erlenmeyer flask at -30mmHg for 10 min with agitation.
3. Prepare a PVC jacket by puncturing flexible PVC tubing (.125 in ID, .25 in OD) at 1 cm intervals with a 20 gauge hypodermic needle (Becton Dickinson model 20G1.5, Becton Dickinson Co., Rutherford, NJ), cutting off a 13 cm section, and straightening at 105° C for 2 hrs.
4. Flush silicone tubing (Dow-Corning model 602-235 medical grade Silastic, .058 in ID, .077 in OD, Dow-Corning Co., Midland, MI) with deionized water (Deionizing Organic Adsorption System, Hydro Services and Supplies, Inc., Durham, NC) and cut off an 18 cm length. Cut 2 cm from the ends of two plastic Eppendorf pipet tips (cat. no. 116, USA/Scientific Plastics, Inc., Ocala, FL).
5. Draw 10 cc of CG suspension into a 10 cc syringe (Becton Dickinson model 5604, Becton Dickinson Co., Rutherford, NJ) and expel air bubbles. Join the silicone tubing to the syringe via a Luer-lock 1.5 mm flexible tubing adaptor. Slide the PVC jacket over the silicone tubing, leaving about 3 cm of tubing extending out of the jacket. Pump suspension through the silicone tube until all air is purged.
6. Force a pipet tip into the end of the PVC jacket, clamping the end of the silicone tubing against the inside wall of the PVC jacket.
7. Slowly extrude CG suspension into the silicone tubing until the tubing swells to touch the inside wall of the PVC jacket along the entire length.

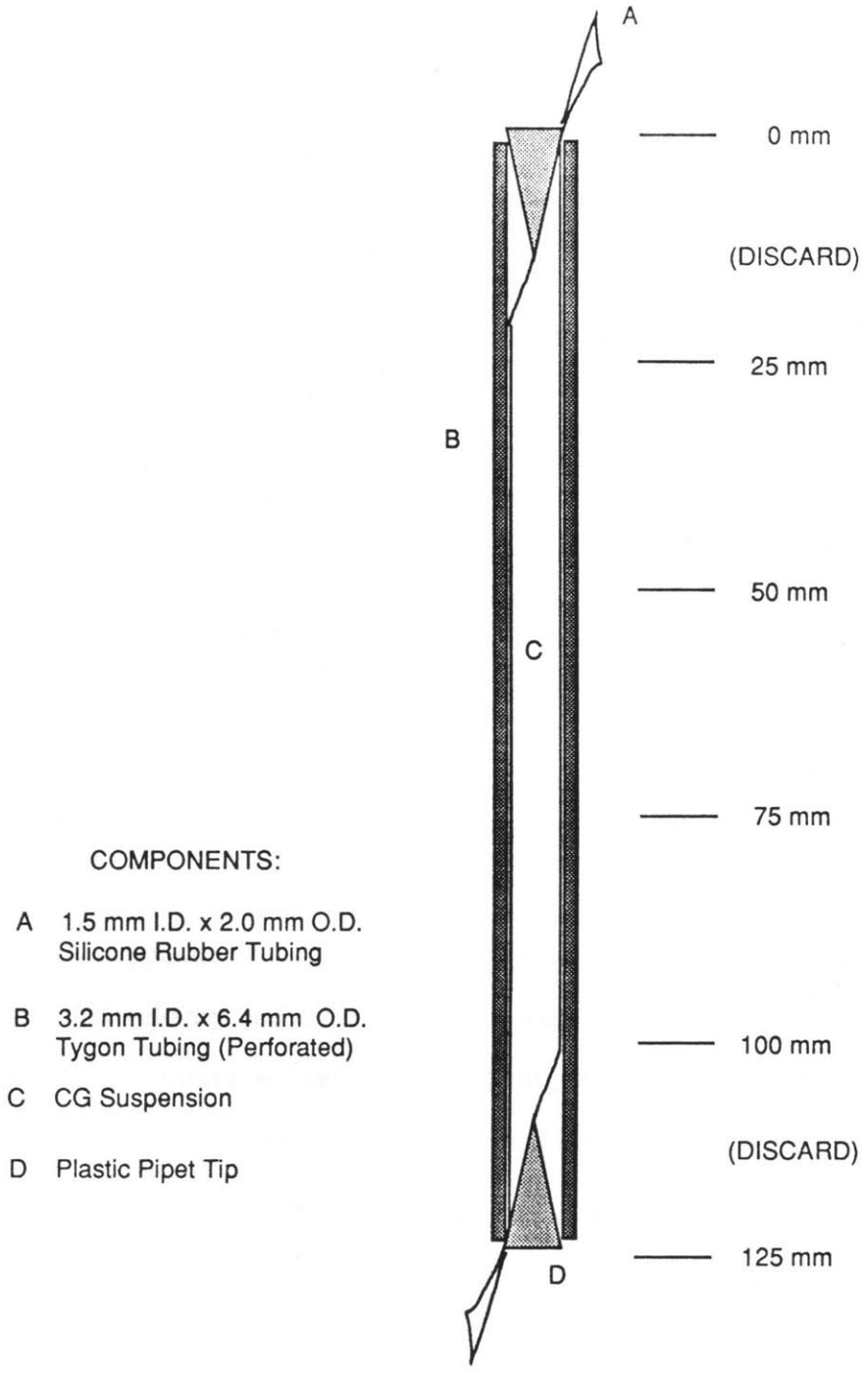

Figure 3-1: PNS Bridge Tube Before Freezing

8. While maintaining pressure on the syringe, force a pipet tip into the end of the PVC jacket closest to the syringe. This seals the CG suspension inside the jacketed silicone tubing. Trim the silicone tubing off just outside of the pipet tip clamps.
9. Using the freezing apparatus described in section 3.4, freeze the jacketed PNS bridge tube at desired lowering velocity and undercooling.
10. Section the jacketed PNS bridge tube into 25 mm lengths.
11. Freeze-dry the sections for 24 hrs (Virtis FreezeMobile 12, Virtis Inc., Gardner, NY).
12. Remove the PNS bridge from each jacket section and package it in an aluminum foil envelope.
13. Put the PNS bridges into a vacuum oven (Fisher Isotemp vacuum oven, Fisher Scientific, Medford, MA) for dehydrothermal (DHT) treatment for 24 hrs at 105° C and -30 mmHg.
14. Store the PNS bridges in a dessicator jar.
15. Just before surgery, the grafts must be trimmed and repackaged. Under sterile conditions, inspect the bridges, trim to desired length, and store in vortex tubes filled with 70% isopropanol.

3.3 Freezing Apparatus

3.3.1 Design

An apparatus has been developed to freeze nerve graft tubes under conditions of controlled velocity and undercooling. Figure 3-2 is a schematic of the apparatus which includes a uniform temperature circulating bath, a liquid nitrogen cooling system,and timing motors to lower the bridge tubes into the bath.

The insulated glass vessel consists of a glass dessicator jar of about 1.5 gallon capacity (Corning Pyrex model 3080, 200 mm ID, Corning Glass Co., Corning, NY) mounted within a 2 foot cube of hard styrofoam insulation. The insulation consists of stiff styrofoam sheet stock (12 in x 30 in x 2 in) cut to shape, stacked, and wrapped with ducttape. Within the vessel is 1.5 gallon of silicone coolant (Dow Corning 200 Fluid, 1.0 Cst., Dow Corning Corp., Midland, MI).

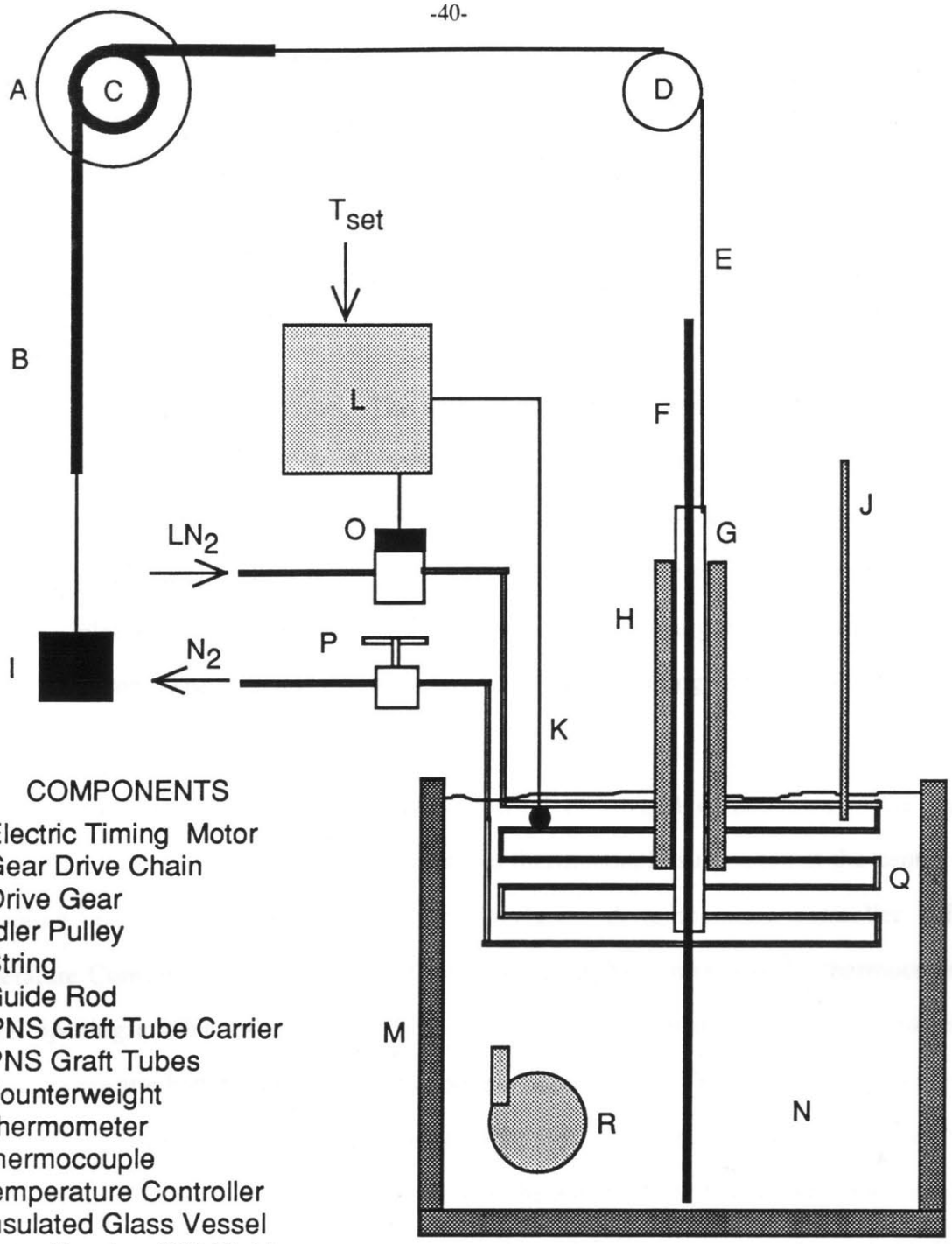

COMPONENTS

A. Electric Timing Motor
B. Gear Drive Chain
C. Drive Gear
D. Idler Pulley
E. String
F. Guide Rod
G. PNS Graft Tube Carrier
H. PNS Graft Tubes
I. Counterweight
J. Thermometer
K. Thermocouple
L. Temperature Controller
M. Insulated Glass Vessel
N. Dow -Corning 200 Fluid
O. LN_2 Solenoid Valve
P. N_2 Throttle Valve
Q. 1/4 " Copper Cooling Coil
R. Circulator

Figure 3-2: Apparatus for Freezing PNS Bridge Tubes

The vessel is capped with a .25 in thick acrylic disc. On this disc is mounted an immersion circulator (from VWR Immersion Circulator Model 1120, VWR Corp., San Francisco, CA) capable of pumping 10 l/min. The circulator consists of a 60 Hz, 115 VAC motor mounted atop the disc and a centrifugal pump hanging below the disc, supported by 8 in standoffs. A .5 in PVC tube directs the output of the pump to cause a circular flow in the vessel.

In the disc are cut three holes. The first hole is a 3 in x 4 in rectangle that provides access to the bath surface. It is through this hole that the bridge tubes, thermometer (-100/50° C model 3134, Walter H. Kessler Co., Inc.), and thermocouple enter the bath. On the two opposing sides of the rectangle are cut holes for #7 rubber stoppers. These stoppers support the inlet and outlet portions of the cooling coil, suspending the coil just below the surface of the bath. The coil is fashioned from .25 in copper tubing and has a 4 in ID and 3 in depth.

The temperature control system is comprised of several components. The bath temperature is measured by a chromel-constantan thermocouple suspended at the center of the cooling coil about .5 in below the bath surface. A temperature controller (LFE Temperature Controller model 232, LFE Corp., Waltham, MA) monitors the thermocouple voltage, opening a solenoid valve (Asco model 8262C13, Automatic Switch Co., Florham Park, NJ) when the bath temperature rises above a desired level. When the solenoid valve opens, liquid nitrogen flows into the copper cooling coil, where it accepts heat and changes phase to become nitrogen gas. A throttle valve at the outlet end of the cooling coil controls the flow rate of liquid nitrogen into the coil. The thermometer provides another measurement of the bath temperature near the surface.

The velocity control system includes several components. There are two 1/30 RPM timing motors (Cramer model 117P, Cramer Division of Conrac Co., Old Saybrook, CT). On the output shafts of these motors can be mounted various sprocket gears (Berg model

GG33S14-12, GGS14-30, and GGS14-64, Winfred M. Berg, Inc., East Rockaway, NY) to change the lowering velocity of the bridge tubes into the bath. The gear heads move 1 foot lengths of gear drive chain (Berg model 326CF-608-E). On one end of each chain is tied a 2 foot length of braided fishing line which runs over a pulley and joins to the lowering bridge tubes. On the other end of each chain is tied a counterweight. All velocity control components are attached to a chassis built from .5 in Aluminum rod, right angle clamps, and .25 in lucite sheet stock.

More than one nerve bridge tube can be lowered into the bath by each timing motor. This is accomplished by fitting a nerve bridge tube carrier to the end of each lowering string. These carriers are 6 in sections of thin walled 5/16 in ID polyethylene tube. As many as 6 nerve bridge tubes can be laid parallel to each carrier and rubber-banded at the top and bottom ends. The carriers ride into the bath on 14 in lengths of 1/8 in wooden dowel that stand vertically in the bath, held in place by test tube clamps. A 3/8 in stainless steel nut is slipped over the top end of the nerve bridge carrier to add mass to the carrier and to keep the lowering string and gear drive chain taut.

3.3.2 Manufacturing Parameters

There are three important parameters in the nerve bridge freezing process: lowering velocity (V), undercooling (ΔT), and concentration of CG in the suspension (C). There are practical and theoretical limits on the values of these parameters.

Lowering velocity ranged between 2.0×10^{-5} and 10^{-4} m/s. 2.0×10^{-5} m/s is a lower limit to avoid sedimentation of the suspension. 10^{-4} m/s is an upper limit to maintain the freezing front at or above the bath surface. Rapid quenching was used for some freezing experiments, but it did not produce uniform pore structure.

Undercooling ranged between 10 and 65 ^{o}C in the experiments. The lower limit on undercooling is 5 ^{o}C to permit freezing. The upper limit on undercooling is 70 ^{o}C because the coolant begins to solidify at this value.

CG concentration in suspension ranged between 0.12 and 0.48 %w/w in the experiments. The lower theoretical limit is 0.12 %w/w to insure a continuous CG matrix in the PNS bridge. A practical upper limit on concentration is 0.96 %w/w to permit dearation and extrusion of the suspension.

3.4 Analysis of Bridge Pore Structure

There are two goals in the analysis of PNS bridge pore structure. The first is measurement of average pore diameter from the image of a bridge cross-section. The second is quantification of pore orientation from the image of a bridge longitudinal section. Figure 3-3 describes the geometric properties of the graft to be measured.

3.4.1 Producing Light Micrographs

The first technique of pore geometry characterization used in this research is based on the work of Mahaney[21]. Because there are some important improvements in her protocol, the methods of embedding, sectioning, and photography are described in detail.

Embedding:

1. Using a surgical scalpel (#11 Bard-Parker, Division of Becton, Dickinson and Co., Rutherford, NJ), trim a 6 mm section from the center of each PNS bridge to be studied.
2. Soak the specimens in methanol for at least 1 hour to dehydrate them. During this step, gently pinch the specimens with fine forceps to remove any air bubbles trapped in the foam. This can best be done in the tray of hexagonal embedding cups (6x8 mm, model 17177A-3, Polysciences, Warrington, PA) one specimen per cup.
3. Following the protocol described in the JB-4 embedding kit (0226, Polysciences, Inc., Warrington, PA) instructions[25], prepare 100 ml of catalyzed infiltration resin. Add 100 ml Solution A and 0.90 gm catalyst C to a 1500 ml Erlenmeyer flask and mix thoroughly with a magnetic stirrer at room temperature.
4. Prepare a second tray of hexagonal embedding cups, filling them with catalyzed Solution A. Remove the specimens from the MeOH and place them one specimen per cup. Allow the specimens to soak for at least three hours.

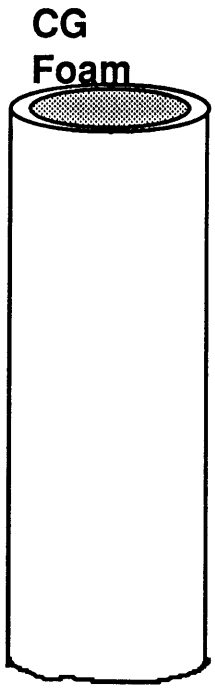

Silicone Rubber Tube
I.D. = 1.5 mm
O.D. = 2.0 mm
length = 20-25 mm

CROSS SECTION:

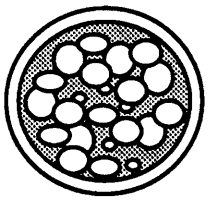

d = average pore diameter

SD_d = standard deviation in pore diameter

LONGITUDINAL SECTION:

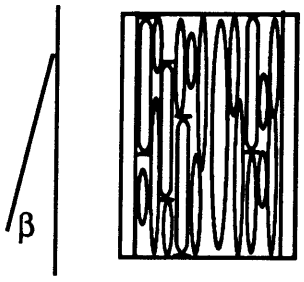

OI = orientation index

$2\cos^2\beta - 1$

Figure 3-3: PNS Bridge Geometry

5. Add exactly 1 ml of JB-4 Solution B (hardener) to 25 ml of catalyzed Solution A. Stir well and place in an ice bath.

6. Prepare a group of rectangular embedding cups (Dupont model 45460, Dupont Co., Instrument Products, Biomedical Division, Newton, CT) by pipetting them half full of activated catalyzed Solution A. Place three infiltrated specimens in each cup, arranging them in parallel orientation along the length of the cup and taking care to note the position of each. Cover the tray with a sheet of Saran wrap and allow the embedded specimens to cure for 24 hours.

7. Remove the resin blocks from the embedding cups and cut them into three separate rectangular pieces, each containing a specimen. The pieces should be 5 mm long and have a 2.5 mm square face. Prepare a tray of hexagonal embedding cups by placing one pre-embedded specimen in each cup. The specimens should stand vertically in the cups.

8. Repeat step 5. Prepare a labelled JB-4 block holder (15899, Polysciences Inc., Warrington, PA) for each specimen. Pipett enough activated catalyzed Solution A into each cup that the upper flat bottom of each cup is just covered with solution. Place the appropriate block holder face down into each cup. Allow the specimens to cure for 24 hours.

9. Remove the embedded, mounted specimens from the cups and store them in a dessicator.

Sectioning and Staining:

1. Place the specimens in a 105° C oven (Fisher Isotemp vacuum oven, Fisher Scientific, Medford, MA) for 15 minutes to harden the methacrylate resin before sectioning.

2. Prepare glass blades for the JB-4 microtome using glass bar stock and a knifemaker (LKB 7800 Knifemaker, LKB Co., Bromma, Sweden). The bars should be washed with glassware cleanser, thoroughly rinsed in distilled water, and air dried before breaking. The bars should be handled only with plastic gloves or with a wrapping of lens paper. Fit a plastic boat onto each blade, taking care not to handle the sharp edge of the blades.

3. Mount a specimen into the chuck of the microtome (Sorvall Microtome model JB-4, Dupont Co. Instrument Products Biomedical Division, Newtown, CT). Using a razor blade, shave the face of the block so that the end of the specimen is just exposed. Trim the face of the block, leaving a 1mm square around the specimen with four facets sloping away from the face at a 20° angle to the face.

4. Fit a blade into the microtome, mounting it at an angle of 4 ° and taking care that the sharp edge of the blade is even with the top of the indicator bar.

5. Prepare a boat solution of 1-2 drops of concentrated NH_4OH in 50 ml of distilled water. Fill the blade boat so that the sharp edge is just wetted. The block and the backface of the knife must remain dry.

6. Set the microtome to cut 3 micron sections. Align the knife so that its left side is nearly in contact with the block. Begin cutting until an intact cross-section of the specimen is sectioned and left floating on the surface of the boat bath. (While cutting, periodically trim the face of the block to expose a 1 mm square around the end of the specimen. After every 10 sections, replace the glass blade. Blades should not be stored more than a fre use.)
7. Wash a glass microscope slide with ethyl alcohol and dry it with a lint-free tissue. Add a drop of distilled water to the center of the slide. Using a wooden applicator stick with an eyelash wax-glued to its end, carefully transfer the section from the boat to the slide.
8. Dry the slide on a hot plate at 60° C for 1 minute.
9. Add a drop of 0.1 % Toluidine Blue to the specimen. After waiting for 1 minute, wash it off with distilled water. Allow the slide to dry on the hotplate.
10. Add a drop of Permamount (SO-P-15, Fisher Scientific Co., Fair Lawn, NJ) to one side of the specimen. Gently place the edge of a #1 coverslip on the slide just outside of the Permamount drop. The Permamount will distribute itself evenly as the coverslip goes down.
11. Examine the specimen using the Wild Stereomicroscope Model M5 (Wild Heerbrugg Ltd., Heerbrugg, Switzerland) at 50x magnification to determine whether the specimen is intact.

Photography:

The specimens were photographed using the Wild Stereomicroscope and an Olypmus OM-2 35 mm SLR camera (Tokyo, Japan) set to auto exposure. Kodacolor 400 print film (Eastman Kodak, Rochester, NY) was used and a medium green filter was placed atop the slide coverslip to enhance contrast.

The process above was developed for examination of PNS bridge cross-sections. To examine longitudinal sections, the process is identical except for the orientation of the bridge specimen with respect to the embedding block.

3.4.2 Producing SEM Micrographs

The SEM can be used to image the pore geometry of PNS bridges. SEM is much faster than embedding and sectioning for producing micrographs of the bridges. It requires less sample preparation and produces images of good quality. The SEM used in this

research was an ISI Scanning Electron Microscope Model DS-130 (International Scientific Instruments, Inc., Santa Clara, CA).

Sample Preparation:

1. Prepare an SEM specimen mounting stub by cleaning it and applying a double sided adhesive pad to its top surface.
2. Prepare a small bath of liquid nitrogen. Quench the PNS bridge to be examined and a #11 surgical scalpel.
3. Using the cold blade, cut a 4 mm section from the middle of the PNS bridge. Place the specimen on end atop the stub.
4. Using an applicator stick, brush silver conducting paint (1481, Ernest F. Fullam, Inc., Schenectady, NY) down the length of the specimen in two diametrically opposed stripes. Brush paint from the base of the specimen across the pad to the edge of the stub surface.
5. Using an SEM Coating Unit E5100 (Polaron Instruments Inc., Doyleston, PA), sputter coat a 150 to 200 A layer of gold over the specimen.
6. Store the coated specimens in a dessicator until ready to view them.

SEM Imaging:

The SEM micrographs were recorded on Polaroid Type 55 film (Cambridge, MA) under the following conditions: Voltage 20KV, working distance 25 mm, magnification 90x, contrast 70% of range, brightness 50% of range, SEI imaging, photo speed 2, f-stop 4.5. The images were made to be as two-dimensional as possible, highlighting the cut edges of the matrix and eliminating as much of the background detail as possible.

The method of producing SEM micrographs can be applied directly to examination of longitudinal sections. SEM magnification should be reduced to 50x.

3.4.3 Analysis of Micrographs Using Line Intercept Method

The simplest method of measuring the average pore diameter in PNS bridge cross-sections is the line intercept method. This method is described in the thesis of Irving[17] but is presented here for completeness.

The mean pore diameter of a CG matrix, or linear intercept diameter (d), can be defined by the following expression:

$$d = \frac{\sum_{i=1}^{N} l_i}{N}$$

where l_i represents the chord of a given pore opening i as it occurs along a given reference line and N represents total number of intersections between the reference line and the pore-matrix boundaries. For each micrograph, measurements were made along five lines rotated at random angles through one reference point, as shown in Fig. 3-4. The values from each reference line were averaged to determine a mean pore diameter (d) for each cross-sectional micrograph.

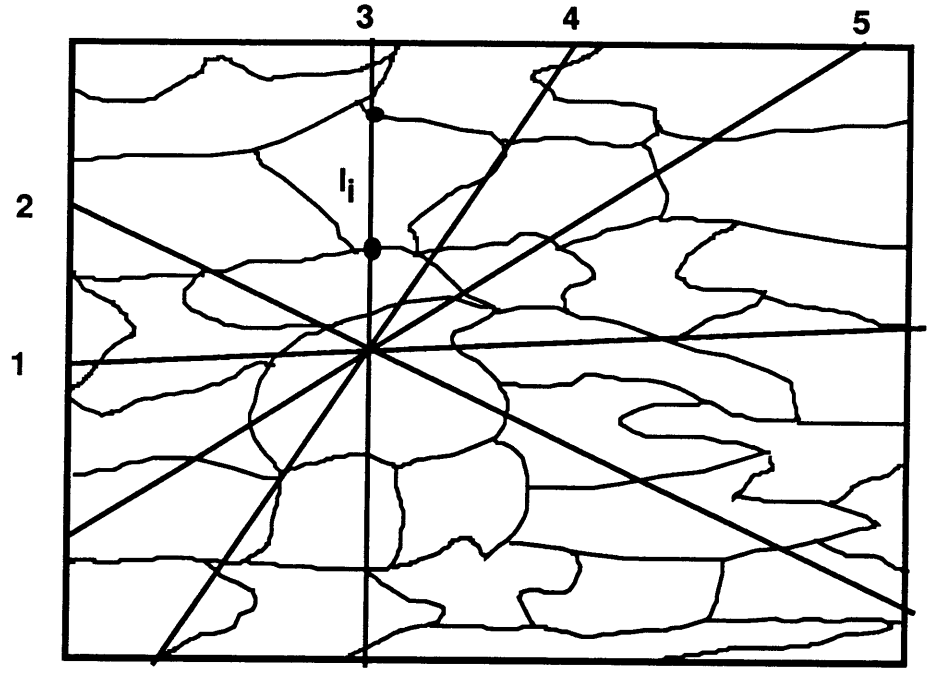

Figure 3-4: Stereological Method of Micrograph Analysis, Irving (1986)

3.4.4 Analysis of Micrographs Using Line Computer Image Analyzer

The use of the computer image analyzer in this research closely follows the protocol described by Wong[20] and Mahaney[21]. The image analysis system used in this research is the Magiscan II Image Analyzer (Joyce Loebl, Tyne and Wear, England). The system uses

an Apple II computer architecture and supports PASCAL programs for data analysis. A video camera (Bosch TYK9A, Robert Bosch Co., West Germany) provides a video input to the Magiscan. The Magiscan manual[26] discusses the features of the system in detail.

The following steps were followed:

1. Boot the Magiscan by inserting the "Boot" diskette in drive 4. When the system is booted, replace the "Boot" diskette with the "System" diskette. In drive 5 place the "Menu" diskette.

2. When the CR key is pressed, the operating system will load and the command line will be displayed. To execute Menu, type X for execute and respond to "Execute what file?" with "menu:menu". The four main operations in Menu are Environment, Program, Xecute, and Results.

3. Choose Environment. Select Set Calibration.

4. Fit a 10 mm extension tube between the video camera and lens. Move the camera to the upper limit of its track. Place the micrograph under the glass plate on the copy stand and turn on the reflective lighting to a dim level. With the aperture fully open, focus the lens, adjusting the zoom so that the image of the PNS bridge cross-section nearly fills the field. Make sure that the micrograph length scale appears in the field. Slowly close the lens aperture and turn up the lighting intensity until a clear image appears on the screen.

5. Hit the spacebar to send a digitized image to the Magiscan. Calibrate the image by entering the desired units (microns), entering the length of the length scale in microns, and marking the ends of the length scale with the light pen. When calibrating a light microscope image, use the 1500 micron dimension across the inside diameter of the silicone tube as a length scale.

6. Choose Quit to return to Menu and select Program. In this submenu, operations for image enhancement and measurement may be selected. For an SEM micrograph, the following settings were used: Video input table- linear, 0 to 63; Segmentation- 0 to 16; Editor-on; Measurements- length, breadth, orientation. For a light micrograph, the following settings were used: Video input table- linear, 35 to 63; Segmentation- 35 to 63, adaptive; Editor-on; Measurements- length, breadth, orientation. Figure 3-5 defines the measurements made . These settings should be adjusted to provide the best contrast between pores and pore walls, with the pores appearing white. Using the Program Management option, programmed settings may be saved on the System disk and loaded again as needed. Note that calibration is saved in the program, so programs should be loaded first and then the calibration should be set in the Environment submenu.

7. Choose Quit to return to Menu and select Xecute. The Magiscan is now ready to analyze an image using the operations selected in the Program submenu. Hit the spacebar to send a digitized image to the Magiscan. The Magiscan will run the programs to enhance the image and the modified image will appear on the screen. The Editor command line will appear on the top of the screen with the options Draw, Erase, Reject, Accept, Cancel, and Quit.

8. By choosing various commands and by using the lightpen to specify regions on the image, the operator can edit the image before the Magiscan takes its measurements. Artifacts in the image may be removed using Draw. Pore structure can be closed using Erase. Regions of the image may be included or excluded from the measurements by using Accept and Reject. When editing is complete, choose Quit.

9. The Magiscan will now take measurements on every closed white region. To see the statistical results of the measurements, choose Statistics. To obtain a hardcopy of the statistics, choose Hardcopy.

10. Choose Quit to return to Menu and select Results. The data from the measurements may be displayed and printed in the form of histograms, three-dimensional plots, or in a table.

11. The listing of measurements from a program execution is automatically stored on the System diskette in the file "datafl.dat". In order to save this data permanently on another disk, choose Quit to return to Menu. Choose Quit again to exit Menu and then type "F" to use Filer to move the files to another disk.

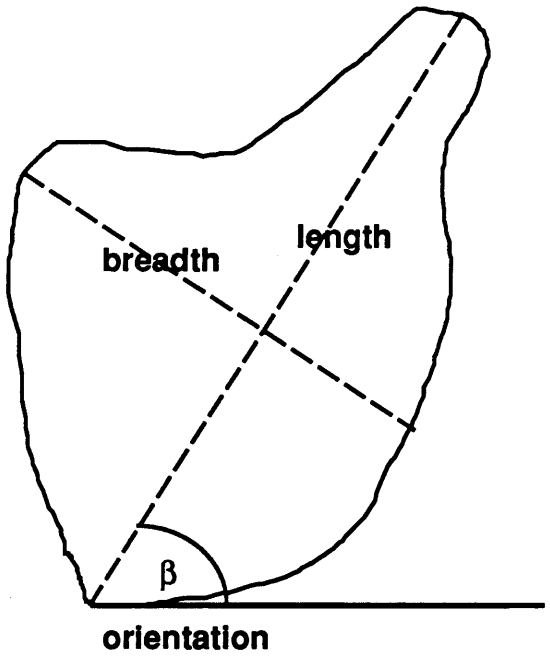

Figure 3-5: Pore Measurements Performed by Magiscan

3.4.5 Reduction of Image Analyzer Data

Data files produced by the Magiscan include a length, breadth, and orientation measurement for each closed bright region in a image. The Statistics option at the end of the Xecute operation reduces this datafile to a maximum, minimum, mean, and standard deviation for each of the three measurements.

To calculate a mean and standard deviation of pore diameter across a batch of nerve bridge tubes, two methods were considered. The first was a PASCAL program by Mahaney[21] that can calculate the mean and standard deviation of measurements stored across as many as 20 datafiles. The second was simply to calculate an average mean, an average standard deviation, and a standard deviation of means based on the results of Statistics for each datafile. The first method in theory gives the most useful results, but was abandoned because the program could not handle datafiles of more than 200 lines (i.e. images of more than 200 pores). The second method was therefore used, implemented on a programmable calculator (HP-33C, Hewlett-Packard Co., Singapore).

The final images analyzed by the Magiscan had numerous artifacts introduced during image enhancement. Most of these artifacts were 1 or 2 pixel white spots, though there were some very large artifacts resulting from nonclosure of pores in the image. Therefore, the data from pore diameter analysis was polluted by very small (less than 10 microns) and very large (greater than 100 micron) pore measurements. The net effect of artifacts was a reduction in the calculated mean pore diameter and a very large (approximately equal to the mean) calculated standard deviation.

There were two possible solutions to the problem of image artifacts. First, a computer program could have been written to filter each data file of any pore measurements less than a certain (say 10 micron) pore measurement. The standard Magiscan statistics program could then be run on the filtered datafile. The second choice was to establish a

theoretical and experimental correlation to convert statistics calculated on polluted datafiles to true values[27]. This could be accomplished by performing Magiscan measurement of a few typical images (small pores, large pores, SEM micrograph, light micrograph), manually filtering the datafile, and calculating the true pore diameter statistics. A simple multiplier could be found to relate the true and polluted mean pore diameter for each general type of image. The percent standard deviation in pore diameter found for each trial image could be considered a standard for its class of image. Since the original datafiles were lost, the latter method of correcting for image artifacts was used. Complete details are given in the Appendix A.

3.5 Apparatus Performance Evaluation

The final design of the the PNS bridge freezing apparatus was reached through a series of three design iterations. Changes in the design included silicone oil rather than propylene glycol coolant, automatic rather than manual temperature control, and a circulating rather than non-circulating bath. The first criterion for a satisfactory apparatus design was uniformity of pore structure within bridges. The second criterion was repeatability of pore structure among bridges produced under the same manufacturing conditions but in different batches. Uniformity and repeatability in pore structure is a function of both the degree of control over the manufacturing parameters and the sensitivity of the the manufacturing process to small variations in these parameters. Mahaney [21] evaluated the uniformity and repeatability of PNS bridges produced under an early design of the freezing apparatus.

The configuration of the freezing apparatus was chosen to insure repeatability and uniformity of bridge pore structure. Manufacturing parameters should vary little during a batch run or from batch to batch. Concentration of CG in suspension should be repeatable as long as sound laboratory technique is observed. The freezing temperature should be

repeatable due to the feedback control incorporated into the freezing apparatus. However, because of the controller design, there are oscillations in freezing bath temperature (1° C above and below the setpoint). In addition, the region above the bath is not insulated from the environment, so changes in the ambient temperature could affect the temperature difference across the bath surface. Finally, the entry velocity of bridge tubes into the bath should not be subject to error since timing motors and slipless chain drives are used. Motor loads are are well within accurate operating range.

Two experiments were designed to test for uniformity and repeatability of pore structure. The uniformity study was performed first in order to justify a single specimen per bridge sampling for the repeatability experiment.

3.5.1 Uniformity Experiment

In the uniformity experiment, four nerve graft tubes were produced under each of six unique manufacturing conditions. Table 3-1 describes these manufacturing conditions. At three points along the length of each bridge tube (l=37,63, and 87 mm as shown in Fig. 3-1), a cross section and a longitudinal section were taken. A light micrograph and a SEM micrograph were made from each cross section. From these micrographs, two different calculations of average pore diameter were made using an image analyzer. In addition, a third calculation of average pore diameter was performed on the light micrographs using the intercept method. Longitudinal sections were subject to a less rigorous visual inspection in order to judge uniformity of pore orientation.

3.5.2 Repeatability Experiment

The object of the repeatability experiment was to to determine whether a given set of manufacturing conditions would yield the same bridge pore structure from batch to batch. Table 3-2 describes a study to determine the variation in bridge pore structure for six cases across three days of production. A batch is a group of three nerve bridge tubes frozen

Table 3-1: Six Cases for Uniformity Experiment

Case	V (m/s)	ΔT (°C)	C (w/w %)	Description
1	$2.0x10^{-5}$	10	0.27	small ΔT, low V
2	$2.0x10^{-5}$	40	0.27	large ΔT, low V
3	10^{-4}	10	0.27	small ΔT, high V
4	$2.0x10^{-5}$	10	0.12	case 1, low C
5	$2.0x10^{-5}$	10	0.48	case 1, high C
6	10^{-4}	40	0.27	large ΔT, high V

simultaneously. Since intrabridge uniformity of pore structure was proven by the uniformity experiment, a sampling of one cross section and one longitudinal section from l=63 mm on each tube was considered sufficient for the repeatability study.

3.6 Transfer Function Experiment

Once the production technique is proven reliable and able to produce bridges that are both uniform and repeatable, then the relationship between manufacturing parameters and graft geometry may be established. These experiments should develop the transfer function for PNS bridge production proposed in Chapter 2.

The data for the transfer function experiment may be taken from results obtained in the uniformity and repeatability experiments. These data bracket the range of manufacturing conditions available. In order to gain a clearer picture of the functions d=f(V,ΔT, C) and OI=g(V,ΔT,C) intermediate manufacturing conditions could have been checked.

Table 3-2: Layout of Repeatability Study

Day	ΔT (°C)	Batches
1	10	1st case 1
		1st case 3
		1st case 4
		1st case 5
2	10	2nd case 1
		2nd case 3
		2nd case 4
		2nd case 5
3	10	3rd case 1
		3rd case 3
		3rd case 4
		3rd case 5
4	40	1st case 2
		1st case 6
5	40	2nd case 2
		2nd case 6
6	40	3rd case 2
		3rd case 6

3.7 CG Freezing Study

In order to understand the mechanism of freezing of CG suspensions, a brief study was conducted using a cryomicroscope. The primary objective was to establish a correlation between dendrite width in freezing study specimens and average pore diameter in PNS bridges produced under similar cooling rates.

In this study, a cryomicroscope system[28, 29] was used to produce images of CG suspension at three concentrations solidifying at two different cooling rates. As shown in

3-6, the system consists of an inverted microscope, freezing stage, computer, and VCR. The freezing process was recorded on videotape. From the videotape, the advancement of the freezing front and the growth of ice dendrites were observed. From these observations, the interface velocity and average dendrite width were measured.

The three concentrations were 0.12 %w/w, 0.27 %w/w, and 0.48 %w/w. The two cooling rates were 4 ^{o}C/min and 20 ^{o}C/min. In each round, the suspension was cooled from 20 to -1 ^{o}C. Each of the 6 rounds were repeated twice, first under a magnification of 40x to observe the growth of dendrites and second at 2.5x to observe the advancement of the freezing front. The substage was maintained at -20 ^{o}C during the experiments.

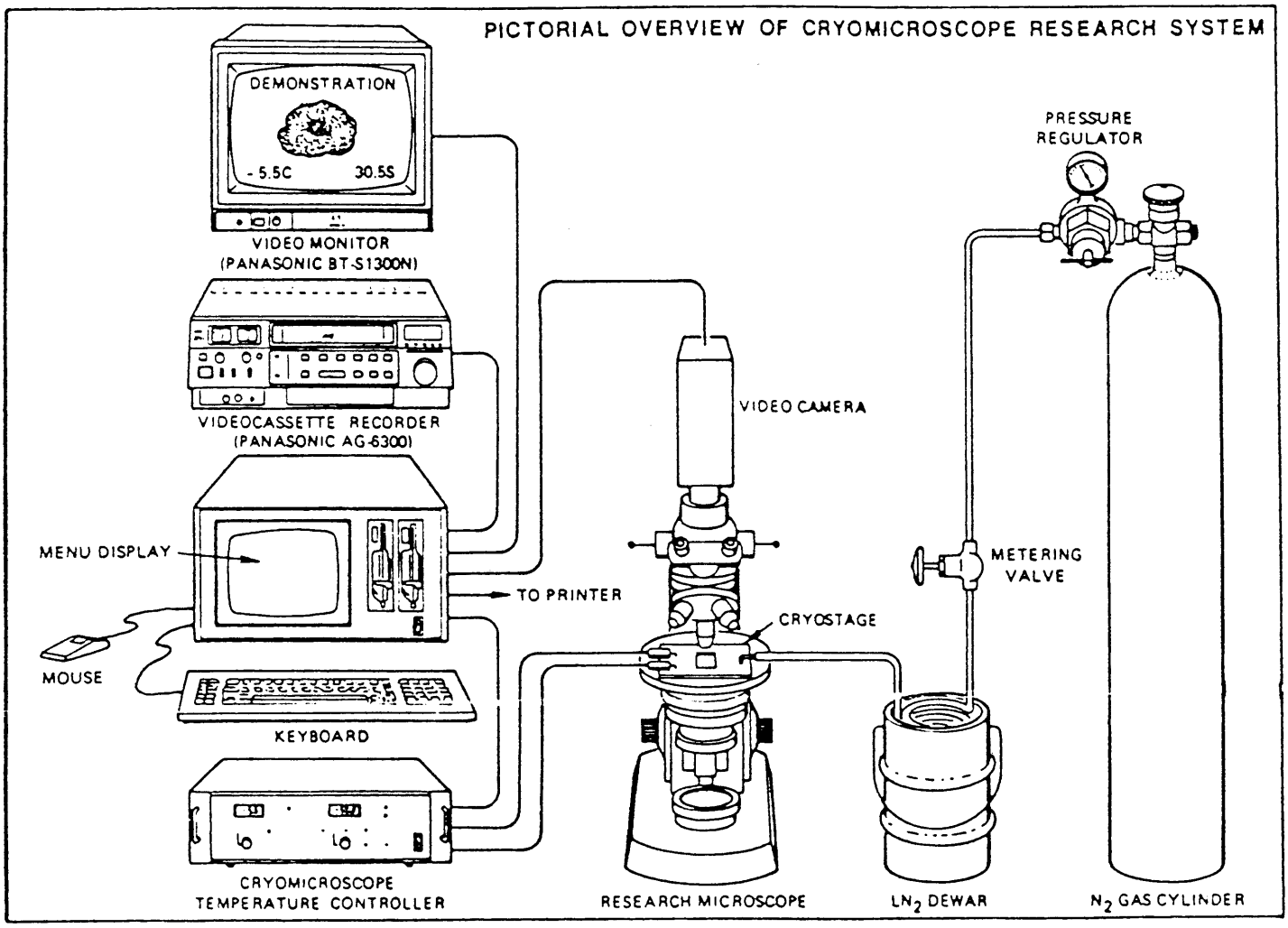

Figure 3-6: Cryomicroscope System Used for CG Freezing Study

Chapter 4

Results and Discussion

The experimental results of this research illuminate four separate issues.

The first is the quality of performance of the freezing apparatus. The two performance criteria employed were uniformity of pore structure within an individual bridge and repeatability of bridge pore structure from one batch of bridges to another.

The second issue addressed by the experiments is the qualitative transfer function relating bridge manufacturing parameters to bridge pore geometry. The three manufacturing parameters considered were entry velocity, undercooling, and concentration of CG in suspension. Their effects on average pore diameter, distribution of pore diameter, and orientation were considered. The predictions of these relations based on data from previous studies and on theoretical modeling are compared to experimentally derived relations.

Third, the differences among the results of three techniques for measurement of bridge pore geometry are discussed. These methods are computerized image analysis of SEM micrographs, computerized image analysis of embedding/sectioned (E/S) light micrographs, and manual image analysis of SEM images using the line intercept method. The efficiency and ease of use of these methods is considered.

Finally, the results of a brief cryomicroscope study are discussed. This study elucidates the process of solidification of CG suspensions.

4.1 Performance Evaluation

4.1.1 Uniformity

The results of the uniformity experiment show that there is no statistically significant difference in d along the length of bridges produced with the PNS bridge freezing apparatus. There is a large value of SD_d for all specimens analyzed, of the same order as d. This fact results from the nature of the CG foam matrix, as well as the process of image enhancement used in the pore diameter analysis

At conditions of slow cooling, (case 1: V= 2.0×10^{-5} m/s, ΔT=10 °C, C=0.27 %w/w) bridge pore structure remains very uniform along the length of the bridge. Figure 4-1 shows SEM micrographs of three cross sections taken along the length of a case 1 bridge. Figure 4-2 shows light micrographs of three E/S specimen cross sections taken along the length of the same case 1 bridge.

At conditions of rapid cooling, (case 6: V=10^{-4} m/s, ΔT=40 °C, C=0.27 %w/w) bridge pore structure remains very uniform along the length of the bridge. Figure 4-3 shows SEM micrographs of three cross sections taken along the length of a case 6 bridge. Figure 4-4 shows light micrographs of three E/S specimen cross sections taken along the length of the same case 6 bridge. Note that the resolution of the E/S is too coarse to adequately show the fine pore structure of a case 6 bridge. For this reason, light micrographs of E/S specimens were not used in the analysis of case 6 bridges.

Figure 4-5 summarizes the results of the uniformity experiment for cases 1-6. The results of the uniformity experiment show that there is no statistically significant difference in d along the length of bridges produced with the PNS bridge freezing apparatus. There is no statistically significant difference between the value of d calculated from SEM and E/S images. The value of SD_d calculated from both SEM and E/S images is 72% of d.

In the uniformity experiment, a few longitudinal sections were collected along the

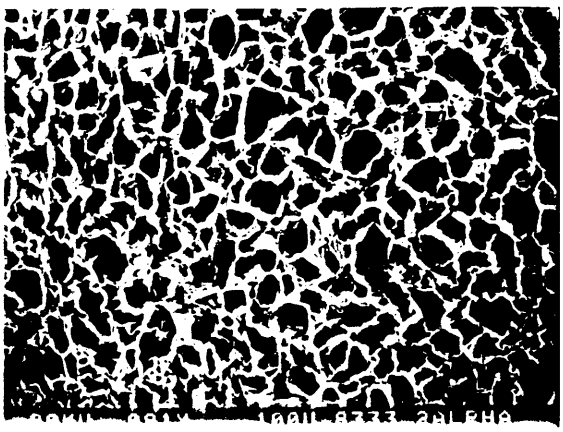

L= 37 MM

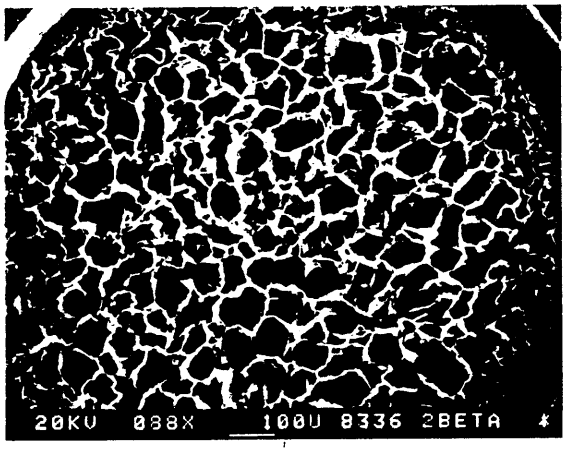

L= 63 MM

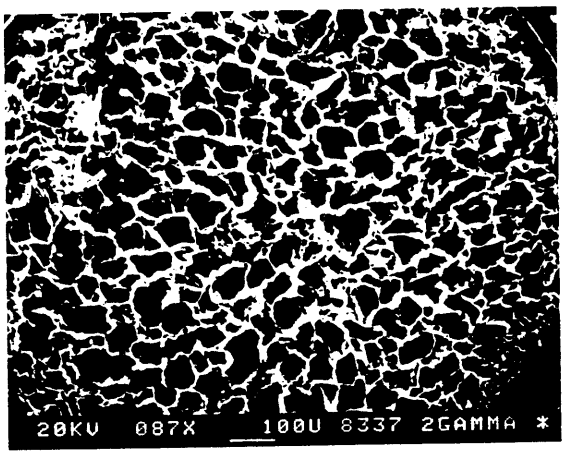

L= 87 MM

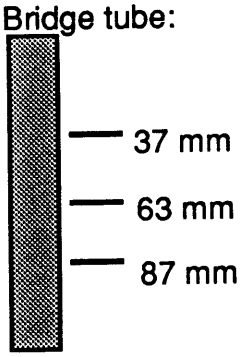

Figure 4-1: Uniformity of Pore Diameter, SEM Micrographs, Case 1

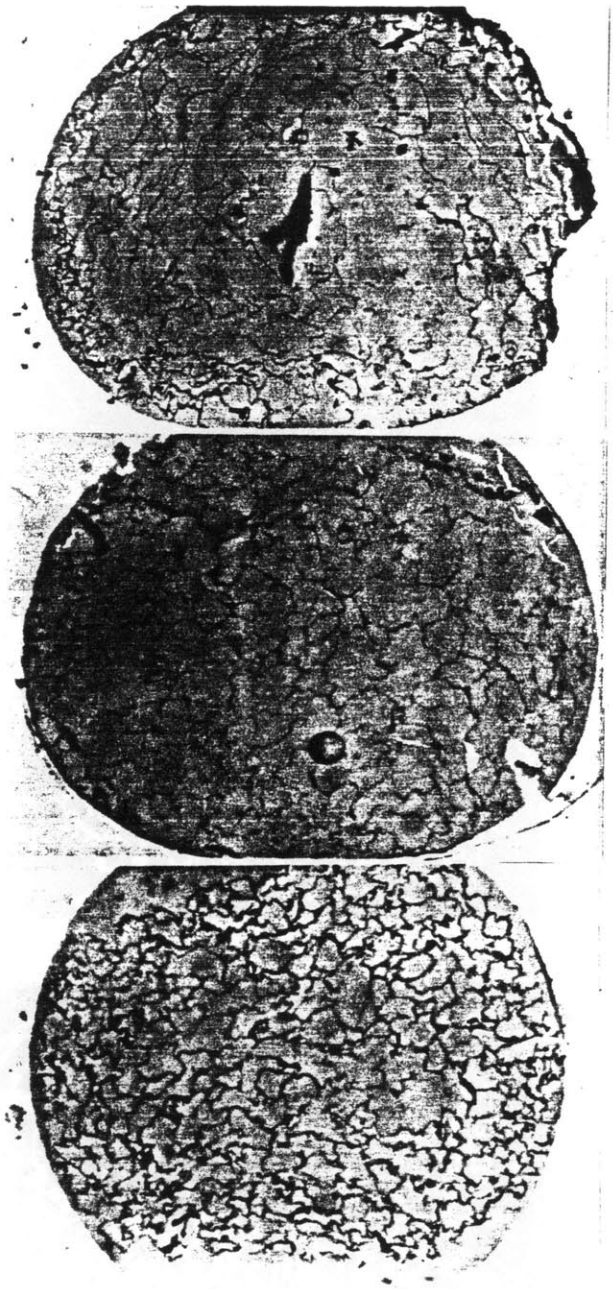

Figure 4-2: Uniformity of Pore Diameter, Light Micrographs of E/S Spec., Case 1

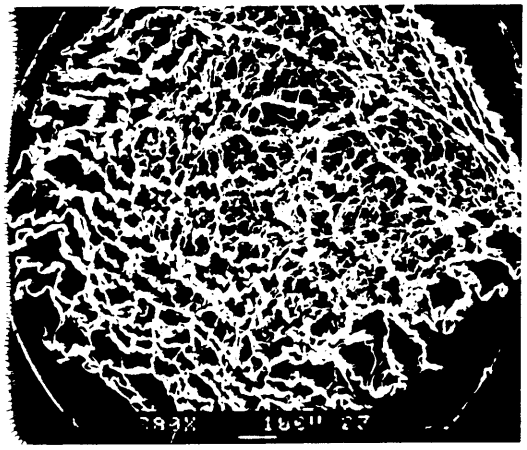

L= 37 MM

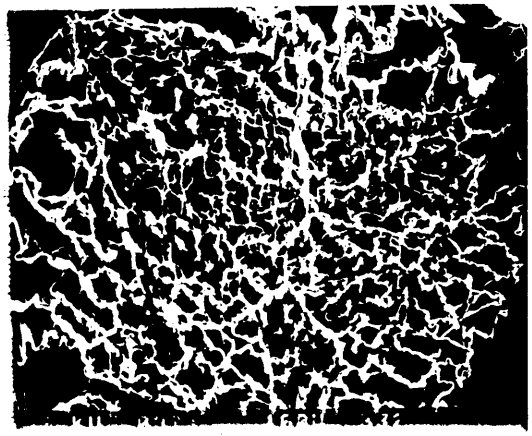

L= 63 MM

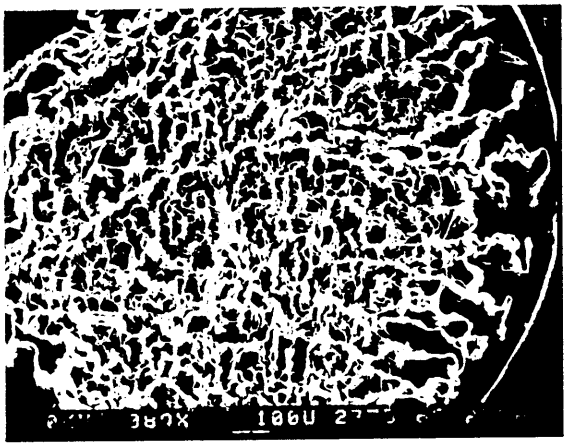

L= 87 MM

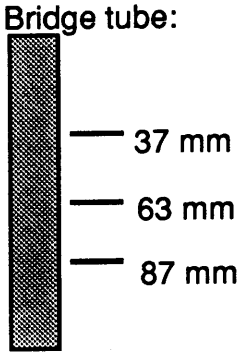

Figure 4-3: Uniformity of Pore Diameter, SEM micrographs, Case 6

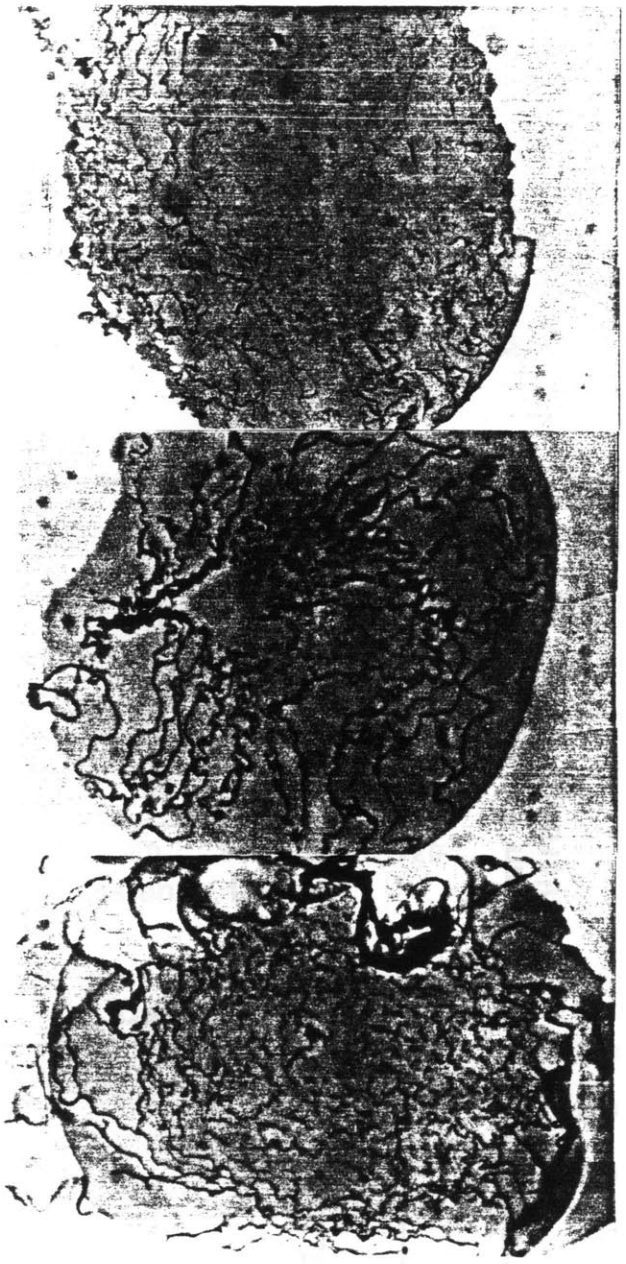

Figure 4-4: Uniformity of Pore Diameter, Light Micrographs of E/S Spec., Case 6

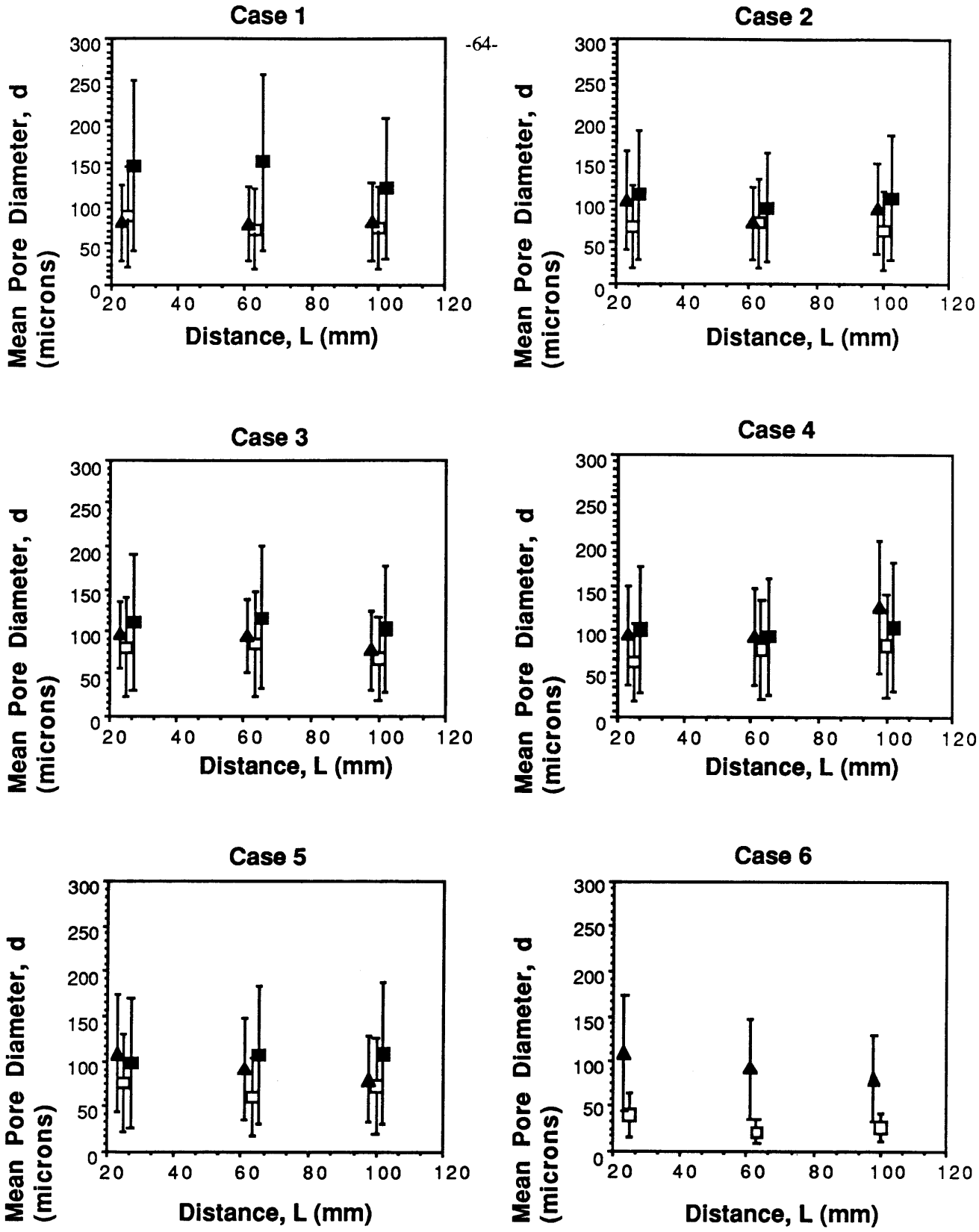

Figure 4-5: Results of Uniformity Experiment, Cases 1-6

length of bridges and studied in the SEM. While no computerized image analysis was performed on the SEM micrographs, Fig. 4-6 clearly shows that pore orientation remains highly uniform along the length of case 1 bridges. The same results were observed for other cases of bridge production. However, because pores are more spherical than elongated when pores become very small or very large, the meaning of pore orientation becomes difficult to define.

4.1.2 Repeatability

The results of the repeatability experiment demonstrate that pore geometry for a given case of manufacturing conditions is repeatable from one bridge production batch to another. As shown in Fig. 4-7, there is no statistically significant difference in d among grafts produced in 3 different batches. All data shown is taken from computer image analysis of cross-sectional SEM micrographs. Pore orientation also remains the same from batch to batch, as shown in Fig. 4-8 which shows longitudinal section SEM micrographs collected from midlength on bridges from three separate case 1 batches.

4.2 Control of Pore Diameter

The thesis research of Chen[18] and Irving[17] showed that pore diameter in pan cast CG foams could be controlled by adjusting the concentration of CG in suspension and the degree of undercooling. Data from the uniformity experiment was used to verify whether these transfer function relationships applied also to the pore diameter in PNS bridges. In addition, the effect of entry velocity on pore diameter was considered. As shown in Fig. 4-5 and Fig. 4-7, computerized image analysis shows little statistically significant difference in d calculated for cases 1-5. Only case 6 is significantly different from all other cases. By "eyeballing" SEM micrographs, very significant differences in pore diameter can be observed from case to case. Because of the natural pore size distribution in the bridges

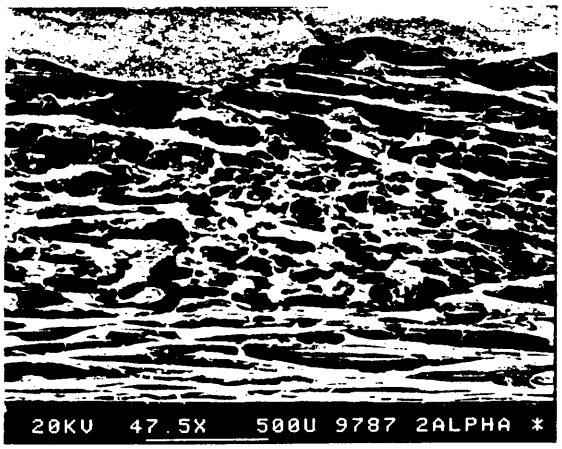

L= 37 MM

L= 63 MM

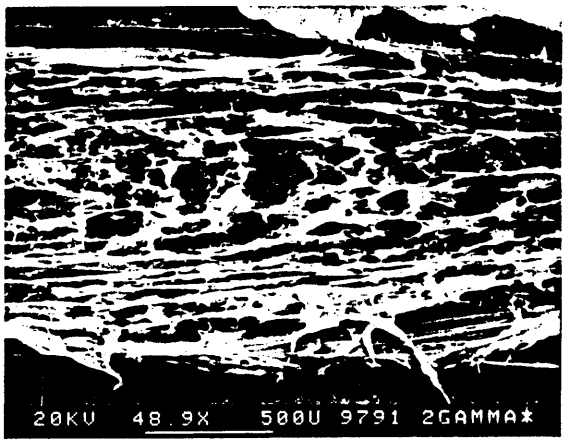

L= 87 MM

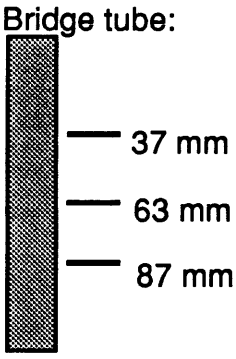

Figure 4-6: Uniformity of Pore Orientation, SEM Micrographs, Case 1

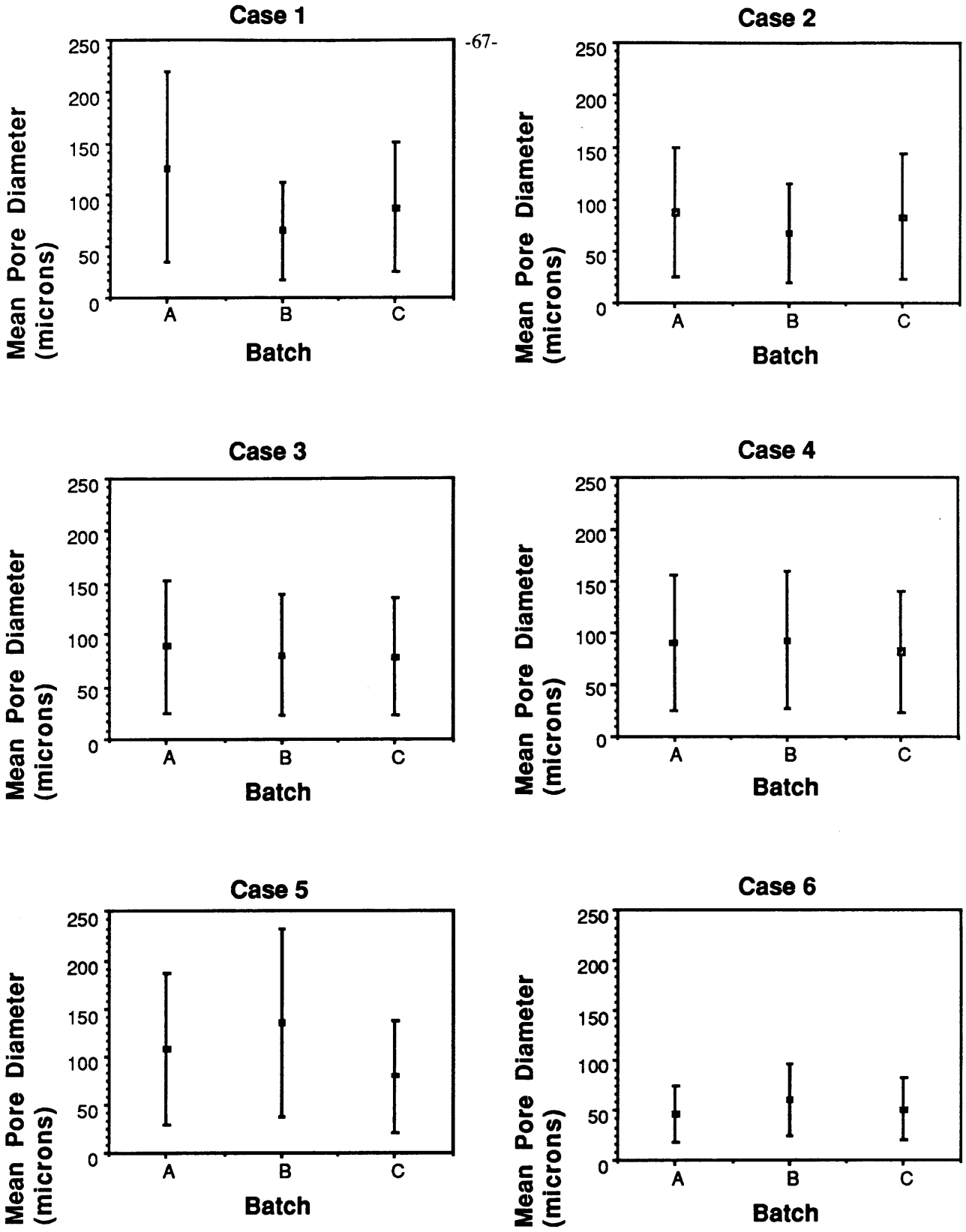

Figure 4-7: Results of Repeatability Experiment, Cases 1-6

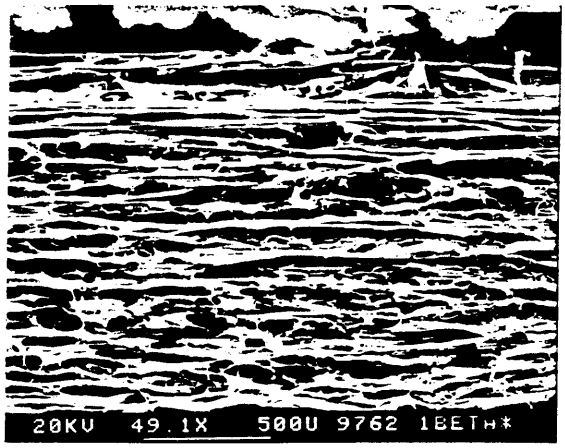

Batch A

Batch B

Batch C

L= 63 MM

Figure 4-8: Repeatability of Pore Orientation, SEM Micrographs, Case 1

and error introduced during image enhancement, a better computerized pore diameter assay would have to be developed in order to rigorously quantify these differences.

4.2.1 Effect of Velocity

The entry velocity certainly has an effect on pore diameter, but the effect is highly dependent on the degree of undercooling.

As shown in Fig. 4-9, increasing velocity has a weak positive effect on pore diameter under conditions of low undercooling. However, the uniformity of pore structure across the bridge cross section tends to decrease dramatically with increased velocity. The orientation of ice dendrite growth goes from axial to radial, forcing CG to the center of the bridge and leading to a smaller pore diameter at the centerline than at the periphery.

Figure 4-10 illustrates the effect of velocity on d at low undercooling. The values of d are taken from analysis of bridges produced under case 1 and case 3 conditions. Note that there is no statistically significant difference between the calculated d at two values of V. Both conditions yield d of about 70 +/- 50 microns measured from SEM images and about 120 +/- 80 microns measured from E/S images.

As shown in Fig. 4-11, increasing velocity has a strong negative effect on pore diameter under conditions of high undercooling. The pore diameter decreases by an order of magnitude. Furthermore, the pore wall structure changes from lamellar to fibrillar. At high undercooling, the velocity change does not affect the uniformity of pore diameter across the bridge cross section.

Figure 4-12 illustrates the effect of velocity on d at high undercooling. The values of d are taken from analysis of bridges produced under case 2 and case 6 conditions. Note that d changes from 70 +/- 50 microns to 27 +/- 16 microns as velocity increases from 2.0×10^{-5} to 10^{-4} m/s.

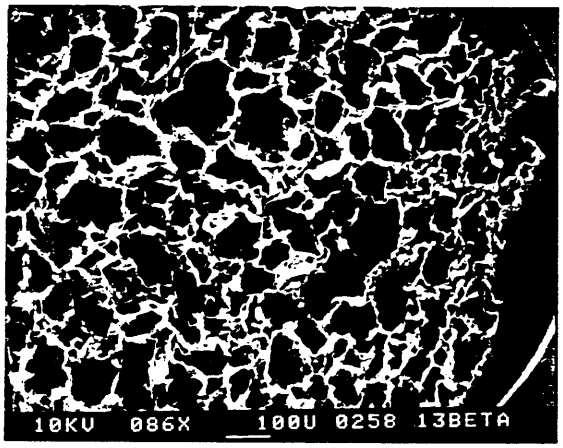

$V = 2.0 \times 10^{-5}$ M/S

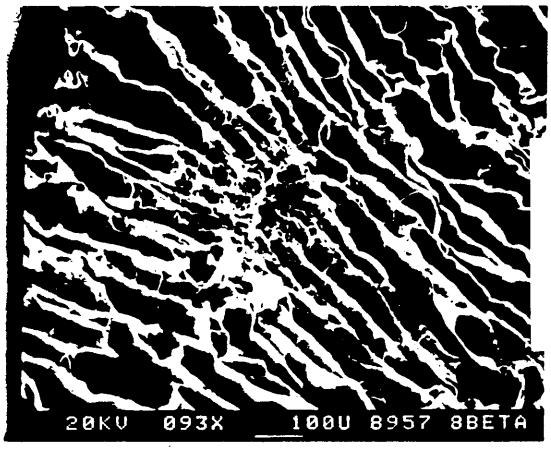

$V = 10^{-4}$ M/S

Figure 4-9: Effect of Velocity on Pore Diameter at Low Undercooling, SEM Micrographs, $\Delta T = 10\ ^{o}C$, C=0.27 %w/w

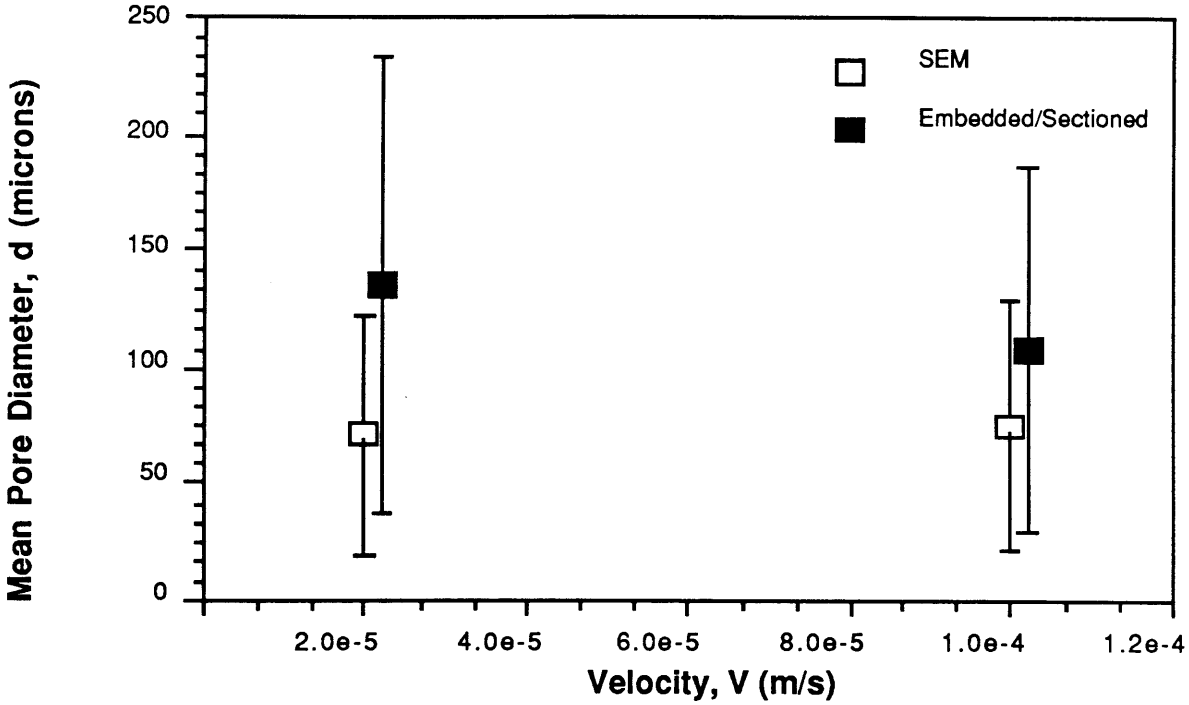

Figure 4-10: Effect of Velocity on Pore Diameter at Low Undercooling, $\Delta T=10\ ^{o}C$, C=0.27 %w/w

4.2.2 Effect of Undercooling

Pore diameter can be controlled by changing the undercooling, but the effect differs depending on the entry velocity.

Figure 4-13 illustrates that increasing undercooling has a very weak positive effect on pore diameter under conditions of low entry velocity. The uniformity of pore diameter remains strong. By visual inspection of micrographs, the pore diameter appears to change from about 60 microns to about 150 microns.

Figure 4-14 shows that there is no statistically significant difference in d is achieved by going from case 1 to case 2 manufacturing conditions. Both conditions yield d of about 70 +/- 50 microns measured from SEM images and about 120 +/- 80 microns measured from E/S images.

As shown in Fig. 4-15, increasing undercooling has a strong negative effect on pore

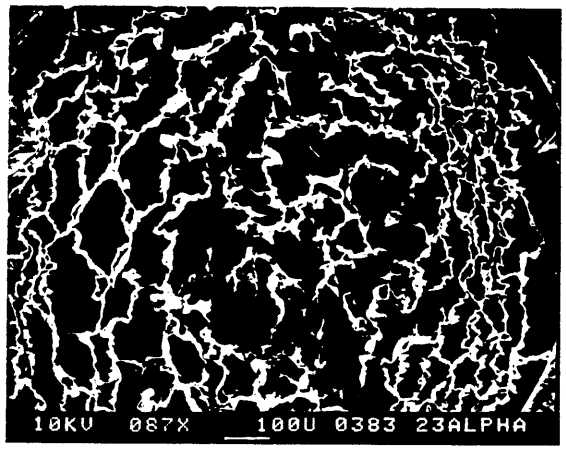

$V = 2.0 \times 10^{-5}$ M/S

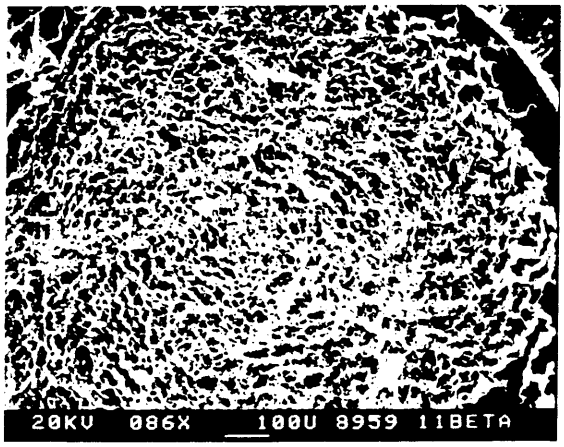

$V = 10^{-4}$ M/S

Figure 4-11: Effect of Velocity on Pore Diameter at High Undercooling, SEM Micrographs, ΔT=40 ^{o}C, C=0.27 %w/w

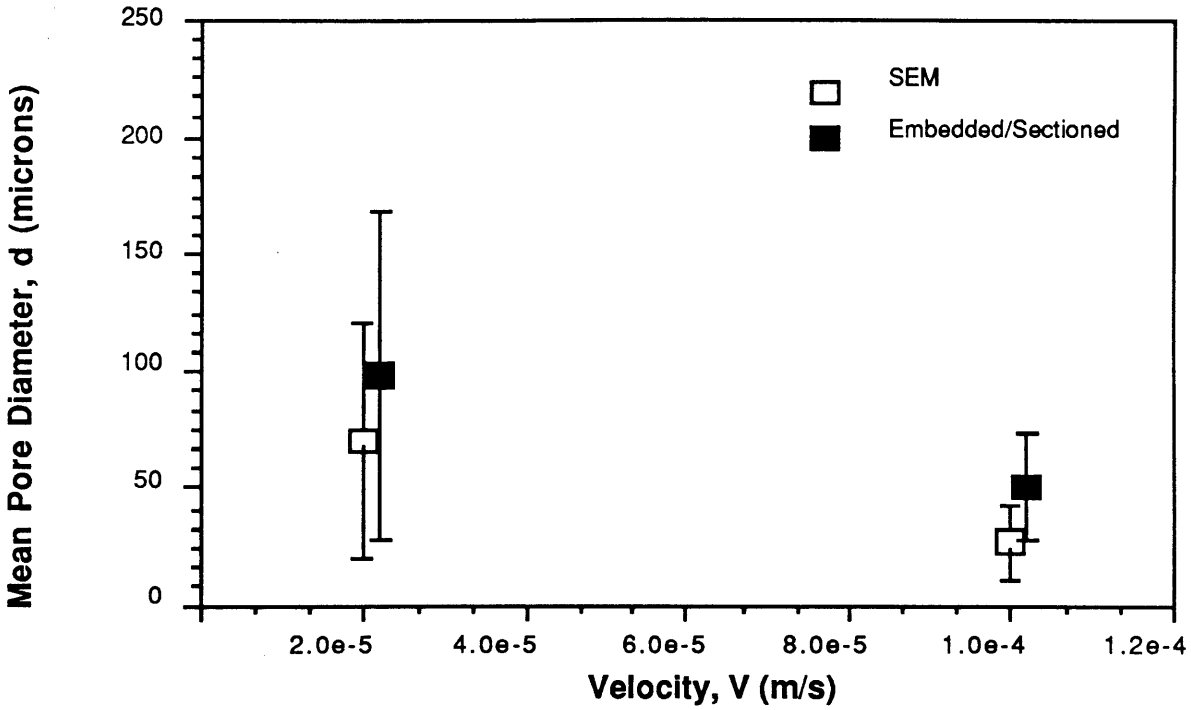

Figure 4-12: Effect of Velocity on Pore Diameter at High Undercooling
ΔT=40 ^{o}C, C=0.27 %w/w

diameter under conditions of high velocity. The pore diameter decreases by an order of magnitude. Furthermore, for low CG concentrations, the pore wall structure changes from lamellar to fibrillar. At high velocity, the change in undercooling greatly increases uniformity of pore diameter across the bridge cross section.

Figure 4-16 illustrates the effect of undercooling on d at high velocity. The values of d are taken from analysis of bridges produced under case 3 and case 6 conditions. Note that d changes from 110 +/- 80 microns to 27 +/- 16 microns as undercooling increases from 10 to 40 ^{o}C.

Irving's relation between pore diameter and undercooling for pan cast foams compares well with the effect of undercooling on pore diameter for PNS bridges produced at high velocity. As illustrated in Fig. 4-17, Irving observed a 60% decrease in pore d when ΔT was changed from 10 to 40 ^{o}C. The data from the uniformity experiment shows a 72% decrease in d for the same change in ΔT. For low velocity, there is no agreement, as shown in Fig. 4-18.

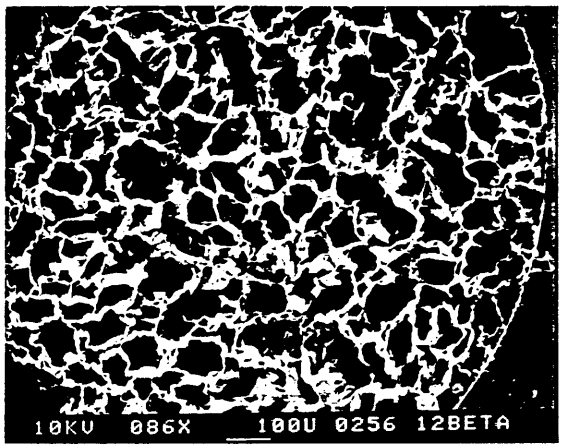

$\Delta T = 10\ ^{o}C$

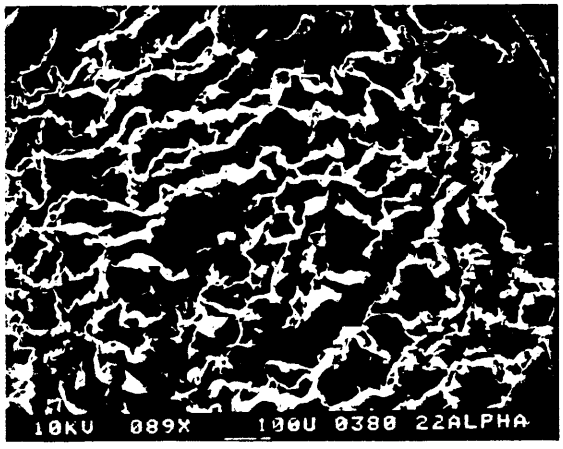

$\Delta T = 40\ ^{o}C$

Figure 4-13: Effect of Undercooling on Pore Diameter at Low Velocity, SEM Micrographs, $V=2.0 \times 10^{-5}$ m/s, C=0.27 %w/w

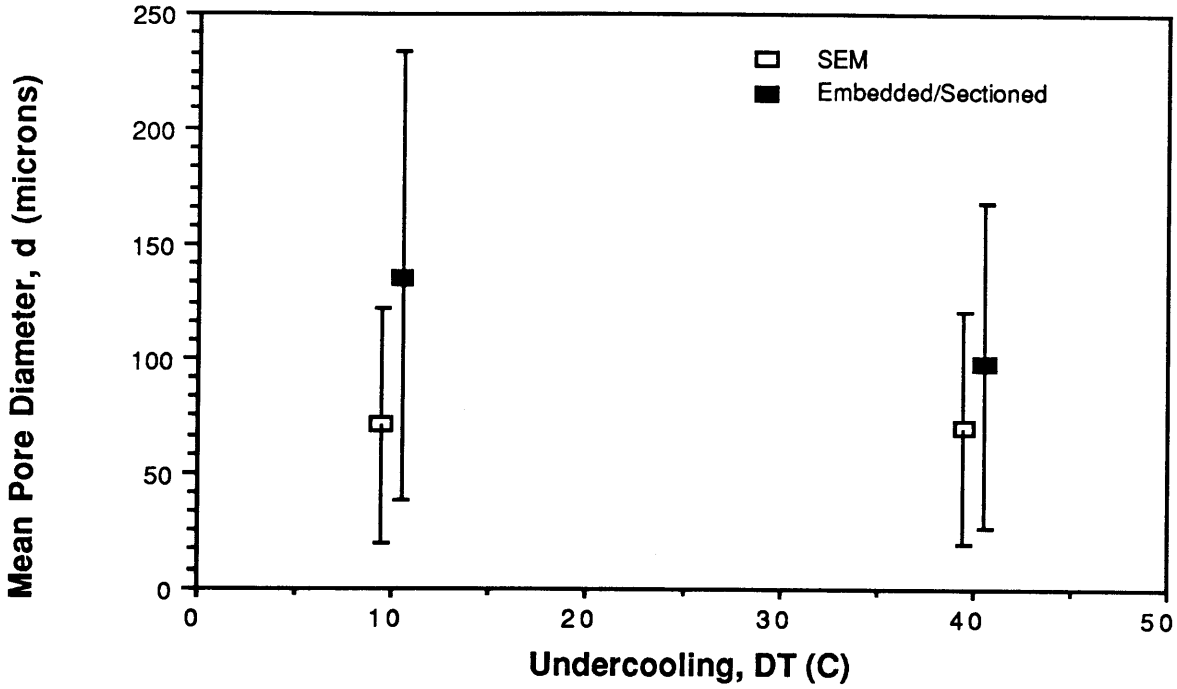

Figure 4-14: Effect of Undercooling on Pore Diameter at Low Velocity, $V=2.0x10^{-5}$ m/s, C=0.27 %w/w

4.2.3 Effect of CG Concentration

There is no observable change in pore diameter as the concentration of CG in suspension is changed from 0.12 %w/w to 0.48 %w/w. However, the pore wall texture changes from fibrillar to lamellar as the concentration is increased. Figure 4-19 shows micrographs of bridges produced under identical slow cooling conditions but at different concentrations. Note that pore diameter is 50-100 microns in each bridge, but the pore walls are much thicker for the 0.48 %w/w bridge. Figure 4-20 illustrates the effect of concentration under rapid cooling conditions. Note that the pore diameter remains about 30 microns in each bridge, but that the pore walls have a wispy fibrillar structure in the 0.12 %w/w bridge.

Figure 4-21 compares Chen's empirical pore diameter vs. CG concentration relation for pan cast foams with the results of the uniformity experiment. Although Chen did not study suspensions of less than 0.48 %w/w concentration, her relation might be extrapolated

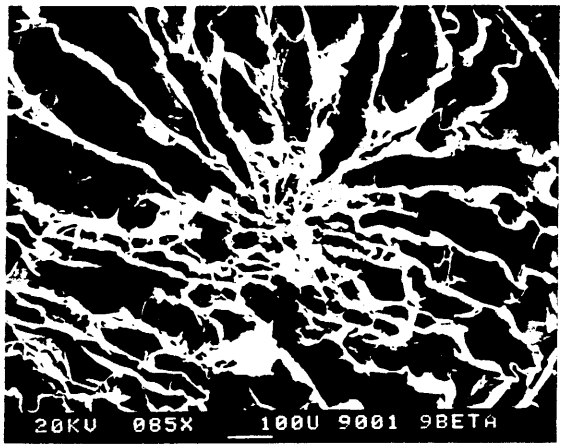

$\Delta T = 10\ ^{o}C$

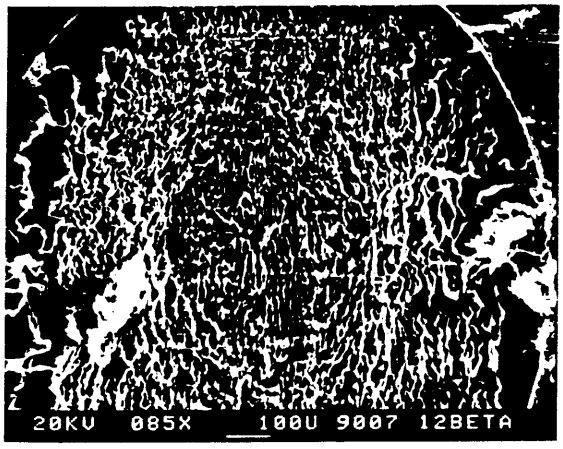

$\Delta T = 40\ ^{o}C$

Figure 4-15: Effect of Undercooling on Pore Diameter at High Velocity, SEM Micrographs, $V=10^{-4}$ m/s, C=0.48 %w/w

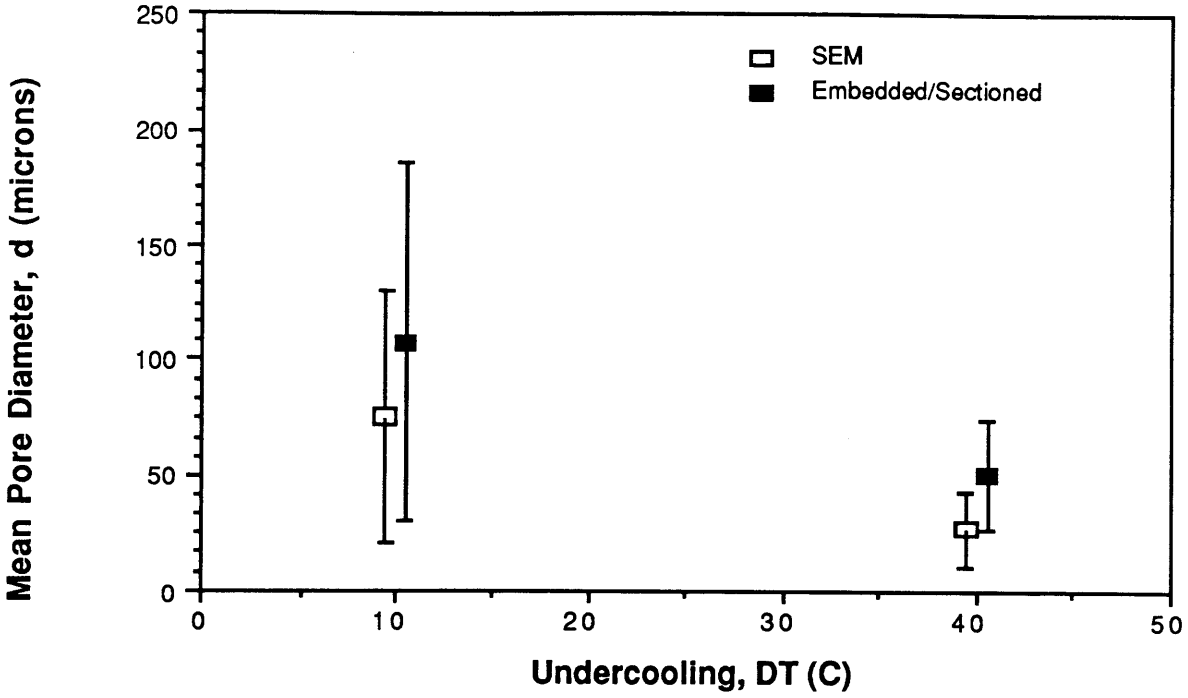

Figure 4-16: Effect of Undercooling on Pore Diameter at High Velocity, $V=10^{-4}$ m/s, C=0.27 %w/w

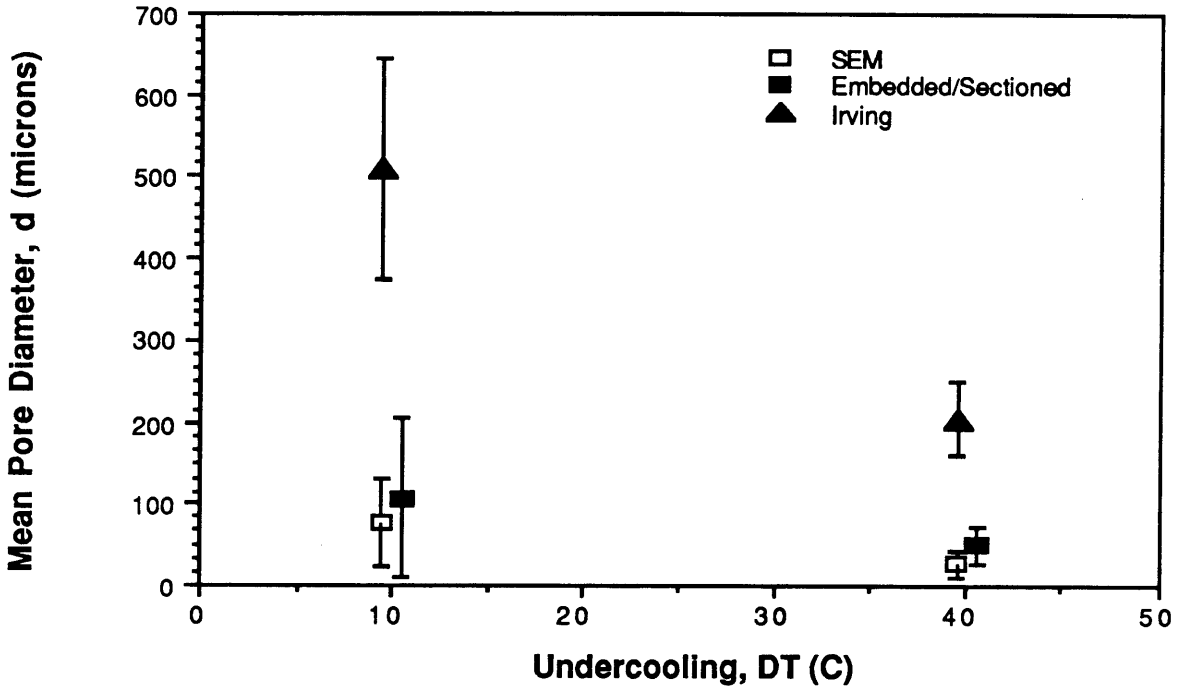

Figure 4-17: Effect of Undercooling on Pore Diameter at High Velocity, Comparison with Irving (1986), $V=10^{-4}$ m/s, C=0.27 %w/w

for low concentrations to predict pore diameters in excess of 200 microns and a continued

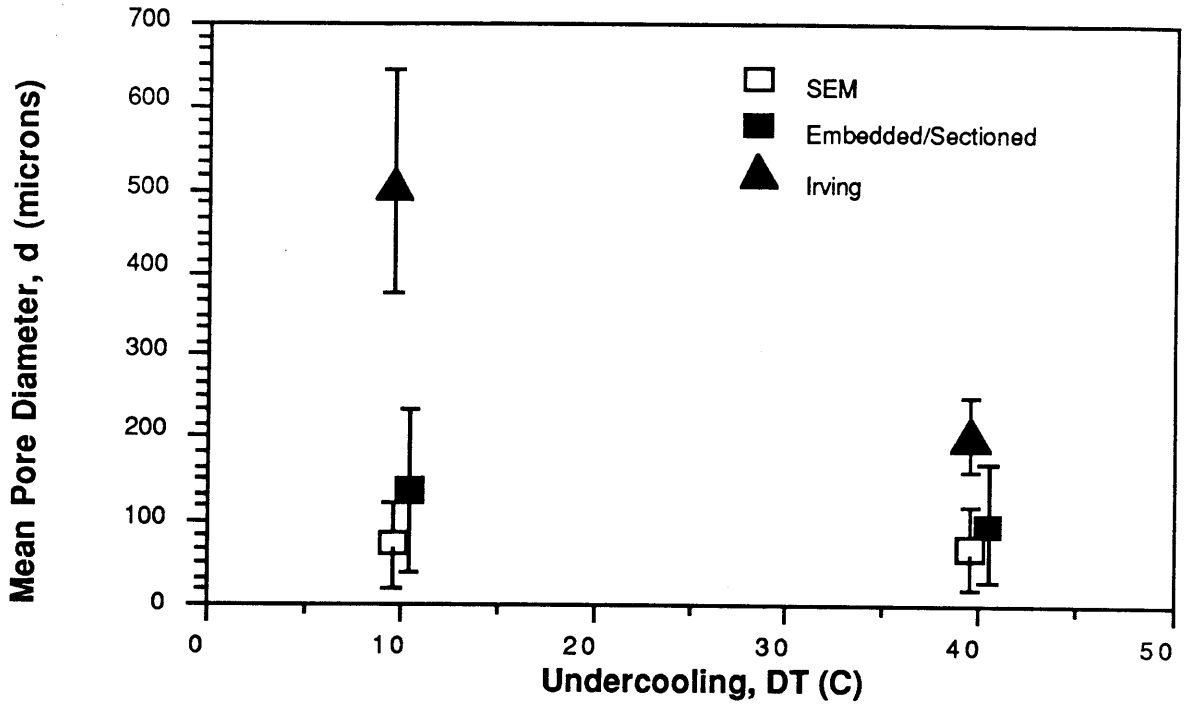

Figure 4-18: Effect of Undercooling on Pore Diameter at Low Velocity, Comparison with Irving (1986), V=2.0x10^{-5} m/s, C=0.27 %w/w

trend of increasing pore diameter with decreasing concentration. The extrapolation is a poor prediction of the actual effect of the uniformity data. Note that the foams cast by Chen were subject to undercooling of 40 to 45 °C while the uniformity test data is for 10 °C undercooling.

4.2.4 Summary of Effects of Velocity and Undercooling on Pore Diameter

Figure 4-22 summarizes the effects of V and ΔT on pore diameter in PNS bridges. The figure gives both the qualitative "eyeball" estimate of pore diameter and the value of d derived from computer image analysis of SEM images. Note that a specimen produced under quench conditions (freefall into the cooling bath) is described.

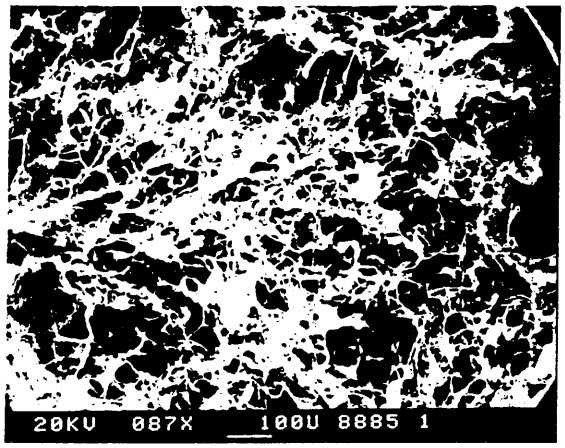

C= 0.12 % W/W

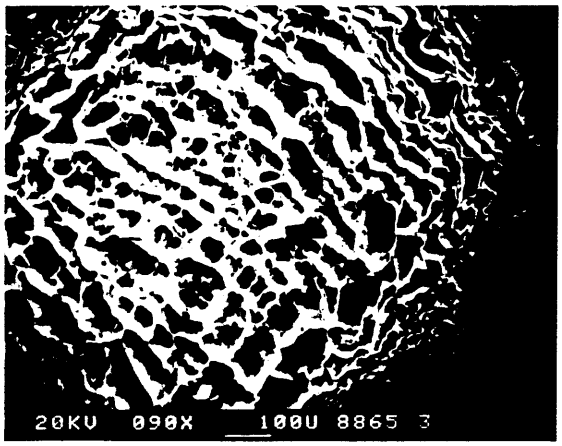

C= 0.48 % W/W

Figure 4-19: Effect of CG Concentration on Pore Diameter at Low Velocity and Low Undercooling, $V=2.0\times10^{-5}$ m/s, $\Delta T=10$ °C

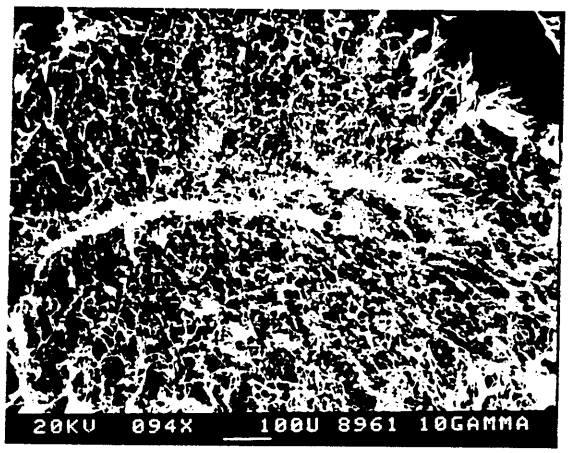

C= 0.12 % W/W

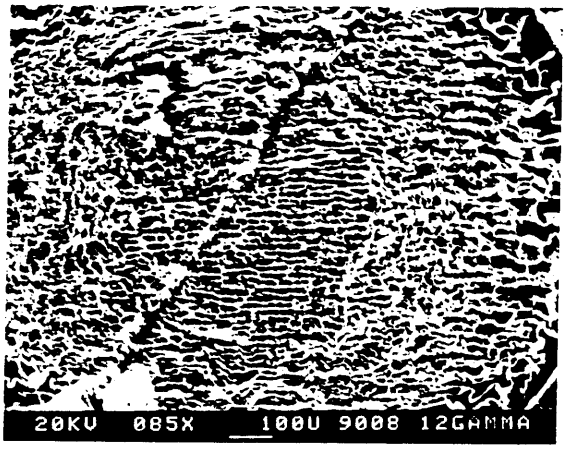

C= 0.48 % W/W

Figure 4-20: Effect of CG Concentration on Pore Diameter at High Velocity and High Undercooling, $V=10^{-4}$ m/s, $\Delta T=40\ ^{o}C$

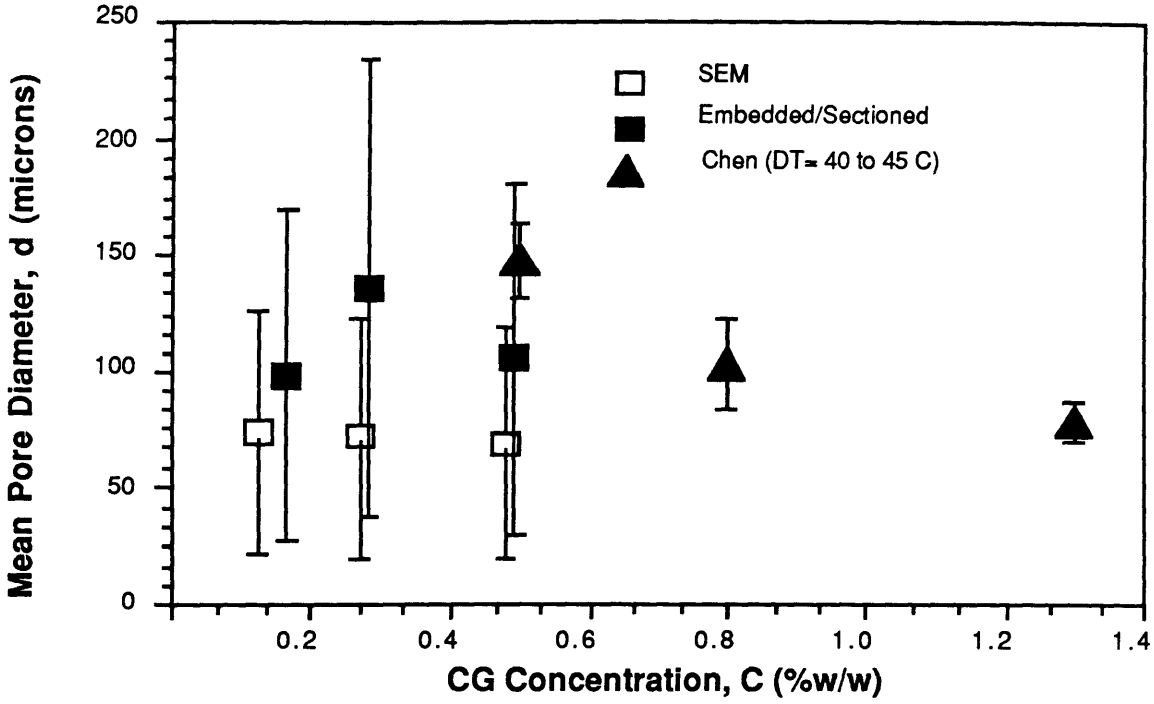

Figure 4-21: Effect of CG Concentration on Pore Diameter, Comparison with Chen (1982), $V=2.0 \times 10^{-5}$ m/s, $\Delta T=10$ °C

4.3 Control of Pore Orientation

Pore orientation in PNS bridges can be controlled by adjusting the velocity and undercooling during the freezing process. Figure 4-6 illustrates a typical axial pore orientation produced under conditions of slow cooling. Figure 4-23 illustrates a strongly radial pore orientation achieved under quench conditions of free fall into the bath and $\Delta T=65$ °C. Radial pore structure is characterized by large elongated pores arranged toward the centerline of the bridge (as observed in the cross section) and a general radial grain of small pores (as observed in the longitudinal section).

Figure 4-24 compares the results of the uniformity experiment with theoretical predictions of pore orientation. The theoretical predictions are based on the Mikic number (Mi) defined in Chapter 2. Note that for $Mi<1$ the orientation tends to be axial while for $Mi=1$ or $Mi>1$ the orientation tends to be radial. This agrees closely with theoretical

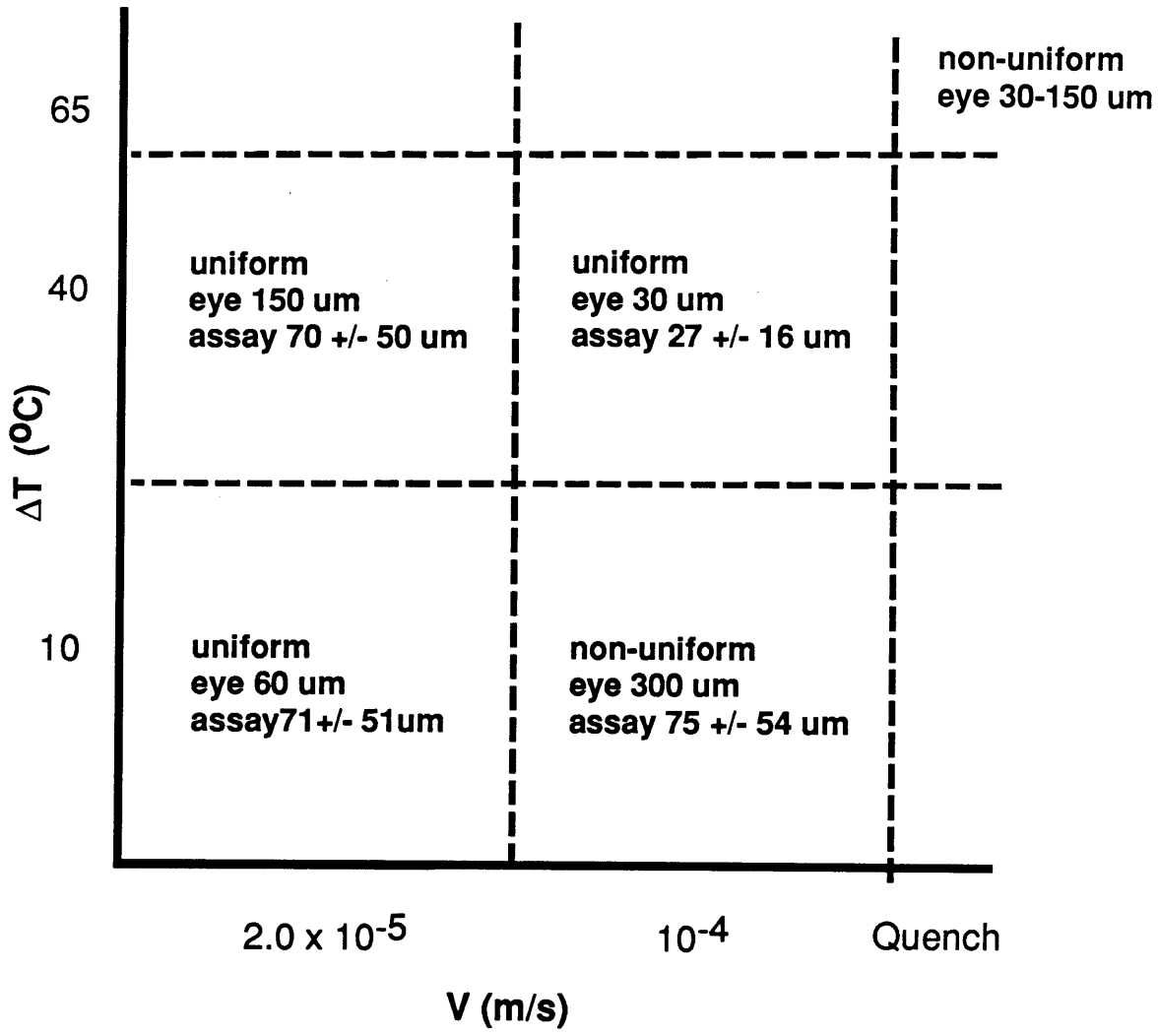

$\delta d/\delta V$ = strong - @ high ΔT
weak + @ low ΔT

$\delta d/\delta \Delta T$ = strong - @ high V
weak + @ low V

Figure 4-22: Summary of Effects of Velocity and Undercooling on Pore Diameter

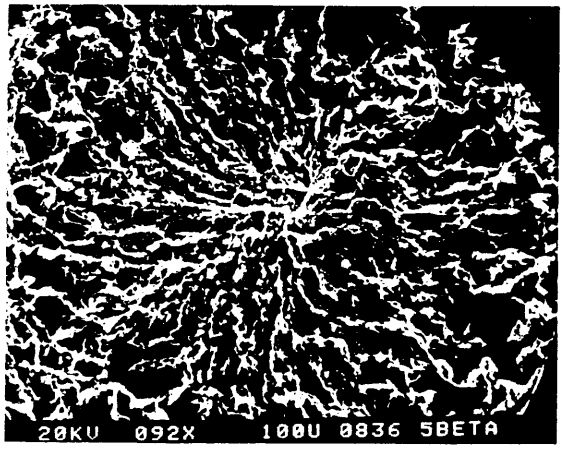

CROSS SECTION

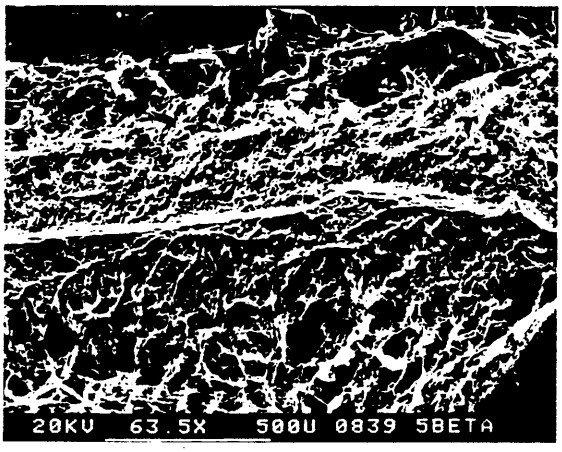

LONGITUDINAL SECTION

Figure 4-23: Radial Pore Orientation through Quenching, ΔT=65 ^{o}C, C=0.27 %w/w

predictions. Increasing velocity at high undercooling leads to a strong radial shift in pore orientation. At low undercooling, the effect is similar but much weaker. Increasing undercooling at high values of velocity leads to a strong radial shift in pore orientation. At velocity, the effect on pore orientation is negligible.

4.4 Methods for Measuring Pore Diameter

An important result of this experimental work are observations about the various methods of pore geometry analysis used. Two types of micrographs were prepared and studied: SEM micrographs of electroplated cross sections and light micrographs of embedded and sectioned cross sections. There were two different methods used to calculate mean pore diameter from micrographs. These were the line intercept method developed by Irving and the method of computer image analysis developed by Wong and Mahaney.

4.4.1 SEM Micrographs vs. Light Micrographs

SEM micrographs are the simplest and least time consuming micrographs to prepare. Principle advantages are the minimal sample preparation required for SEM and the immediate development of Polaroid micrographs. Image contrast is easily enhanced by adjusting the microscope. Therefore, high contrast images can be produced that require little editing on the image analyzer screen.

Light micrographs of embedded and sectioned (E/S) specimens take a great deal of effort to produce. The process of embedding and sectioning is very laborious and often needs to be repeated in order to obtain acceptable specimens for microscopy. The micrographs must be developed and printed, so the results are not as immediate as with SEM. When used in computer image analysis, more time is required for editing light micrographs than for editing SEM micrographs. Unfortunately, the resolution of an E/S light micrograph is too coarse to adequately show the fine fibrillar pore structure. For this

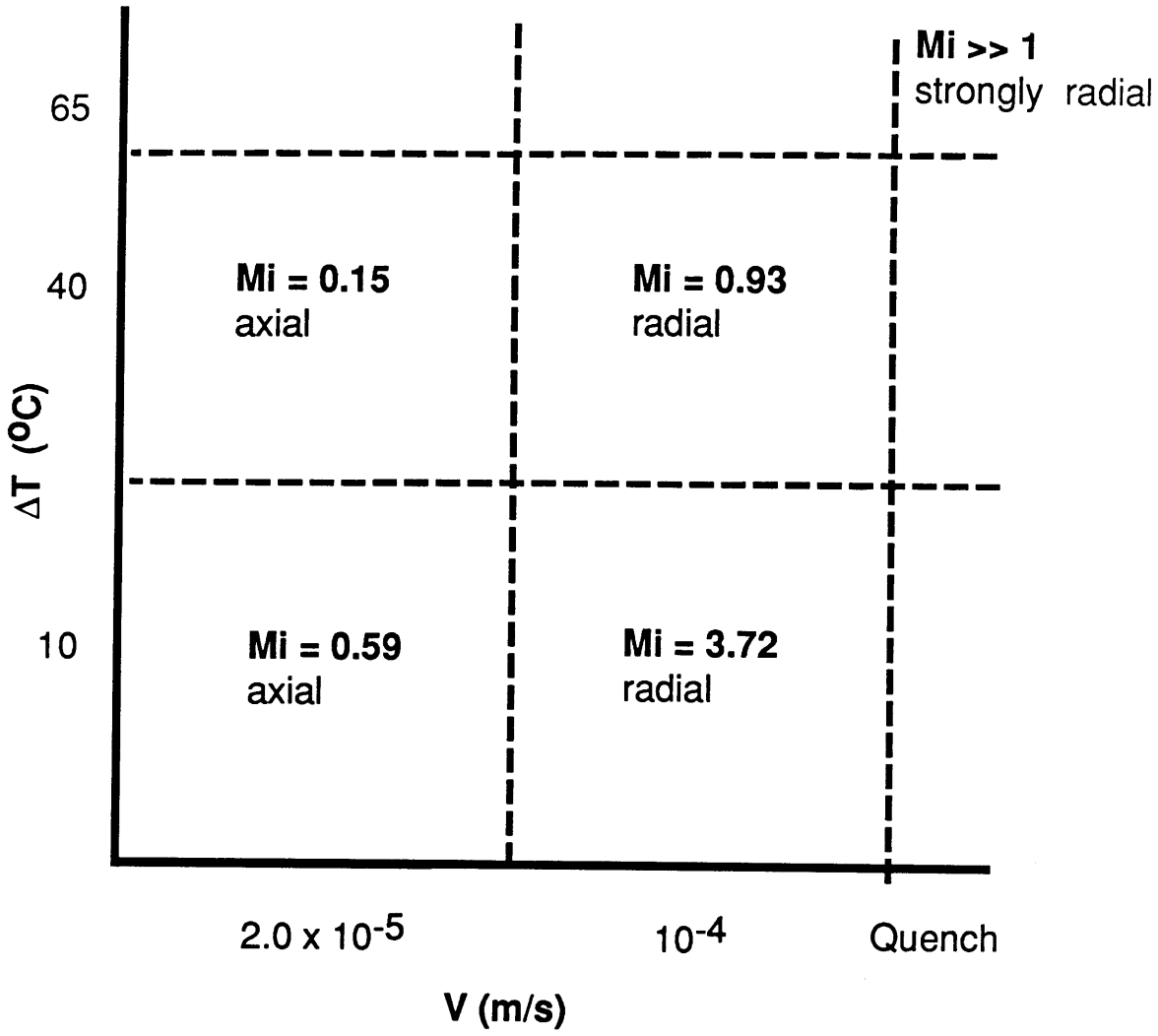

$$\delta radial/\delta V = \begin{matrix} strong + @\ high\ \Delta T \\ weak + @\ low\ \Delta T \end{matrix}$$

$$\delta radial/\delta \Delta T = \begin{matrix} strong + @\ high\ V \\ 0 \qquad\quad @\ low\ V \end{matrix}$$

Figure 4-24: Control of Pore Orientation, Correlation of Experimental Results with Theoretical Predictions

reason, light micrographs of E/S specimens could not be used in the analysis of case 6 bridges.

4.4.2 Line Intercept Method vs. Computer Image Analysis

The line intercept method is the simplest method for calculating mean pore diameter. It was used in to calculate d for the the uniformity experiment. Micrographs need to be enlarged to at least 8.5 x 11 in size to permit easy measurement and provide good resolution of line-pore wall intercepts.

Computerized image analysis was used for both the uniformity and repeatability experiments. It can be adapted for both light micrographs and SEM micrographs with no or little statistically significant difference in calculated d. The major drawback to this method is time and cost. Editing images with the light pen is a tedious and subjective task that can consume as much as 10 minutes per micrograph. The rate for image analyzer time is $25.00 per hour, so any rigorous study can become very expensive. Even with careful editing of images, there are many one or two pixel light spots on the image that are measured as very small pores. Therefore, the datafiles of pore measurements must themselves be edited before statistics are calculated on pore measurements. Otherwise, there is a unrealistically low calculated d and a very large SD_d. Editing of datafiles requires additional computer programs or laborious manual correction.

4.5 Freezing Study

The brief freezing study verified that under the freezing conditions used in the freezing apparatus, solidification occurs by dendritic growth. The freezing study showed two things. First, for a cooling rate of 4 ^{o}C/min (corresponding to the conditions of slow cooling in the freezing apparatus), an ice interface velocity of 2.0×10^{-5} m/s and a mean primary dendrite width of about 100 microns were observed. Second, for a cooling rate of

20 ^{o}C/min (corresponding to the conditions of fast cooling in the freezing apparatus), an ice interface velocity of $1.2x10^{-4}$ m/s and a mean primary dendrite width of about 50 microns were observed. Third, for the three different suspension concentrations tested, the freezing front velocity was independent suspension concentration. Unfortunately, the ice-collagen interactions could not be studied because the unstained suspension exhibited poor contrast between these constituents.

Chapter 5

Conclusions

This thesis research has contributed in several ways to the development of a production method for peripheral nerve bridges. First, it has led to an apparatus that produces nerve bridges with uniform pore structure repeatably from batch to batch. Second, there is now a qualitative understanding of how bridge pore structure can be controlled by changing parameters of the freezing process. Third, several methods of pore geometry analysis have been evaluated. Finally, there is a better theoretical understanding of the microscopic and macroscopic solidification processes involved in the production of peripheral nerve bridges. These contributions establish a good basis for routine production of PNS bridges and provide direction for further process development.

5.1 Apparatus Performance Evaluation

Based on the criteria of bridge uniformity and repeatability discussed in section 3.5, the bridge freezing apparatus offers very good performance.

5.1.1 Uniformity

For conditions of either slow cooling or rapid cooling, The apparatus produces bridges of uniform pore diameter. There is no statistically significant change in mean pore diameter along the length of bridges. This result is due to several factors.

First is the nature of the bridge pore structure. Since, the pore structure evolves from a stochastic process of ice nucleation and growth, the standard deviation in pore diameter is about 72% of the mean value. Therefore, small changes in mean pore diameter along the length of the bridge are insignificant when compared with the variability in pore diameter

within a bridge cross section. Second, the manufacturing parameters are controlled closely enough in the apparatus design that they cannot change to any significant degree during the time required to freeze a nerve bridge.

Additionally, the bridges produced show excellent uniformity of pore orientation along their length. The freezing process is a stable process, insensitive to changes in the manufacturing parameters that might otherwise cause perturbations in the local temperature gradient responsible for dendritic solidification at the freezing front. This is not surprising, since there is a significant thermal lag associated with the PVC jacket surrounding the freezing PNS bridge.

5.1.2 Repeatability

The freezing apparatus produces grafts of repeatable pore geometry from batch to batch. For either slow cooling or rapid cooling conditions. There is no statistically significant change in mean pore diameter across three batches of bridges produced on different days. In addition, there is no noticeable change in pore orientation from batch to batch.

The repeatability of pore geometry suggests that, once calibrated, the freezing apparatus reliably maintains the manufacturing parameters from batch to batch. In addition, the freezing process is insensitive to ambient air temperature which changed by as much as 10 ^{o}C from day to day during the repeatability tests.

5.2 Control of Pore Geometry

By adjusting the entry velocity (V) across the range of 2.0×10^{-5} to 10^{-4} m/s and changing undercooling (ΔT) across the range of 10 to 40 ^{o}C, mean pore diameter could be varied across the range of 150 to 30 microns. In addition, the orientation of pores could be changed from strongly axial to strongly radial. By adjusting the CG concentration in

suspension across the range of 0.12 to 0.48 %w/w, pore wall structure could be varied from fibrillar to lamellar. Changes in CG concentration did not directly affect mean pore diameter, however. Figure 5-1 summarizes the effects of manufacturing parameters velocity and undercooling on mean pore diameter and pore orientation.

5.2.1 Effect of Velocity and Undercooling on Pore Diameter

In general, a large d is obtained by using slow cooling rates (low V and low ΔT). A small d is obtained by through rapid cooling (high V and high ΔT). The effects of V and ΔT appear to be coupled. An increase in V has the strongest negative effect on d at high values of ΔT. Similarly, an increase in ΔT has the strongest negative effect on d at high values of V.

The influence of ΔT on d closely parallels observations made by Irving, but only under conditions of high V. Irving observed a 60% decrease in pore d when ΔT was changed from 10 to 40 ^{o}C. The data from the uniformity experiment shows a 72% decrease in d for the same change in ΔT.

For uniformity of pore diameter across a bridge cross section, slow cooling rates are most favorable. At quench conditions, pores are very large (100's of microns) near the periphery of the bridge but decrease to less than 10 microns near the center of the bridge. The exception to this rule is the case of V= 10^{-4} m/s and ΔT= 40 ^{o}C, where d becomes small (30 microns) and very uniform, with a few large collapsed pores along the periphery.

5.2.2 Effect of Velocity and Undercooling on Pore Orientation

The effects of V and ΔT on pore orientation are very closely coupled and correlate well with theory. When the dimensionless number Mi relates material properties of the bridge, geometric properties of the bridge and the ratio $V/\Delta T$ to the orientation of dendrite growth in the solidifying CG suspension. When Mi is less than 1, the pore orientation is axial. When Mi is equal to or greater than 1, the pore orientation becomes radial.

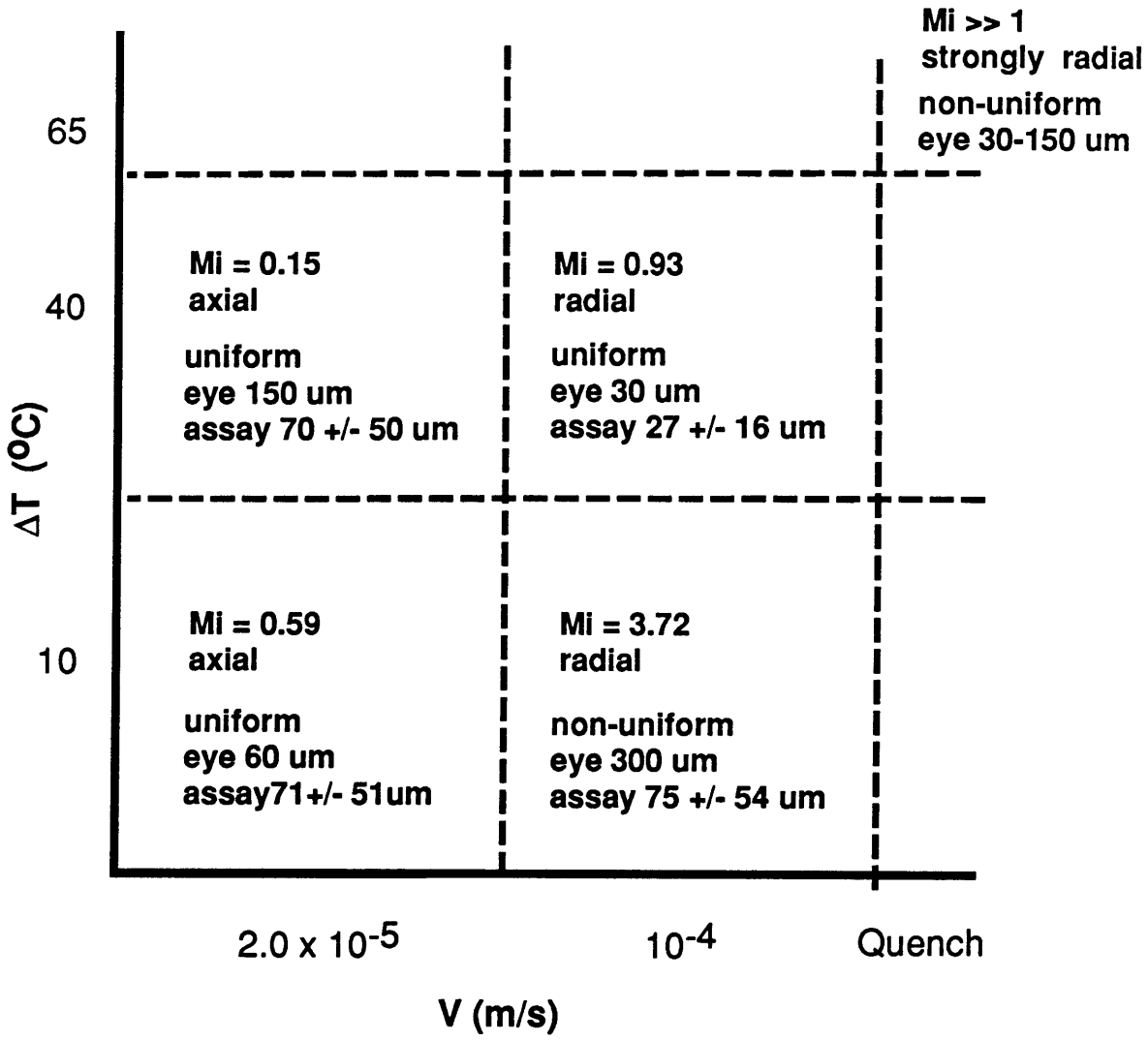

$\delta d/\delta V$ = strong - @ high ΔT
weak + @ low ΔT

$\delta radial/\delta V$ = strong + @ high ΔT
weak + @ low ΔT

$\delta d/\delta \Delta T$ = strong - @ high V
weak + @ low V

$\delta radial/\delta \Delta T$ = strong + @ high V
0 @ low V

Figure 5-1: Summary of Effect of Velocity and Undercooling on Pore Structure

5.3 Preferred Method for Pore Geometry Analysis

Of the imaging methods used in this research, preparation of high contrast SEM micrographs of plated specimens was by far the easiest. Much less effort and skill are required for SEM micrographs than for light micrographs of embedded and sectioned (E/S) specimens. In addition, work did not have to be repeated as frequently with SEM micrographs as with E/S light micrographs to get a good image for analysis. The two types of micrographs gave mean pore diameter results that were statistically the same.

The best technique of pore diameter analysis was the line intercept method. It was much easier and less expensive than computer image analysis and yet gave calculations of d that were statistically the same as those obtained through the more sophisticated computer technique. Both methods are insensitive to very small (~10 micron) or very large (500 micron) pores in micrographs. The computer image analysis results are distorted by artifacts that come into the micrograph image during contrast enhancement. Therefore, data files of individual pore measurements need to be filtered of very small measurements before statistical analysis.

5.4 Solidification Processes in Nerve Bridge Production

By studying CG suspensions in a cryomicroscope under conditions of controlled cooling rate, it was concluded that solidification occurs by dendritic growth. By modeling the cooling rates employed in actual nerve bridge freezing, it was found that freezing front velocity was roughly the same as entry velocity. The primary dendrite diameters were about the same as the mean pore diameter of nerve bridges produced under similar cooling rates.

1. Chang, A.S.-P., ''Electrophysiological Recovery of Peripheral Nerves Regenerated by Biodegradable Polymer Matrix'', Master's thesis, Mechanical Engineering, Massachusetts Institute of Technology, 1988.

2. Williams, L.R., Longo, F.M., Powell, H.C., Lunborg, G., Varon, S., ''Spatial-Temporal Progress of Peripheral Nerve Regeneration within a Silicone Chamber: Parameters for a Bioassay'', *J. Comp. Neurology*,218 1983.

3. Henry, E.W., Chiu, T.H., Nyilas, E., Brushart, T.M., Dikkes, P., Sidman, R.L., '' Nerve Regeneration through Biodegradable Polyester Tubes'', *Exp. Neurology*,90 1985.

4. Dunn, G.A. and Ebendal, T., ''Contact Guidance on Oriented Collagen Gels'', *Experimental Cell Research*,111 1978.

5. Lee, E., ''Effects of Degradation Rate and Crosslink Density of Artificial Skin on Wound Contraction'', Master's thesis, Mechanical Engineering, Massachusetts Institute of Technology, 1986.

6. Yannas, I.V., Orgill, D.P., Silver, J., Norregaard, T.V., Zervas, N.T., Schoene, W.C., ''Polymeric Template Facilitates Regeneration of Sciatic Nerve across 15-mm Gap'', *Trans Soc Biomaterials*,8 1985.

7. Yannas, I.V., Orgill, D.P., Silver, J., Norregaard, T.V., Zervas, N.T., Schoene, W.C., ''Regeneration of Sciatic Nerve across 15-mm Gap by Use of a Polymeric Template'', *Advances in Biomedical Polymers, C.G. Gebelein (ed)*, Plenum Publishing Corp., 1987.

8. Yannas, I.V. and Burke, J.F., ''Design of Artificial Skin. I. Basic Design Principles.'', *Journal of Biomedical Materials Research*,14 1980.

9. Yannas, I.V., Burke, J.F., Orgill, D.P., and Skrabut, E.M., ''Wound Tissue Can Utilize a Polymeric Template to Synthesize a Functional Extension of Skin.'', *Science*,215 1982.

10. Aubourg, Patrick F., *Interaction of Second-Phase Particles with a Crystal Growing from the Melt*, PhD dissertation, Materials Science and Engineering, Massachusetts Institute of Technology, 1978.

11. Myers, M. and Flemings, M.C., ''Behavior of Silica Inclusions in a Partially Solidified Iron Base Alloy'', *Metallurgical Transactions*,August 1972.

12. Korber, C., Rau, G., Cosman, M.D., and Cravalho, E.G., ''Interaction of Particles and a Moving Ice-Liquid Interface'', *Journal of Crystal Growth*,72 1985.

13. Uhlmann, D.R., Chalmers, B. ,and Jackson, K.A., ''Interaction Between Particles and a Solid--Liquid Interface'', *Journal of Applied Physics*,October 1964.

14. Cisse, J.and Bolling, G.F., ''A Study of the Trapping and Rejection of Insoluable Particles during the Freezing of Water'', *Journal of Crystal Growth*,10 1971.

15. Doillon, C.J., Whyne, C.F., Brandwein, S., and Silver, F.H., ''Collagen-Based Wound Dressings: Control of the Pore Structure and Morphology'', *Journal of Biomedical Materials Research*,20 1986.

16. MacKenzie, A.P., ''Factors Affecting the Mechanism of Transformation of Ice into Water Vapor in the Freeze-Drying Process'', *Annals of New York Academy of Sciences*,125 1965.

17. Irving, H., ''The Effect of Freeze Drying Temperature on Pore Size in Collagen-GAG Artificial Skin''. Bachelor's thesis, Mechanical Engineering, Massachusetts Institute of Technology, 1986

18. Chen, E.H.-Y., ''The Effect of Porosity and Crosslinking of a Collagen Based Artificial Skin on Wound Healing'', Master's thesis, Mechanical Engineering, Massachusetts Institute of Technology, 1982.

19. Dagalakis, N., Flink, J., Stasikelis, P., Burke, J.F., and Yannas, I.V., ''Design of Artificial Skin. III. Control of Pore Structure.'', *Journal of Biomedical Materials Research*,14 1980.

20. Wong, M., ''Quantification of Pore Size in Collagen-GAG Artificial Skin''. Bachelor's thesis, Mechanical Engineering, Massachusetts Institute of Technology, 1985

21. Mahaney, H.K., ''A Method for Quantification of Pore Structure in Collagen-Glycosaminoglycan Peripheral Nervous System Grafts''. Bachelor's thesis, Materials Science and Engineering, Massachusetts Institute of Technology, 1987

22. Mikic, B.. Personal commmunication, 1988

23. Rohsenow, W.M. and Choi, H., *Heat, Mass, and Momentum Transfer*, Prentice Hall, 1961.

24. Skrabut, E.S., ''Protocol for Collagen/GAG Foam''. Unpublished protocol, Fibers and Polymers Laboratory, Massachusetts Institute of Technology, 1980, rev. 1985

25. Polysciences, Warrington, PA, *JB-4 Embedding Kit Data Sheet No. 123B*, 1985.

26. Joyce-Loebl division of Vickers Co.,Tyne and Wear, England, *Magiscan II Operator's Manual*, 1983.

27. Ferdman, A.. Personal commmunication, 1988

28. Cosman, M.D.; Toner, M.; Kendal, J.; Cravalho, E.G., ''An Integrated Cryomicroscopy System'', Tech. report, Interface Techniques, Inc.; Harvard-MIT Division of Health Sciences and Technology, January 1988.

29. Scheiwe, M.W. and Korber,C., ''Thermally Defined Cryomicroscopy and Some Applications on Human Leucocytes'', *Journal of Microscopy*,April 1982.

30. Dionne, M., ''Protocol for Collagenase Assay''. Unpublished protocol, Fibers and Polymers Laboratory, Massachusetts Institute of Technology, 1984, rev. 1985

Appendix A
Mean Pore Diameter Correlation

Both a theoretical and an experimental correlation were developed to convert the mean pore diameter calculated from an artifact-polluted image to a true mean pore diameter [27].

A.1 Theoretical Correlation

Figure A-1 describes how a true mean pore diameter (R) can be derived from the mean pore diameter (P) calculated from an image that is filled with numerous small artifacts of diameter r<R. This models the calculation of mean pore diameter for a large pore specimen (cases 1-5). P is modeled as the weighted average pore diameter of two pore populations n_r and n_R (A). The expression for P can be rewritten (B) to show the dependence of P on the ratios given in C. If the assumed small artifact diameter is much less than the assumed real mean, and if the number of artifacts is less then the number of pores, then the expression for P can be simplified (D). Finally, a simple multiplier relating R to P is found that depends on the population ratio (E).

Figure A-2 extends the model to include the effect of large image artifacts of diameter R^*>R on P. This simulates the calculation of mean pore diameter for a small pore specimen (case 6). Here, P is modeled as the weighted average pore diameter of three pore populations n_{R^*}, n_R, and n_r (A). The expression for P can be rewritten (B) to show the dependence of P on a different set of ratios (C). The same assumption used in the two population model (D) simplifies the expression for P (E). Now, however, R is a linear function of both P and R^*.

$$P=\frac{n_R R+n_r r}{n_R+n_r} \qquad \text{A}$$

Where n_R = number of pores at **R**, the true mean pore diameter.

Where n_r = number of small image artifacts of diameter **r**.

Where **P** is the mean pore diameter calculated by the image analyzer.

$$P=\frac{1+\frac{n_r r}{n_R R}}{\frac{n_R+n_r}{n_R R}}=\frac{1+\frac{n_r r}{n_R R}}{\frac{1}{R}+\frac{n_r}{n_R R}} \qquad \text{B}$$

$$\text{If } \frac{n_r}{n_R}<1 \text{ and } \frac{r}{R}<1, \text{ then } \frac{n_r r}{n_R R}<<1 \approx 0 \qquad \text{C}$$

$$P=\frac{R}{1+\frac{n_r}{n_R}} \qquad \text{D}$$

$$R=P\left(1+\frac{n_r}{n_R}\right) \qquad \text{E}$$

Figure A-1: Correlation of True Mean pore Diameter with Image Analyzer Result: Cases 1-5

$$P = \frac{n_{R^*}R^* + n_R R + n_r r}{n_{R^*} + n_R + n_r} \quad \text{A}$$

Where n_{R^*} = number of large image artifacts of diameter R^*.

$$P = \frac{1 + \frac{n_{R^*}R^*}{n_R R} + \frac{n_r r}{n_R R}}{\frac{1}{R} + \frac{n_{R^*} + n_r}{n_R R}} \quad \text{B}$$

$$\text{If } \frac{n_{R^*}}{n_R} < 1, \frac{n_r}{n_R} < 1, \frac{r}{R} < 1, \text{ and } \frac{R^*}{R} > 1 \quad \text{C}$$

$$\text{Then } \frac{n_r r}{n_R R} << 1 \approx 0 \text{ and} \quad \text{D}$$

$$P = \frac{R + \frac{n_{R^*}R^*}{n_R}}{1 + \frac{n_{R^*} + n_r}{n_R}} \quad \text{E}$$

$$R = P\left(1 + \frac{n_{R^*} + n_r}{n_R}\right) - R^*\left(\frac{n_{R^*}}{n_R}\right) \quad \text{F}$$

Figure A-2: Correlation of True Mean pore Diameter with Image Analyzer Result: Case 6

A.2 Experimental Correlation

A set of experimental correlations were found between the mean pore diameter calculated from an artifact-polluted (unfiltered) image and the true mean pore diameter calculated from a filtered image. The first step was to perform computer image analysis of SEM and E/S light micrographs of both case 1 and case 6 bridges. For each image, this analysis gave both a datafile of pore measurements and a set of pore diameter statistics. The statistics included P, the unfiltered mean pore diameter, and SD, the unfiltered standard deviation in pore diameter. Second, the data files for each image were manually filtered of artifact measurements. Manual filtering involved reviewing a printout of the datafile and crossing off measurements that were outside of a chosen range. Third, a true mean pore diameter was calculated by performing statistical calculations on the filtered data. These calculations were done on a VAX 11/750 (Digital Equipment Corp., Maynard, MA) by typing the filtered data into a new datafile and calculating the simple mean and the standard deviation with a FORTRAN program. For each image, the unfiltered mean pore diameter (P), the filtered mean pore diameter (R), and the filtered standard deviation (SD_f) could now be compared.

Figure A-3 shows a histogram of pore diameters measured by the Magiscan from a case 1 SEM micrograph. A P of 61.7 and a SD of 65.6 were calculated. After filtering the pore diameter datafile of all measurements less than 20 microns, an R of 90.6 and a SD_f of 65.3 were calculated. This gave an experimental multiplier $(R/P)_e$ of 1.47 and a percent SD_f of 72%.

Figure A-4 shows a histogram of pore diameters measured by the Magiscan from a case 1 light micrograph of an embedded and sectioned specimen. A P of 42.1 and a SD of 79.8 were calculated. After filtering the pore diameter datafile of all measurements less than 20 microns, an R of 87.8 and a SD_f of 63.6 were calculated. This gave an $(R/P)_e$ of 2.08 and a percent SD_f of 72%.

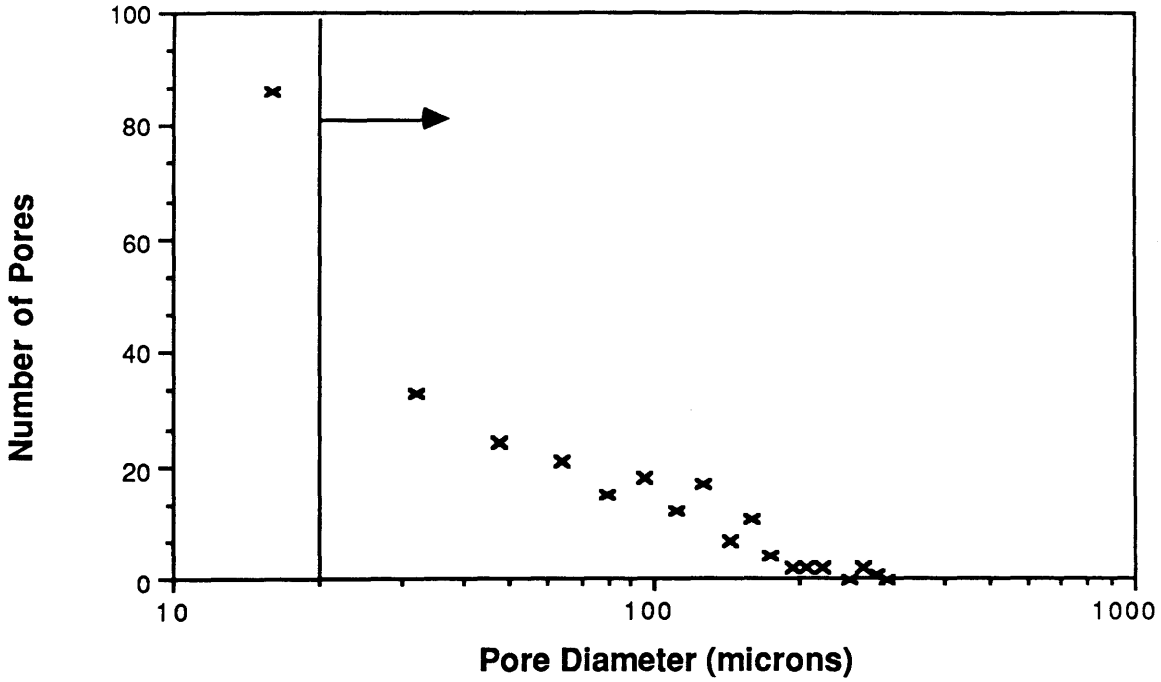

Figure A-3: Histogram of Pore Diameters Measured by Magiscan: Case 1, SEM Micrograph

Figure A-5 shows a histogram of pore diameters measured by the Magiscan from a case 6 SEM micrograph. A P of 49.8 and a SD of 55.8 were calculated. After filtering the pore diameter datafile of all measurements less than 10 microns and greater than 100 microns, an R of 44.4 and a SD_f of 26.8 were calculated. This gave an $(R/P)_e$ of 0.89 and a percent SD_f of 60%.

Figure A-6 shows a histogram of pore diameters measured by the Magiscan from a case 6 light micrograph of an embedded and sectioned specimen. A P of 39.9 and a SD of 45.0 were calculated. After filtering the pore diameter datafile of all measurements less than 10 microns and greater than 100 microns, an R of 51.2 and a SD_f of 23.3 were calculated. This gave an $(R/P)_e$ of 1.28 and a percent SD_f of 46%.

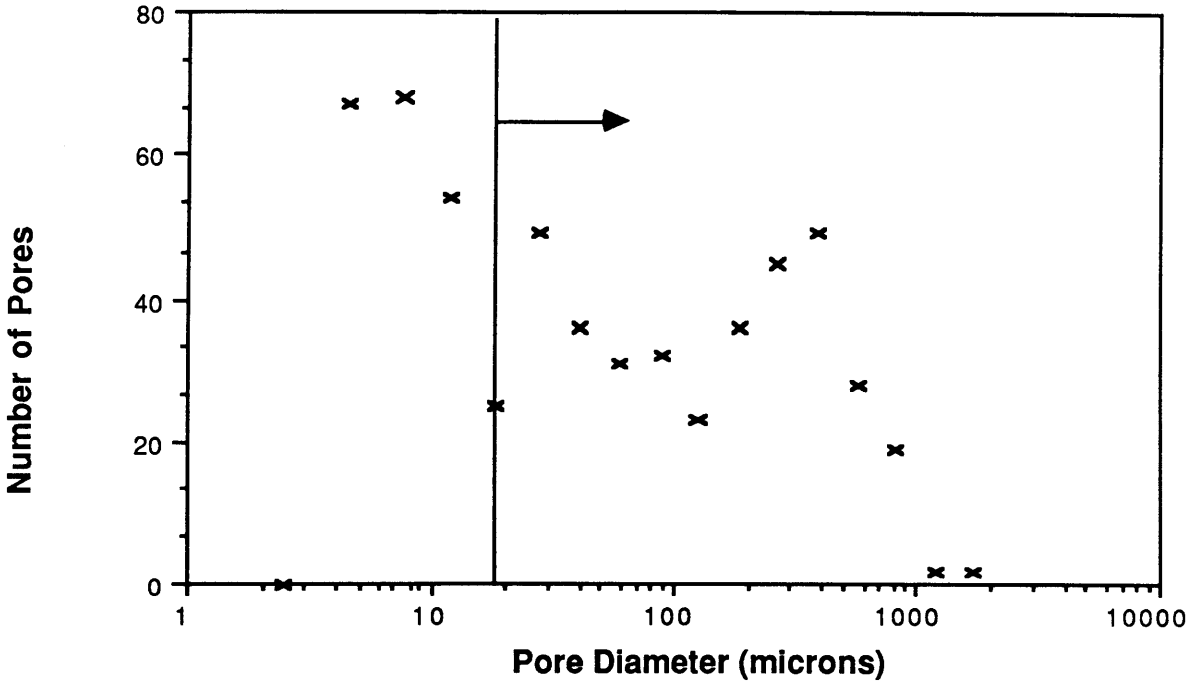

Figure A-4: Histogram of Pore Diameters Measured by Magiscan: Case 1, Light Micrograph of E/S Spec.

A.3 Discussion of Theoretical and Experimental Correlations

The data shown in the histograms was used in the theoretical correlations shown in Eqn. A-1-E and A-2-F to check the agreement of the theoretical and experimental correlations for each of the four micrographs.

For the case 1 SEM micrograph, r= 20 microns and R= 90 microns were assumed. From the histogram, n_r= 120 and n_R= 142 were measured. Therefore, n_r/n_R= 0.85 and r/R= 0.2. Thus the theoretical multiplier $(R/P)_t$ was 1.85, 20% greater than $(R/P)_e$.

For the case 1 light micrograph, r= 20 microns and R= 90 microns were also assumed. From the histogram, n_r= 263 and n_R= 304 were measured. Therefore, n_r/n_R= 0.86. Thus $(R/P)_t$ was 1.86, just 10% greater than $(R/P)_e$.

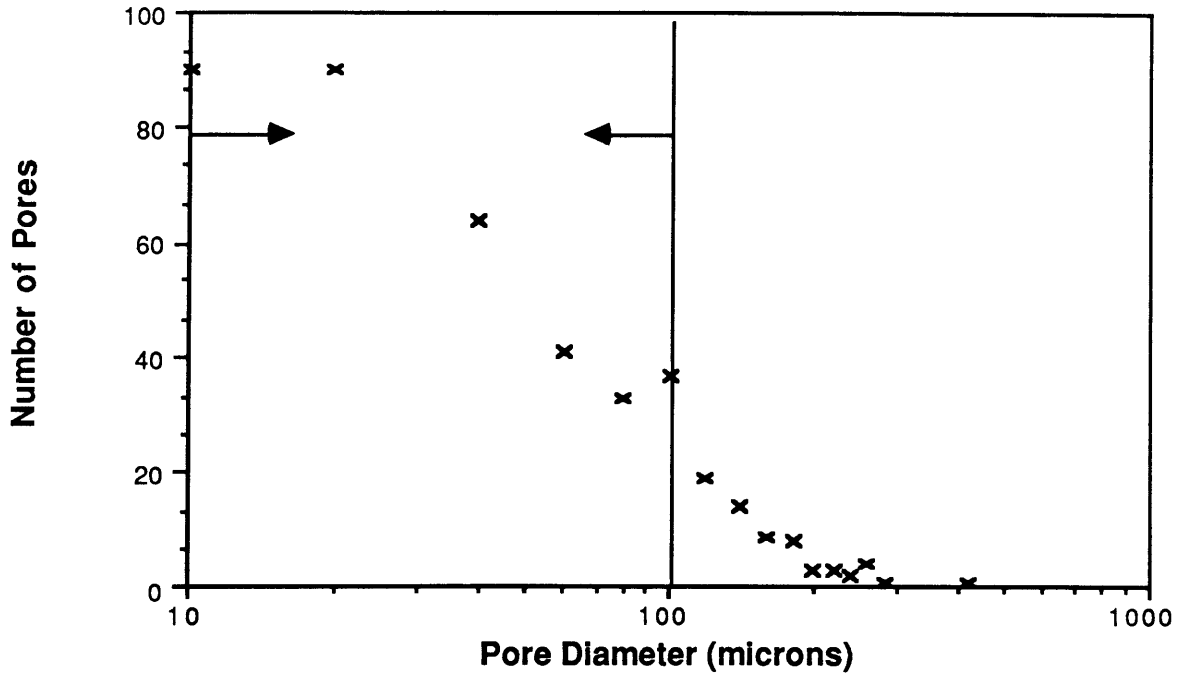

Figure A-5: Histogram of Pore Diameters Measured by Magiscan: Case 6, SEM Micrograph

For the case 6 SEM micrograph, r= 10 microns, R= 50 microns, and R^*= 100 microns were assumed. From the histogram, n_r= 100, n_R= 255, and n_R= 64 were measured. Therefore, $[n_{R^*} + n_r]/n_R$= 0.64, n_{R^*}/n_R= 0.25. Thus $(R/P)_t$ was 1.04, 16% greater than $(R/P)_e$.

For the case 6 light micrograph, r= 10 microns, R= 50 microns, and R^*= 100 microns were again assumed. From the histogram, n_r= 104, n_R= 96, and n_R= 180 were measured. Therefore, $[n_{R^*} + n_r]/n_R$= 2.95, n_{R^*}/n_R= 1.87. Thus $(R/P)_t$ was 0.21, 83% less than $(R/P)_e$.

For large pore specimens, the theoretical and experimental (R/P) correlations closely agreed (within 20%) and were about 1.5 for SEM micrographs and 2.0 for light micrographs. By filtering the pore diameter measurements, and acceptable SD_d= 72% was achieved. The experimental correlations were used to correct all calculated case 1-5 mean pore diameters.

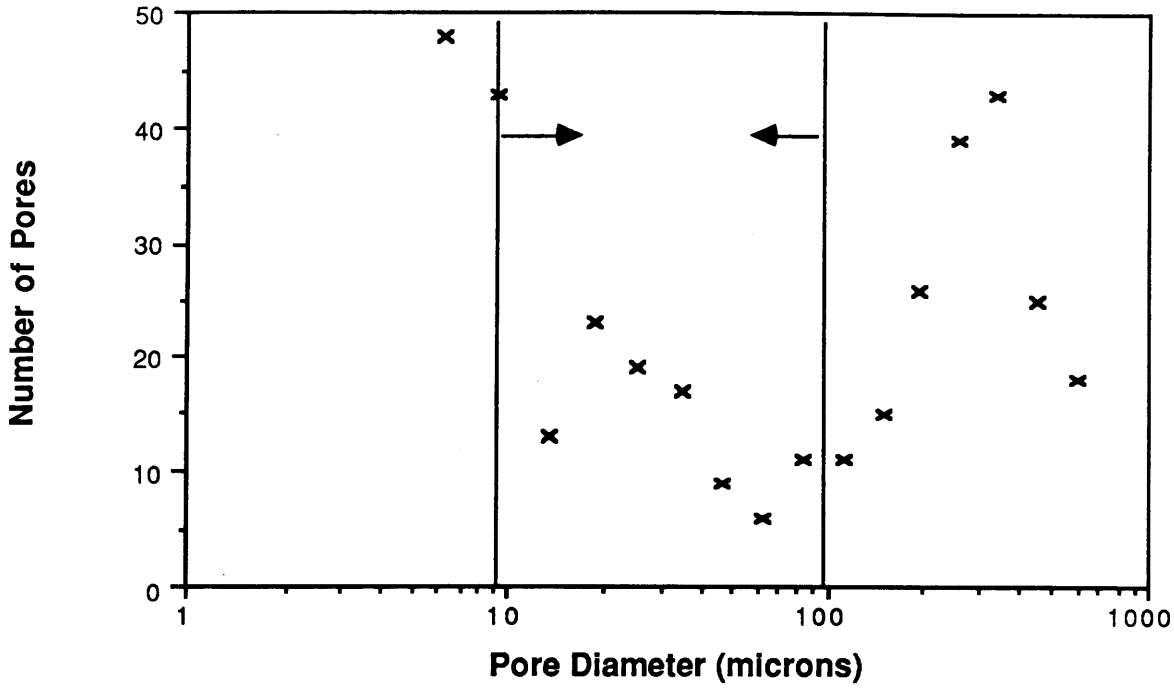

Figure A-6: Histogram of Pore Diameters Measured by Magiscan: Case 6, Light Micrograph of E/S Spec.

For small pore specimens, the theoretical and experimental (R/P) correlations agreed well for the SEM micrographs (within 16%) but very poorly for the light micrographs (an 83% difference). The experimental correlation was used to correct all calculated case 6 SEM micrograph mean pore diameters. Because of the poor agreement of theory and experiment for the case 6 light micrograph correlation and the very large standard deviation in the unfiltered data, this data was thrown out. Embedding and sectioning offers unacceptably low resolution for analysis of very fine (less than 50 micron) pore structures.

Appendix B
Special PNS Bridge Protocols

B.1 5-10 Micron Pores

Observe the following conditions: V= 10^{-4} m/s, ΔT= 80 °C, C= 0.27 %w/w.

B.2 2 mm Bridges

PNS bridges for rabbits have been produced in 2 mm I.D. silicone tubes. The manufacturing steps in Section 3.2 are followed, with the following components substituted:

1. Dow Corning model 602-305 medical grade Silastic Tubing, .078 in ID, .125 in OD (Dow-Corning Co., Midland, MI)
2. Clay Adams Plastic Tubing Adapter model A-1025 D(7543) (Clay Adams Division of Becton Dickinson Co., Parsippany, NJ)

2 mm bridges have been produced with 10 micron pores by observing the following conditions: V= 10^{-4} m/s, ΔT= 65 °C, C= 0.27 %w/w.

B.3 Suspended Particle Bridge

PNS bridges with suspended particle (amorphous) structure have been produced to determine whether continuous pore structure is important to the performance of a bridge in nerve regeneration. The graft contains the same 0.007 gm/ml density of CG as the conventional PNS bridge produced under conditions of C= 0.27 %w/w. A sterile saline suspension of CG is made and then injected into empty silicone tubes placed between the nerve stumps. The average particle diameter is 246 microns with a standard deviation of 106 microns. microns, measured by examination of Trypan blue stained suspension under 10x magnification with a hemocytometer. The following procedure was developed for the production of the suspended particle bridges:

1. Sterilize the following in a steam autoclave: 1 Ederbach blending cup, cap, cap nut, blade, bearing cap, 2 Socket wrenches, 1 Teflon sheet. Collect Ederbach blender (model 8590, Ederbach Corp., Ann Arbor, MI), Lauda cooler, and sterile scalpel.
2. Soak cup and bearing seal washer in 25% glutaraldehyde overnight. Rinse thoroughly with sterile deionized water.
3. Assemble Ederbach blender under sterile conditions.
4. Test blender cup for leaks by filling cup with sterile deionized water and running at high speed for 10 min. Cool to -4 °C.
5. Prepare 550 ml sterile saline solution.
6. Add saline and sterile CG foam to make .007 gm/ml suspension. Cut foam into 1/2 in squares using sterile scalpel on Teflon sheet.
7. Titrate to pH 3 with HCl.
8. Blend suspension at high speed for 20 minutes at 4 °C.
9. Dearate at low speed for 15 minutes at 4 °C.

Appendix C
Control of Biodegradation Rate

The protocol for aqueous glutaraldehyde crosslinking of PNS bridges closely follows that described in the thesis of Lee[5]. The crosslinking solution is 0.25% glutaraldehyde in 0.05 M acetic acid. One measure of crosslink density in CG polymers is the collagenase assay developed by Dionne[30]. Figure C-1 illustrates the relation between assay units and aqueous crosslinking time for pan cast CG foams. This relation was assumed to apply to PNS bridges, since the CG composition is identical and the long soaking times will overcome any effects of geometry on diffusion processes employed in crosslinking.

The following protocol for crosslinking was observed under sterile conditions:

1. Rehydrate in 0.05 M acetic acid (pH 3) for 24 hr.
2. Crosslink for desired time in 0.25% glutaraldehyde.
3. Twice rinse in deionized H_2O.
4. Soak 24 hrs in deionized H_2O.
5. Rinse in deionized H_2O.
6. Store in 70% isopropanol at 4 ^oC.

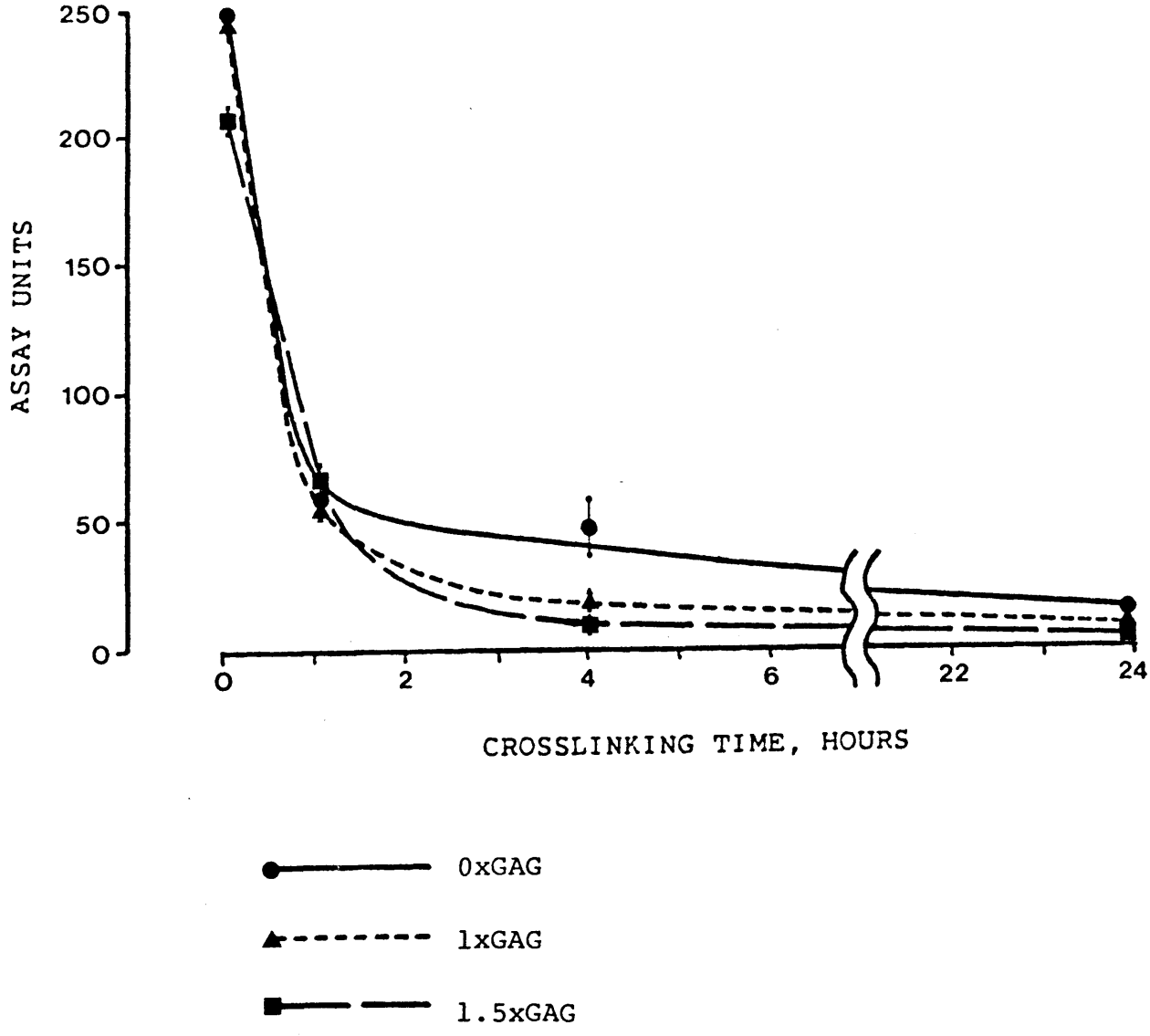

Figure C-1: Assay Units vs. Aqueous Crosslinking Time, Lee (1986)